



Fakultät für Medizin

Molekulare Kardiologie

I. Medizinische Klinik und Poliklinik

Klinikum rechts der Isar

Patient-specific iPSC-based models of hypoplastic left heart syndrome

Vollständiger Abdruck der von der Fakultät für Medizin der Technischen Universität München zur Erlangung des akademischen Grades eines

Doktors der Naturwissenschaften (Dr. rer. nat.)

genehmigten Dissertation.

Svenja Laue

Vorsitzender:

Prof. Dr. Dr. Stefan Engelhardt

Prüfer der Dissertation:

1. Prof. Dr. Karl-Ludwig Laugwitz

2. Prof. Dr. Wolfgang Wurst

Die Dissertation wurde am 04.10.2017 bei der Technischen Universität München eingereicht und durch die Fakultät für Medizin am 03.01.2018 angenommen.

Abstract

Hypoplastic left heart syndrome (HLHS) is one of the most fatal congenital heart defects (CHD) represented by a severely underdeveloped left ventricle. Human genetic studies of the past decade have highlighted a complex genetic basis for CHDs in general, and HLHS in particular, but failed to delineate a common genetic trait. Human induced pluripotent stem cells (hiPSCs) now allow examining key processes of human heart development in the context of the complex genetic background of the patient. hiPSCs from three individuals affected by HLHS were generated and differentiated into cardiovascular cell lineages for molecular characterization. HLHS-affected hiPSCs formed cardiomyocytes (CMs) that did not show any structural abnormalities but exhibited transcriptional reduction of key cardiac markers that can be assigned to left cardiac structures. Similar expression profile changes were observed in cardiovascular progenitor cells (CVPCs). Moreover, while apoptosis rate was not affected in HLHS-CVPCs, their specification was altered due to a cell cycle progression delay. This correlated to impaired cilia function and reduced response to autophagy induction. Inhibition of autophagy in healthy CVPCs was sufficient to recapitulate the observed HLHS disease phenotype.

Remarkably, whole exome sequencing of the three HLHS patients and their parents revealed *de novo* mutations in genes involved in cilia and autophagy processes occurring in all three probands, namely *MACF1*, *FGFR1* and *DENND5B*. Such genes or related gene family members were found to be target of *de novo* mutations in other HLHS affected patients in a larger scale whole exome screening of 78 HLHS trios. Further analysis of the potential role of *DENND5B* in HLHS demonstrated that the identified *de novo* mutation impairs binding of *DENND5B* to *RAB39*, a key player in autophagosome formation. Moreover, morpholino knockdown of *DENND5B* in *Xenopus* and zebrafish revealed a crucial and novel role of this gene in cardiogenesis and cilia formation and function.

Together, this work uncovered an unprecedented role of autophagy in human cardiovascular cell lineage specification and demonstrated defective primary cilium/ autophagy/ cell-cycle axis in HLHS.

Zusammenfassung

Das hypoplastische Linksherzsyndrom (HLHS) gehört zu den schwerwiegendsten angeborenen Herzfehlern und ist durch eine ausgeprägte Unterentwicklung der linken Herzkammer gekennzeichnet. Genetische Analysen von Patienten mit angeborenen Herzfehlern, unter anderem auch von Patienten mit HLHS, legen nahe, dass eine genetische Komponente bei der Entstehung der Krankheit besteht. Allerdings konnte dieser Zusammenhang bisher keiner eindeutigen genetischen Veränderung zugeordnet werden. Human induzierte pluripotente Stammzellen (hiPSC) ermöglichen es zentrale Schritte der menschlichen Herzentwicklung darzustellen und dabei den Einfluss des komplexen patientenspezifischen genetischen Hintergrunds zu untersuchen. Im Rahmen dieser Arbeit wurden hiPSCs von drei Patienten mit HLHS generiert, in kardiovaskuläre Zellen differenziert und auf molekularer Ebene analysiert. HiPSCs von Patienten mit HLHS konnten in Kardiomyozyten (CM) differenziert werden, die keine strukturellen Auffälligkeiten zeigten. Auf transkriptioneller Ebene zeigte sich jedoch eine Reduktion des Expressionslevels von zentralen kardiovaskulären Transkriptionsfaktoren, die mit der Entwicklung des linken Herzens in Verbindung gebracht werden können. Ähnlich Änderungen in der Transkription fanden wir auch in kardiovaskulären Vorläuferzellen (CVPCs) dieser Patienten. Darüber hinaus konnten wir zeigen, dass die Spezifizierung dieser Zellen auf Grund einer veränderten Zell-Zyklus Dynamik gestört war, während andere Prozesse, wie Apoptose, normal verliefen. Gleichzeitig mit der veränderten Zell-Zyklus Dynamik beobachteten wir eine gestörte Induktion von Autophagie sowie Veränderungen in der Ziliogenese. In gesunden Zellen konnte mittels Inhibierung der Autophagie der HLHS-Phänotyp induziert werden.

Interessanterweise fanden sich in whole-exome Sequenzierungsdaten der drei HLHS-Patienten und ihrer Eltern *de novo* Mutationen in Genen, die in Autophagie und Ziliogenese eine wesentliche Rolle spielen: MACF1, FGFR1 und DENND5B. Dies bestätigte sich in einer größeren Kohorte von 78 HLHS-Trios, die ebenfalls *de novo* Mutationen in verwandten Genen mit ähnlichen Funktionen zeigten. In einer weiterführenden Analyse, die die Rolle von DENND5B in der Entstehung des HLHS untersuchte, konnten wir zeigen, dass die identifizierte *de novo* Mutation die Bindung von DENND5B an RA39 stört, welches wiederum eine zentrale Rolle bei der Bildung des Autophago-

soms spielt. Darüber hinaus haben wir durch Morpholino-knockdown Experimente in *Xenopus* und Zebrafisch zeigen können, dass DENND5B eine, bis dahin noch nicht beschriebene Rolle in der kardialen Entwicklung sowie der Entstehung und Funktion von Zilien spielt.

Zusammenfassend lässt sich sagen, dass diese Arbeit erstmalig die Bedeutung von Autophagie bei der Spezifizierung von humanen kardiovaskulären Vorläuferzellen aufzeigt und Defekte der „primären Zilium/Autophagie/Zell-Zyklus“ Achse als wesentliche Ursache für die Entstehung von HLHS identifiziert.

Table of contents

Abstract	I
Zusammenfassung	II
Table of contents	IV
Abbreviations	VI
1. Introduction	1
1.1. Congenital heart diseases	1
1.1.1. Inheritable vs non-inheritable factors in CHD	1
1.1.2. Hypoplastic left heart syndrome as a defined phenotype in CHD ...	3
1.1.3. Onset of hypoplastic left heart syndrome: current theories	6
1.2. Signalling and processes in cardiogenesis	8
1.2.1. Early cardiogenesis	8
1.2.2. Signalling pathways involved in cardiogenesis	11
1.2.3. Regulation of cardiogenesis by cilia	14
1.2.4. Regulation of cardiogenesis by autophagy	21
1.3. Congenital heart disease modelling	27
1.3.1. <i>In vivo</i> cardiac disease modelling	27
1.3.2. <i>In vitro</i> cardiac disease modelling using hiPSCs	29
2. Methods	37
2.1. Reprogramming of human fibroblasts to hiPSCs	37
2.2. Cell culture	38
2.2.1. hiPSC cell culture	38
2.2.2. Directed differentiation of hiPSCs into cardiovascular progenitors (CVPCs)	39
2.2.3. Directed differentiation of hiPSCs into cardiomyocytes	39
2.2.4. Spontaneous differentiation of hiPSCs into EBs	40
2.2.5. mESC cell culture	40
2.2.6. Spontaneous differentiation of mESCs into EBs	41
2.3. Cloning	41
2.3.1. Human DENND5B expression vector	41
2.3.2. PiggyBac™ NKX2.5 Enhancer	43
2.4. Transfection generating stable cell lines	44
2.4.1. Clonal selection	45
2.5. Immunofluorescence	45
2.6. Flow cytometry	46

2.7. RNA isolation, RT-PCR and qRT-PCR.....	48
2.7.1. qRT-PCR for pluripotency and embryonic germ layer markers and cardiac specific genes	50
2.7.2. qRT-PCR of PiggyBac™ integration numbers.....	50
2.7.3. PCR of Sendai transgenes and endogenous pluripotency marker expression	51
2.8. Western Blot	51
2.8.1. Protein sample preparation	51
2.8.2. SDS-PAGE and Blotting.....	52
2.8.3. Staining and detection.....	53
2.9. List of oligonucleotides	53
3. Results.....	55
3.1. Identification of <i>de novo</i> mutations by whole exome sequencing in HLHS trios.....	55
3.2. Generation of hiPSCs from HLHS patients	57
3.3. Marker gene expression during cardiac differentiation of HLHS-hiPSCs.....	58
3.4. Proliferation analysis during cardiac differentiation of HLHS-hiPSCs ..	62
3.5. Apoptosis analysis during cardiac differentiation of HLHS-hiPSCs	64
3.6. Cell cycle analysis during cardiac differentiation of HLHS-hiPSCs.....	64
3.7. Ciliogenesis analysis in HLHS-hiPSC-derived CVPCs	66
3.8. Autophagy analysis in HLHS-hiPSC-derived CVPCs.....	69
3.9. Induction of the HLHS phenotype by autophagy inhibition in control hiPSCs	70
3.10. Analysis of disease-causing <i>de novo</i> mutations of interest.....	71
3.11. Molecular and functional analysis of DENND5B.....	74
3.12. Generation and evaluation of NKX2.5 Enhancer-GFP hiPSC lines for identification of cardiac subpopulations.....	79
4. Discussion	81
4.1. Challenges in modelling complex cardiac disease as CHD.....	81
4.2. Perturbations in cilia and autophagy as basis for defective cardiogenesis and CHD	86
4.3. Limitations of the study	93
5. References.....	96

Abbreviations

AAVS	Adeno-associated virus
ACTA2	Smooth muscle alpha (α)-2 actin
AFP	Alpha-fetoprotein
AIM1L	Absent In Melanoma 1-Like
AMPK	AMP-activated protein kinase
ANF	Atrial natriuretic peptide
APC	Adenomatous polyposis coli
APD	Action potential duration
ARVC	Arrhythmogenic right ventricular cardiomyopathy
ATF6	Activating transcription factor 6,
ATG	Autophagy-related protein
AV	Atrioventricular
BAI2	Brain-specific angiogenesis inhibitor 2
BAV	Bicuspid aortic valve
BCL1	B-cell CLL/lymphoma 1
BMP	Bone morphogenetic protein
BSA	Bovine serum albumine
BSA	Bovine serum albumin
CaMKII	Ca ²⁺ /calmodulin-dependent protein kinase II
CASQ2	Calsequestrin-2
CD	Cluster of differentiation
CDH	Cadherin
CDK	Cyclin-dependent kinase
CER	Cerebus
CHD	Congenital heart disease
CIM	CVPC induction medium
clCASP3	Cleaved Caspase 3
CM	Cardiomyocyte
CMLC2	Cardiac myosin light chain 2

CMV	Human cytomegalovirus
c-MYC	Myelocytomatosis Viral Oncogene Homolog
CNV	Copy number variation
COPD	Chronic obstructive pulmonary disease
CPVT	Catecholaminergic polymorphic ventricular tachycardia
CQ	Chloroquine
CRISPR	Clustered Regularly Interspaced Short Palindromic Repeats
cTNT	Cardiac troponin T
Ctrl	Control
CVPC	Cardiovascular progenitor cell
DAAM	Disheveled-associated activator of morphogenesis
DAD	Delayed After Depolarization
DAPI	4',6-diamidino-2-phenylindole
DCM	Dilated cardiomyopathy
DENND5B	DENN Domain Containing 5B
DES	Desmin
DKK1	Dickkopf-related protein 1
DMEM	Dulbecco's modified medium
DMSO	Dimethyl sulfoxide
DNA	Deoxyribonucleic acid
DORV	Double outlet right ventricle
DSH	Dishevelled
EAD	Early afterdepolarization
EB	Embryonic body
ECG	Electrocardiogram
ECL	Enhanced chemiluminescence
EDTA	Ethylenediaminetetraacetic acid
EdU	5-ethynyl-2'-deoxyuridine
ELC	Essential light chain of myosin
EMT	Epithelial-mesenchymal transition
END-2	Endodermal-like cells 2
ER	Endoplasmic reticulum
ERBB	Erythroblastic leukemia viral oncogene homolog

ETV2	ETS Variant 2
FACS	Fluorescence-activated cell scanning
FBN1	Fibrillin-1
FBS	Fetal bovine serum
FGF	Fibroblast growth factor
FGFR	Fibroblast growth factor receptor
FHF	First heart field
FIP200	FAK family kinase-interacting protein of 200 kDa
FOX	Forkhead box protein
FS	Forward scatter
FZ	Frizzled
GABRR2	Gamma-Aminobutyric Acid Type A Receptor Rho2 Subunit
GAPDH	Glyceraldehyde 3-phosphate dehydrogenase
GATA	GATA-binding protein
GDP	Guanosine diphosphate
GEF	Guanine nucleotide exchange factor
GFP	Green fluorescent protein
GJA	Gap junction protein alpha 1
GLI	Glioma-associated oncogene
GRB2	Growth factor receptor-bound protein 2
GSK3 β	Glycogen synthase kinase 3 beta
GTP	Guanosine triphosphate
GWAS	Genome-wide association studies
HAND	Heart- and neural crest derivatives-expressed protein
HCM	Hypertrophic cardiomyopathy
hCO	Human cardiac organoid
HEY	Hairy/enhancer-of-split related with YRPW motif protein
HIF	Hypoxia-inducible factor
hiPSC	Human induced pluripotent stem cell
HIV	Human immunodeficiency virus
HLHS	Hypoplastic left heart syndrome
IFT	Intraflagellar transport
IGF-1	Insulin-like-growth-factor-I

IP ₃	Inositol trisphosphate
IRE1	Inositol-requiring enzyme 1
ISL1	Insulin gene enhancer protein 1
ITR	inverted terminal repeat sequences
JNK	c-Jun N-terminal kinase
KCN	Potassium Voltage-Gated Channel
KLF4	Kruppel-like factor 4
KRT	Keratin
KSR	Knockout serum replacement
LAMP2	Lysosome-associated membrane protein 2
LC3	Microtubule-associated protein 1A/1B-light chain 3
LIF	Leukemia inhibitory factor protein
LKB1	Liver kinase B1
LMNA	Lamin A/C
LQTS	Long-QT syndrome
MACF1	Microtubule-Actin Crosslinking Factor 1
MAPK	Mitogen-activated protein kinase
MCS	Multiple cloning site
MEF	Mouse embryonic feeder cell
MEF2C	Myocyte-specific enhancer factor 2C
mESC	Mouse embryonic stem cell
MESP	Mesoderm posterior protein
mHtt	Mutant huntington
miRNA	microRNA
MLL1	Mixed lineage leukemia protein-1
MMP2	Matrix metalloproteinase-2
MOI	Multiplicity of infection
mRNA	Messenger RNA
mTOR	Mechanistic Target of Rapamycin
MYH	Myosin heavy chain
MYL	Myosin light chain
MYRF	Myelin Regulatory Factor
NaCl	Sodium Chloride

NCAM	Neural cell adhesion molecule
NDE	Nuclear distribution protein nudE homolog 1
NDUFB10	NADH:Ubiquinone oxidoreductase subunit B10
NEAA	Non-essential amino acids
NeoR	Neomycin resistance
NFAT	Nuclear factor of activated T-cells
NICD	Notch intracellular domain
NKX2.5	NK2 homeobox 5
NO	Nitric oxide
OCT	Octamer-binding transcription factor
OFD1	Oral-facial-digital syndrome 1 protein
OFT	Outflow tract
PARP1	Poly(ADP-ribose)-Polymerase 1
PBMC	Peripheral blood mononuclear cell
PBS	Phosphate buffered saline
PCP	Planar cell polarity
PCR	Polymerase chain reaction
PDGFR α	Platelet-derived growth factor receptor α
PDX1	Pancreas/duodenum homeobox protein 1
PERK	Protein Kinase RNA-like ER Kinase
PFA	Paraformaldehyde
PFN	Profilin
PI	Propidium Iodide
PI3K	Phosphoinositide 3-kinase
PITX2	Paired-like homeodomain transcription factor 2
PKC	Protein kinase C
PKP2	Plakophilin-2
PLC γ	Phospholipase C γ
PPAR γ	Peroxisome proliferator-activated receptor- γ
PSF	Primary skin fibroblasts
PTA	Persistent truncus arteriosus
PTC	Patched
PTNP11	Protein tyrosine phosphatase nonreceptor type 11

qRT-PCR	Quantitative reverse transcriptase-PCR
RAB	Ras-related in brain
RAC1	Ras-related C3 botulinum toxin substrate 1
RAS	Rat sarcoma
REX1	Reduced expression protein 1
Rho	Ras homolog gene family
RNA	Ribonucleic acid
ROCK	Rho-associated, coiled-coil containing protein kinase
ROS	Reactive oxygen species
RPMI	Roswell Park Memorial Institute medium
RYR	Ryanodine receptor
SAG	Smoothened agonist
SCF	Stem cell factor
SCL	Stem cell leukemia
SDS	Sodium dodecyl sulfate
SeV	Sendai Virus
SHF	Second heart field
SHH	Sonic hedgehog
SHP2	Src homology-2 domain containing protein
siRNA	Small interfering RNA
SLN5A	Sodium voltage-gated channel alpha subunit 5
SMAD	Portmanteau of small and mothers against decapentaplegic
SMO	Smoothened
SOX2	Sex determining region Y-box 2
SQSMT1	Sequestosome-1
SR	Sarcoplasmic reticulum
SS	Side scatter
STAT	Signal Transducers and Activators of Transcription
SV	Sinus venous
SVC	Superior vena cava
SYBU	Syntabulin
T	Brachyury
TALEN	Transcription activator-like effector nuclease

TBX	T-box
TCTEX	T-complex testis-specific protein 1
TDGF1	Teratocarcinoma-derived growth factor 1
TGF β	Transforming growth factor β
TH	Tyrosine hydroxylase
TLR	Toll-like receptor
TOF	Tetralogy of Fallot
TRA1	Transcription-associated protein 1
TRIS	Tris(hydroxymethyl)-aminomethan
TTN	Titin
ULK	UNC-51-Like Kinase-1
UPR	Unfolded protein response
VE	Vascular endothelial
VEGF	Vascular endothelial growth factor
WNT	Wingless-Type MMTV Integration Site Family, Member
WT1	Wilms tumour protein 1
YFP	Yellow fluorescent protein
ZIC3	Zinc finger of the cerebellum 3
ZNF	Zinc finger

1. Introduction

1.1. Congenital heart diseases

Cardiovascular malformations are one of the major causes for infant mortality in the western world and represent an immense challenge for cardiac surgeons as well as researchers. The manifestation of these defects is complex and treatment is very problematic requiring advanced technological interventions. Additionally, the origin of the occurrence of these defects is not even partially understood yet despite major progress in disease modelling along with intensive cardiovascular and developmental biology research throughout the past decades.

Congenital heart diseases (CHD) describe a class of cardiovascular malformations arising during embryonic development. This group includes a huge variety of structural as well as functional deficits, ranging from cyanotic heart disease, left-sided obstruction defects to septation defects¹. The incidence of CHD is reported with 0.5-0.7% of all live births and severe forms of these birth defects are present in around 1.5 cases per 1000 newborn infants², thus representing the most common congenital abnormality³.

1.1.1. Inheritable vs non-inheritable factors in CHD

Up to date, it remains elusive to name a cause for the onset of CHD. Ongoing controversial debates about potential genomic variations versus environmental coincidences highlight the complexity of this group of malformations. First evidence of a genetic component in CHD dates back to previously geographically isolated populations, in which hotspots of particular cardiac defects could be assigned to specific geographical regions, most likely due to their divergent genetic histories⁴⁻¹³. Reoccurrence rates in families of affected individuals are markedly increased up to 40-fold compared to the overall population. The risk of a sibling to be diagnosed with a type of CHD is thus estimated with 1-4%¹⁴⁻²⁵. Another finding that supports the idea of autosomal recessive inheritance is the amplification of cases of cardiovascular malformations in regions with high consanguineous rates²⁶⁻³¹. Additionally, the heritability of a number of cardiovascular malformations is described with 50-90%^{8,9,14,32-34}. Studies in animal models revealed more than 300 genes crucial for proper cardiogenesis³⁵. Therefore, even though

individual mutations occur very rarely, the elevated number of target loci might explain the high prevalence of CHDs. Hence, several research groups claim a genetic component causative for the onset of congenital cardiac disorders.

However, assigning single variants to specific cardiovascular disorders remains challenging. So far, researchers identified only a few genetic loci that exhibit an elevated level of mutation rates³⁶. Illustrating karyotypes of liveborn infants showing a congenital malformation, chromosomal abnormalities were identified in 10-12% of all cases³⁷. The regions affected by these alterations can often be associated with syndromic congenital disorders that present predominant cardiac defects³⁶. Until now, numerous genomic duplications and deletions could be allocated to congenital cardiovascular malformations, thus the instability of local regions in the genome appears to represent an important trigger in the development of these cardiac disorders³⁸⁻⁴¹. Initial definition of larger regions affected in CHD and subsequent screening of those regions for potential candidate genes, indeed led to the identification of a small number of defined genes predicted to be causative. Some of those genes are dosage sensitive, implying that an imbalanced expression or haploinsufficiency due to the mutations is responsible for exhibiting the phenotype and the degree of severity. The reason is most likely the high sensitivity of developmental pathways to temporally and spatially dynamical changing of gene product levels. Often, transcription factors and chromatin modifiers are affected³⁶. The interaction of *de novo* mutations with mutations carried on from the parents and their respective importance in the onset of CHD is still controversially discussed. Zaidi *et al.* could account *de novo* mutations for around 10% of the congenital disorders investigated in a large exome sequencing analysis⁴² leaving space to interpret the causative factor in the remaining cases.

This brings forth the additional potential role of non-inherited environmental risk factors in this assumed interaction. Discussed is the maternal health state regarding infections and other illnesses during early stages of the pregnancy, in particular maternal rubella, upper respiratory tract infections or diabetes^{43,44}. Moreover, metabolic disorders such as phenylketonuria as well as altered levels of retinoic acid could influence cardiogenesis in the embryo⁴⁵. Maternal intake of therapeutic and nontherapeutic drugs as well as foetal exposure to thalidomide and indomethacin, used to delay preterm delivery, might also lead to an elevated risk. Instead, folic acid has been described to positively act on embryonic development preventing birth defects⁴⁶. Neonatal asphyxia or

hypoxia, maternal B-mode ultrasound examinations and the number of previous pregnancies are named as risk factors as well. Finally, social factors such as the maternal educational background and maternal mental stress are also assumed to play a role^{47,48}. A recent study combines these two factors unravelling a higher impact of functional convergence compared to direct convergence in the development of congenital heart defects. This means that genetic and environmental risk factors do not directly influence distinct genes and proteins but rather converge in defined networks of molecules that drive discrete steps of cardiogenesis and are responsible for the formation of explicit cardiac structures⁴⁹.

1.1.2. Hypoplastic left heart syndrome as a defined phenotype in CHD

In most cases of congenital malformations, specific cardiac structures such as particular heart valves, parts of the cardiac chambers or the outflow tract are missing or severely underdeveloped. A clinically clearly defined CHD is the hypoplastic left heart syndrome (HLHS) where the left ventricle represents the cardiac structure mainly affected. It occurs in the second half of gestation in the foetus⁵⁰ and has a prevalence of 4-8% of all congenital cardiovascular defects^{2,51}. With a survival rate of only 50-70% of infants⁵² born with HLHS, an interstage mortality of 12%⁵³ and poor long-term prognosis, it is one of the most fatal congenital malformations. HLHS patients represent a sharply defined phenotype with a crucially underdeveloped left ventricle, hypoplasia of the ascending aorta as well as of the aortic arch and additional aortic and mitral valve stenosis. Accordingly, the systemic circulation is interrupted which would lead to rapid death without instant postnatal interventions (Fig. 1).

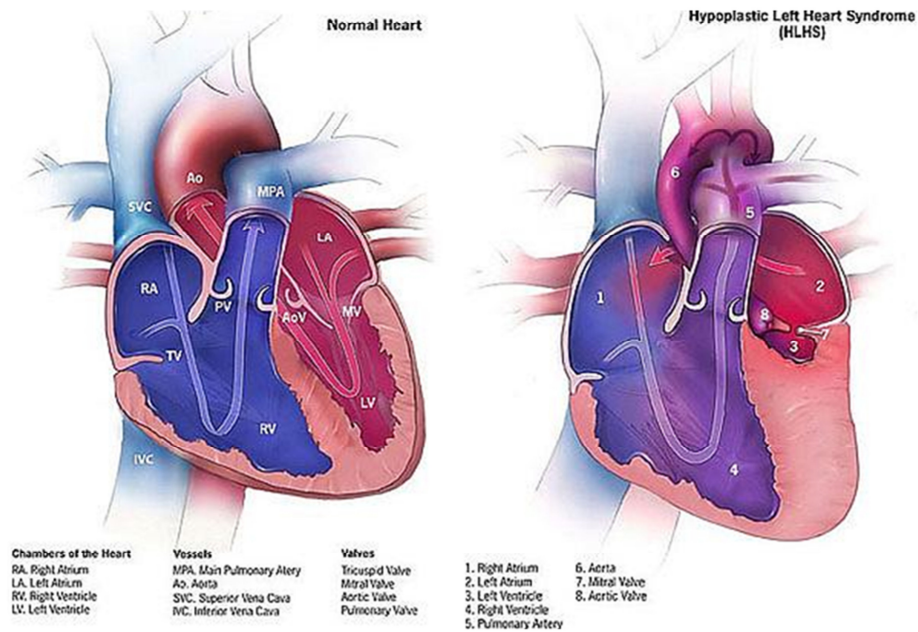


Figure 1: Structural differences between a normal heart and a hypoplastic left heart. (A) Morphology of a normal heart. (B) Schematic heart of HLHS patients with an underdeveloped left ventricle. Source: Centers for Disease Control and Prevention, National Center on Birth Defects and Developmental Disabilities.

In the recent years, enormous advances in cardiac surgery approaches made it possible to save the lives of an increasing number of newborns with a manifested hypoplastic left heart. To achieve this survival, either a heart transplant or the so-called Norwood procedure, first successfully accomplished by Dr. William Imon Norwood, Jr. and colleagues in 1981, is required immediately after birth to secure blood supply. During this three-stage procedure, the function of the left ventricle is restored utilizing existing parts of the cardiovascular system. In brief, in stage 1 (Norwood procedure), which the newborns need to undergo directly postnatally, the fully functional right ventricle adopts the supply of the systemic circulation with blood. Therefore, an atrial septectomy as well as the transection and ligation of the distal main pulmonary artery are performed. Subsequently, the underdeveloped aortic arch is coupled with the pulmonary artery and the aortic coarctation is repaired applying a patch to the disrupted part, thereby enlarging the vessel and thus increasing the blood flow. Moreover, since the lungs are no longer supplied with deoxygenated blood from the right ventricle, the aorta needs to be connected to the main pulmonary artery by creating an aortopulmonary shunt resulting in restored pulmonary blood flow. The second stage (Glenn procedure) is carried out

roughly three to six months after stage 1 once there is a reduction of the pulmonary vascular resistance detected, leading to a separated pulmonary and systemic circulation after replacement of the aortopulmonary shunt by a bidirectional superior vena cava (SVC)-pulmonary shunt. Consequently, the pulmonary system is now protected from the high systemic arterial pressure and moreover, mixture of upper venous and oxygenated blood in the right ventricle is prevented. Still, some venous blood from the lower body part is reaching the right ventricle reducing the total oxygen saturation of the blood leaving the right ventricle. Hence, stage 3 (Fontan procedure) is required to finalize the restoration of blood-, and thus, oxygen supply throughout the whole body by eliminating the flow of deoxygenated blood to the right ventricle directing it towards the pulmonary artery^{54,55}. Consequently, the heart consists of a single pumping chamber responsible for the body circulation, built out of the right ventricle, whereas passive venous flow to the lungs maintains the pulmonary circulation (Fig. 2).

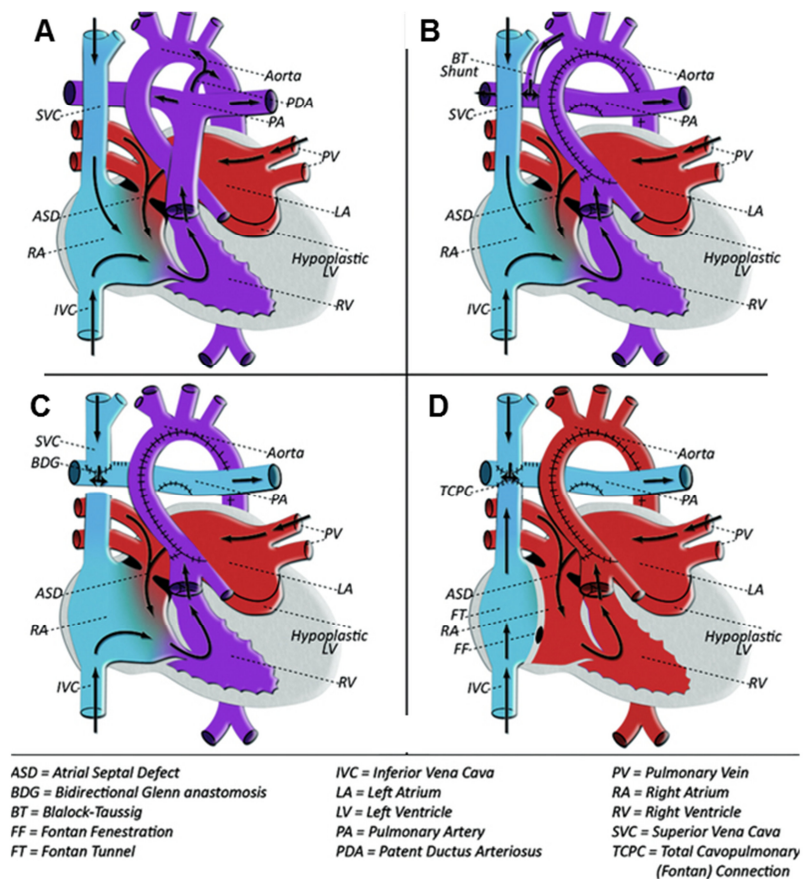


Figure 2: Visualization of the cardiac surgery intervention in HLHS patients. (A) HLHS heart before surgery. (B) Norwood procedure (C) Glenn procedure (D) Fontan procedure. Source: New Approaches to Neuroprotection in Infant Heart Surgery. Erin L Albers, David P Bichell and Bethann McLaughlin.

This intervention impacted the outcome of patients born with HLHS dramatically, raising the expectations of long term survival of successfully operated HLHS patients to around 70% of today newborns. Unfortunately, despite this giant progress made in improving the outcome of infants born with a hypoplastic left heart, life-long monitoring of the patients is obligatory and often, patients that underwent the Norwood procedure show impaired cardiac function over time and require pacemaker implantation to compensate the heavy systemic load permanently pumped through the rebuilt, weaker left ventricle⁵⁶. Therefore, the understanding of possible mutations and/or mechanisms leading to this dramatic congenital heart defect is essential and the key for managing the disorder and developing a successful therapy to overcome the disease.

1.1.3. Onset of hypoplastic left heart syndrome: current theories

As described already for CHD in general, also for HLHS it is still not well understood which defect is causing this dramatic phenotype. Theories include altered blood flow patterns during early stages of cardiac development as well as mutations in crucial genes of cardiogenesis affecting the formation of the chambers which will be discussed in this chapter.

The “flow theory”

One current hypothesis of the origin of HLHS is described as “flow theory”. This builds on the postulation that blood flow-mediated remodelling is a crucial aspect for the morphogenesis of the cardiovascular system. Foetuses developing a hypoplastic left heart display abnormal flow patterns in the left atrium and pulmonary vein indicating a possible connection of disturbed embryonic circulation and HLHS⁵⁷. Supporting the theory, first models of a hypoplastic left heart in chick embryos could be achieved by temporal disruption of the blood flow through the developing left ventricle⁵⁸. The impact of hemodynamic changes on cardiogenesis has been further studied by Groenendijk *et al.*, suggesting that these alterations result in higher intraventricular pressure leading to the phenotype. While this increased ventricular load results in amplified radial force, perpendicular to the blood flow, another force, the frictional force, acting parallel to the blood flow instead and inducing shear stress, could also be a trigger in forming a hypoplastic ventricle⁵⁹. Moreover, the extent to which the hemodynamic flow is changed

most likely defines the severity of the cardiac malformation⁶⁰. However, flow dynamics are complex in the developing myocardium. Especially profound morphological changes such as cardiac tube looping along with receptor-mediated signal transduction processes transferring flow changes into the cells make it difficult to understand how flow dynamics could lead to severe congenital malformations such as HLHS⁶¹.

Genetic variants in HLHS

As already mentioned above, another aspect that has been controversially discussed not only for the occurrence of CHD in general, but also for HLHS in particular, is the association with genetic variants as a possible motive. Evidence could be an observed familiar clustering of HLHS and congenital disorders^{8,19,62}. Moreover, linkage analysis revealed significant loci on specific chromosomes confirming that HLHS rather represents a genetically heterogeneous disorder^{63,64}. Data has been generated claiming specific genetic mutations being at least partially involved in the development of the disease thus presenting the disease as inheritable. Already in 1974, first suggestions of an autosomal recessive background were stated⁶⁵. Until now, mutations in several genetic clusters have been postulated to be causative for HLHS. Also copy number variations (CNVs) and chromosomal abnormalities, often associated with genetic syndromes^{41,63,66,67} as well as microdeletions have been reported^{41,68,69}. The majority of variants described belong to chamber-specific regulatory genes such as *Gap Junction Protein Alpha 1 (GJA1)*⁷⁰, *NK2 Homeobox 5 (NKX2.5)*⁷¹, *NOTCH1*^{72,73}, *Myosin heavy chain (MYH) 6*⁷⁴ and *Heart- and neural crest derivatives-expressed protein (HAND) 1*⁷⁵, suggesting a primary defect of heart formation and growth^{76,77}. Other mutations found in HLHS patients include *SMAD3*⁷⁸, *erythroblastic leukemia viral oncogene homolog 4 (ERBB4)*⁷⁹, *Zinc finger of the cerebellum 3 (ZIC3)*⁸⁰ and *Forkhead box protein (FOX) C2* and *LI*⁸¹. Recent studies found an enrichment of *de novo* variants in histone-modifiers that influence accurate differentiation timing as well⁸².

Nevertheless, strong evidence for a complex rather than a Mendelian inheritance pattern is given by the fact that identical mutations lead to diverse cardiac malformations, best illustrated in a study describing identical twins with inconsistent phenotypical manifestations, one showing a mild bicuspid aortic valve (BAV) while the other one is suffering from severe HLHS⁶². This argues in favour of theories proposing an interplay of ge-

nostic variants, genetic modifiers and environmental risk factors to define the ultimate phenotype.

1.2. Signalling and processes in cardiogenesis

Not only the role of inheritable versus non-inheritable factors is yet not clarified, another important question remains unanswered: which pathways and molecular mechanisms are affected by those intrinsic and extrinsic factors to establish the severe cardiac phenotype? Although some theories exist aiming to describe the molecular basis of this birth defect, none of them could be proven correct so far.

1.2.1. Early cardiogenesis

The first step in unravelling the molecular mechanisms leading to congenital heart defects is to understand cardiogenesis in general and to discover important pathways and molecules within this complex process.

First steps in cardiogenesis

The heart is the first functional organ to develop and starts to beat and pump blood at around 4 weeks of development in human embryogenesis. Heart formation starts 18 to 19 days after fertilisation. In brief, the primitive heart tube arises from embryonic mesoderm after gastrulation, by the fusion of two endocardial tubes, consisting of cardiac progenitor cells. Subsequently, this tube loops, being the first organ showing left-right asymmetry, and the primitive cardiac structures truncus arteriosus, bulbus cordis, sinus venosus, primitive ventricle and primitive atrium, are formed. Septation of these primitive structures builds the four chambers as well as the aorta and the pulmonary artery⁸³. Initial experiments performed in chick grafts in the 1940s aimed at illustrating early cell fate decisions in order to understand how the vertebrate heart is formed and specialized. Here, gastrulation was described as the process in which the three germ layers mesoderm, endoderm and ectoderm are formed. At this stage, cardiac precursor cells are already visible⁸⁴. Looking at amphibians such as *Xenopus* and in zebrafish, mesoderm, the germ layer from which the heart arises, is separated from an intermediate germ layer, the mesendoderm, whereby the process leading to this segregation is still not completely

discovered. A known regulator of mesoderm induction is *Brachyury (T)* and mice with a homozygous knockout of *T* die at E10 due to incomplete mesoderm formation.⁸⁵ Moreover, a proximal-distal gradient of NODAL/SMAD seem to be involved in the segregation of the cardiac mesoderm⁸⁶. The factors specifying the earliest primitive mesoderm and endoderm are GATA-binding protein (GATA) 4, 5, 6 NODAL and ACTIVIN interacting with Wingless-Type MMTV Integration Site Family, Member (WNT)/ β -catenin signalling⁸⁷. Bone morphogenetic protein (BMP) 2 has been identified as a factor defining early cardiac structures rising from the early mesoderm⁸⁸ and positioning the heart⁸⁹, confirmed by BMP2 deficient mice exhibiting severe cardiovascular malformations⁹⁰.

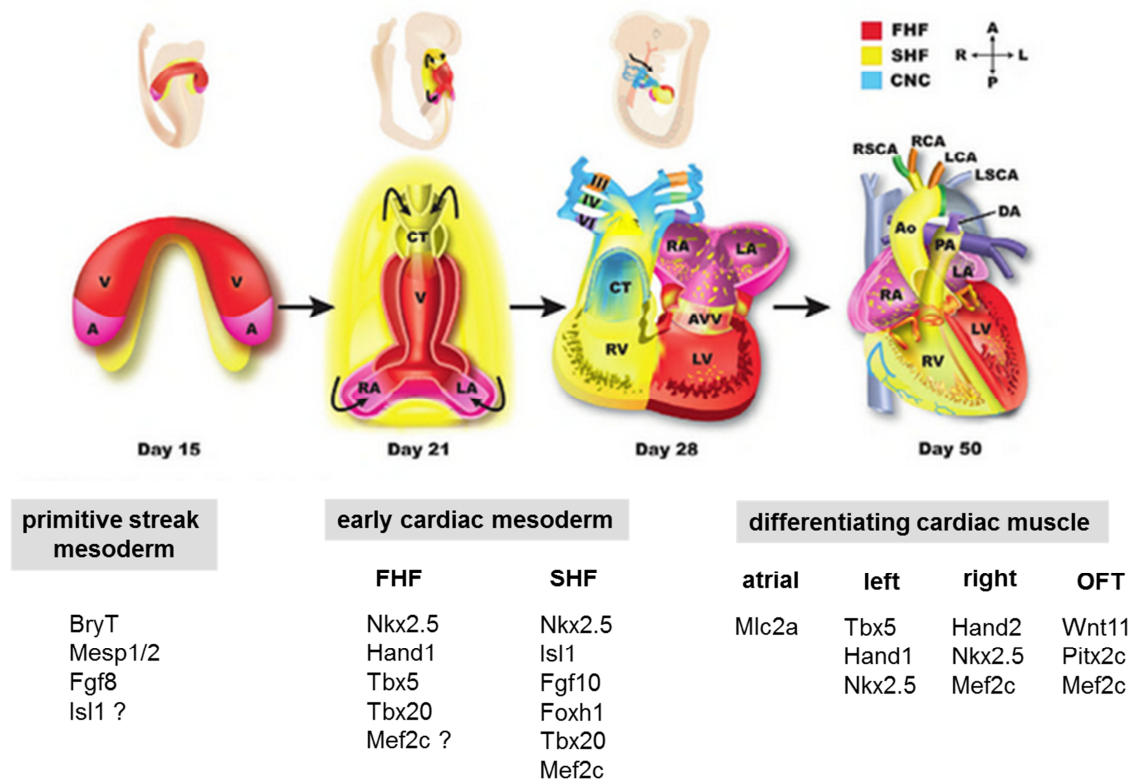


Figure 3: Scheme of cardiogenesis and the involvement of marker gene expression of FHF and SHF cardiac precursors. A: Atrium, V: Ventricle, CT: conotruncal valve, AVV: Atrio-ventricular valve, RA: right atrium, LA: left atrium, RV: right ventricle, LV: left ventricle, Ao: Aorta, DA: Ductus arteriosus, LCA: left carotid artery, RCA: right carotid artery, LSCA: left subclavian artery, RSCA: right subclavian artery, RCC: right common carotid, LCC: left common carotid, PA: pulmonary artery. Source: Intercellular Signalling in Development and Disease: Cell Signalling Collection, Edward A. Dennis, Ralph A. Bradshaw.

Additionally, expression of Mesoderm posterior protein 1 (MESP1) between E6.5 and E7.5 in mice determine a cardiovascular fate of mesodermal cells⁹¹. Cardiac determination of the mesoderm towards prospective myocardial, endocardial and epicardial cell

fate occurs at E7.5 in mouse embryos^{92,93} and is molecularly defined by expression of GATA4, 5, 6, HAND1, 2, NKX2.5 and Wilms tumour protein 1 (WT1)⁹⁴. Hereby, the expression of the mesoderm-specific transcription factor MESP1 is essential for cardiovascular progenitor formation in mice⁹⁵ and also subsequently required for the migration of cardiac precursor cells⁹¹ (Fig. 3).

Development of cardiac progenitors

Cardiac progenitors can be identified for the first time in the cardiac crescent, originating from splanchnic mesoderm, that undergoes a fusion to create the primitive heart tube which will contribute to the left ventricle, major parts of the atria, the atrioventricular (AV) canal and the sinus venosus (SV). This population is called first heart field (FHF) but its proceeding patterning including cardiac looping and elongation of the heart tube is strictly dependent on the presence of another population of cardiac precursors, defined as second heart field (SHF)⁹⁶. This group of cells, located medial and dorsal to the cardiac crescent within the pharyngeal mesoderm, forms the right ventricle, the outflow tract (OFT) and parts of the arterial and venous pole of the heart tube^{97,98} and of the great arteries. SHF is characterized by the expression of TBX1, Insulin gene enhancer protein 1 (ISL1), Fibroblast growth factor (FGF) 8 and 10 and GATA4⁹⁸⁻¹⁰⁰. However, key cardiac markers such as the transcription factors NKX2.5 and ISL1 are expressed in both heart fields, but in defined temporal and spatial patterns. Hence, a major difference between these two heart fields is the timing of differentiation^{101,102} whereby FHF cells are specializing earlier towards myocytes than their SHF counterpart, which is still in a premature proliferative state, maintained by NKX2.5 inhibition of SMAD1 and BMP2¹⁰³. The formation of those heart fields relies on several signalling pathways including BMP, SHH, FGF, WNT and NOTCH, mainly emitted from the adjacent endoderm¹⁰⁴ and the FHF-derived myocytes build a scaffold for the still immature proliferative SHF progenitor population. However, the lack of specific markers for these heart fields makes it difficult to get a more detailed insight in the heart field division and further definition. One key step is the establishment of a septum between the left and right ventricle regulated by asymmetric T-box 5 (TBX5) and Paired-like homeodomain transcription factor 2 (PITX2) expression¹⁰⁵.

Besides the cardiogenic mesoderm, from which FHF and SHF populations arise, two other progenitor sources exist that “shape” the heart later on. On one hand, cardiac neu-

ral crest cells represent precursors of aorta smooth muscle cells and the cardiac autonomic nervous system and on the other hand the proepicardium, that forms coronary arteries and cardiac fibroblasts¹⁰⁶.

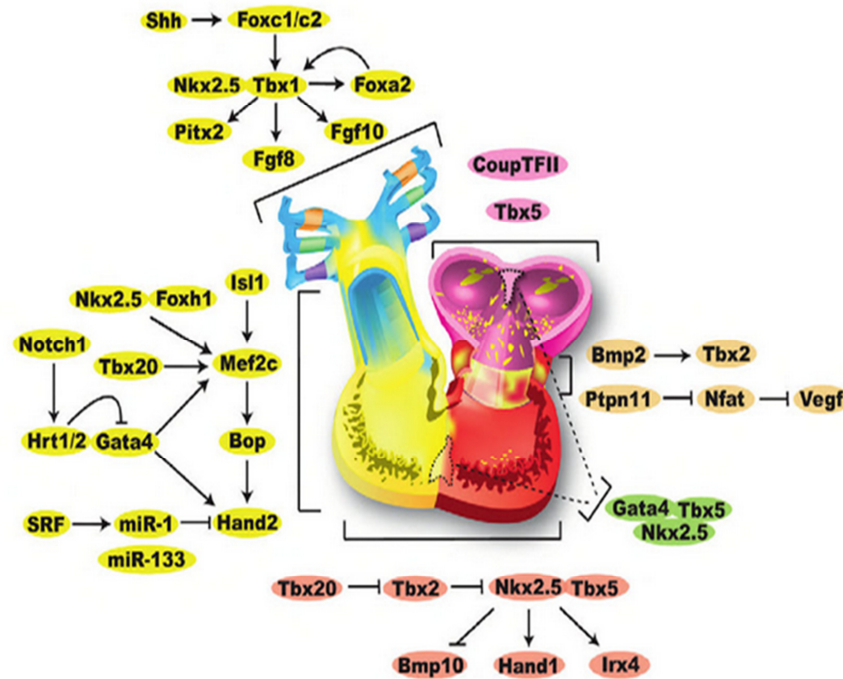


Figure 4: Signalling and transcriptional networks in cardiogenesis. Cardiac structure-specific involvement. Source: Intercellular Signalling in Development and Disease: Cell Signalling Collection, Edward A. Dennis, Ralph A. Bradshaw.

1.2.2. Signalling pathways involved in cardiogenesis

In the recent years, several animal models have been developed to understand key signalling pathways and related genes responsible for specification of these clearly defined cardiac structures as well as to examine how irregularities in the expression of those particular genes, pathways or specific mechanisms might lead to cardiac malformations. Important discovered pathways include the canonical and noncanonical WNT pathways along with transforming growth factor β (TGF β), SHH, FGF and NOTCH signalling (Fig. 4).

Canonical and non-canonical WNT signalling

Canonical WNT pathway activation stimulates proliferation of early cardiac precursors, thus maintaining their progenitor state and preventing formation of structures of the myocardium. Overexpression studies in *Xenopus* could show, that in very early cardiogenesis, inhibition of WNT signalling is necessary for NKX2.5 and TBX5 expression

to induce heart formation¹⁰⁷. Interestingly, this downregulation of the WNT pathway is only effective in specific regions, in which BMP is highly expressed¹⁰⁸. WNT expression is also required to maintain the SHF progenitor population in a premature state¹⁰⁹, emphasizing the crucial spatial and temporal regulation of expression patterns during development. Following induction of cardiogenesis by the inhibition of canonical WNT, a switch to the activation of the non-canonical WNT pathway enables the progression of cardiac differentiation^{110,111}.

The non-canonical WNT pathway, also referred to as planar cell polarity (PCP) pathway, is described to play a role in cardiac morphogenesis. More in detail, it regulates cell migration of early cardiac progenitors during heart tube formation, mainly by modulating cytoskeleton remodelling through induction of down-stream pathways such as RhoA/ROCK, RhoA/JNK, Ca²⁺/PKC, and Ca²⁺/CaMKII signalling. Upon morpholino knockdown of WNT11, a noncanonical WNT, the fusion of cardiac primordia is interrupted in *Xenopus*, leading to a phenotype called cardia bifida where two separate hearts are developed in lateral positions¹¹². Moreover, WNT11 together with WNT5a, another non-canonical WNT, are expressed in the developing murine OFT and mutations in these genes lead to OFT defects, such as double outlet right ventricle (DORV)^{113,114}.

TGFβ signalling

Another important player during the progression of heart development is the TGFβ superfamily that comprises mainly BMPs acting as ligands and signals via SMADs. Mice lacking BMP4 are able to form primitive heart structures but die soon after heart tube formation¹¹⁵. From a chronological point of view, BMPs act at the same stage when the non-canonical WNT pathway is activated. Hereby, BMP2 and 4 activate the expression of NKX2.5 and GATA4 thus inducing myocardial formation^{116–118}. Again, distinct spatial and temporal coordination of BMP signalling after myocardial induction is necessary to guide SHF progenitors towards myocardial specification¹¹⁹. But in both heart fields, high levels of activated BMP are necessary to proceed from cardiogenic mesoderm to the working myocardium; only the time of expression differs with a delay in SHF progenitors to allow an extended proliferation period necessary to generate an adequate cardiac cell mass¹²⁰.

Shh signalling

The essential step of extended proliferation of SHF cells is taking place in a very narrow time window and is also driven by SHH signalling¹²¹. Early in embryogenesis, SHH is expressed in the pharyngeal endoderm and mice lacking smoothed (SMO), a downstream target of SHH signalling, display a delayed expression of NKX2.5 in cardiomyocytes¹²². Moreover, ectopic expression of SHH in zebrafish results in heart looping defects, which goes in line with the additional role of SHH signalling in left-right patterning of the embryo^{123,124}. Hereby, SHH is asymmetrically expressed on the left side of Hensen's node, stimulating NODAL and LEFTY expression, which belong to the TGF β family, in the left lateral mesoderm, mediated by secretion of Cerebus (CER), also known as Caronte, from the node to the lateral mesoderm. CER release leads to a left-sided inhibition of BMP and an induction of NODAL and associated PITX2 expression in the mesoderm while FGF and ACTIVIN A inhibit CER expression on the right side resulting in active BMP and suppression of right-sided NODAL expression^{125–128}. During the signalling cascade, SHH binds to Patched (PTC) receptors located at the primary cilium leading to internalization of the complex thereby releasing SMO from vesicles to proceed to the membrane tip of the cilium membrane where it activates glioma-associated oncogene (GLI) proteins that subsequently translocate into the nucleus to induce gene expression.

FGF signalling

FGF receptor (FGFR) signalling, mediated by receptor tyrosine kinases, is required at many steps of cardiogenesis¹²⁹. Especially FGF8, released from adjacent endoderm, is mandatory for an upregulation of the cardiac transcription factors NKX2.5 and Myocyte-specific enhancer factor 2C (MEF2C) in the precardiac mesoderm¹³⁰. This induction of differentiation by endodermal-mediated FGF signalling is again restricted to a very narrow time frame and alterations of this signalling outside of this window do not cause any cardiac defects¹³¹. Instead, targeting the FGF pathway inside this time frame will lead to early heart looping defects as well as cardiac neural crest deficiencies that cause defects in cardiac outflow tract septation^{132,133}. Later on, FGF8 is required for the addition of SHF-derived structures, in particular outflow tract myocardium, to the already existing cardiac scaffold¹³⁴ indicating likewise spatial differences in induction and function of FGFR signalling.

NOTCH signalling

NOTCH signalling is involved in several fate decisions required during embryonic development. During heart development, NOTCH1 activity is detected soon after upregulation of MESP1 and 2. NOTCH1 null mice exhibit extended progenitor cell mass that is not able to differentiate further towards myocytes, most likely since NOTCH1 acts as an inhibitor of the canonical WNT pathway under physiological conditions¹³⁵. Equally, NOTCH2 null mice show a reduced myocardial size¹³⁶. Thus, the role of NOTCH during cardiogenesis is pre-patterning of cardiac mesoderm and subsequently determining the fate of cardiac precursors by maintaining them in their pre-cardiogenic state, acting downstream of NKX2.5 and GATA4¹³⁷. Moreover, it defines the embryonic left-right axis and is responsible for proper cardiac looping and subsequent separation of the atrial and ventricular blood circulation by the AV canal upon Hairy/enhancer-of-split related with YRPW motif protein (HEY) gene activation, mediated by BMP2 and TBX2. After AV canal formation, cardiac valves are formed by epithelial–mesenchymal transition (EMT) of a subpopulation of endothelial cells arising from the AV canal and this EMT is disrupted if NOTCH signalling is abundant. Hereby, NOTCH is acting via vascular endothelial (VE)-cadherin and Vascular endothelial growth factor (VEGF) pathway suppression as well as Matrix metalloproteinase-2 (MMP2) activation^{138–140}.

1.2.3. Regulation of cardiogenesis by cilia

Many signalling pathways important for early cardiac development are bundled in cilia, antenna-like protrusions of the membrane found on many types of cells during specific time points of development as well as on adult tissues. This structure has been described to play a crucial role in cardiogenesis as well and malfunctioning could be connected to several congenital disorders.

Cilia structure and ciliogenesis

In eukaryotes, two types of cilia exist, motile cilia and non-motile primary cilia, which both exhibit essential functions in motility or cellular signalling, respectively. Both cilia types show many conserved structures. They are built of microtubule-based membrane protrusions, called axonemes, arising from a mother centriole during cilia formation which migrates towards the cell surface and is then attached to the membrane at the

base of the cilium, representing the basal body of the cilium. The main difference between the two forms of cilia is the pattern of the axoneme: while both types are built of an outer ring of 9 doublet microtubules, only the motile cilia has an additional central pair of 2 singlet microtubules, described as “9+2” pattern versus the “9+0” pattern in the non-motile cilia¹⁴¹ (Fig. 5).

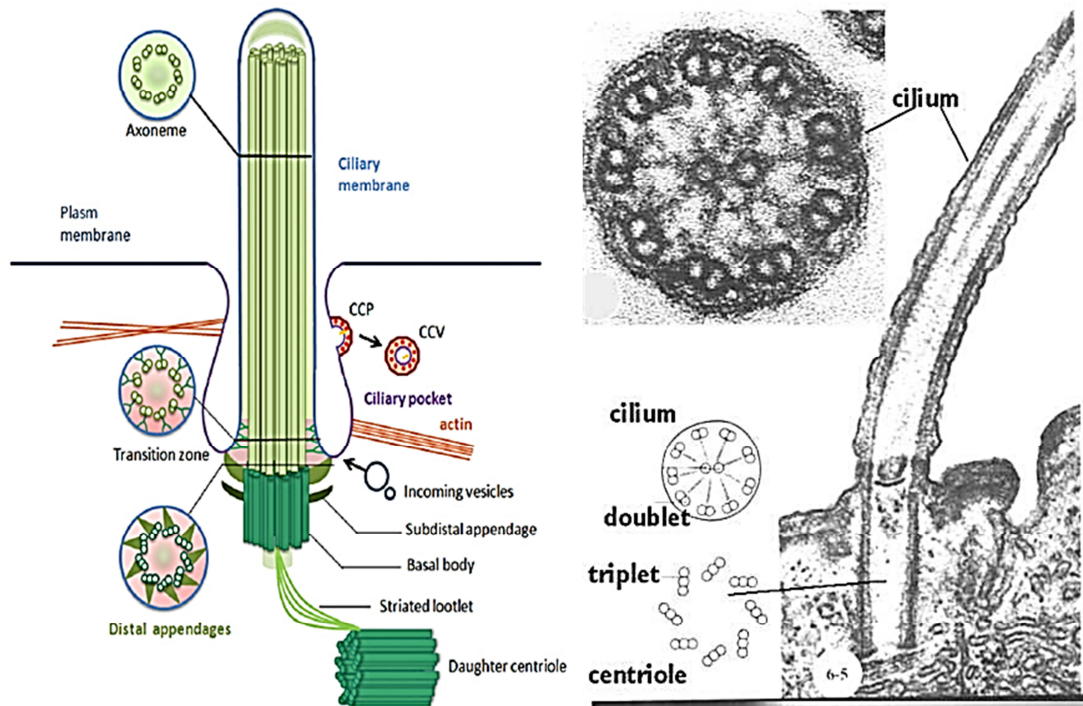


Figure 5: Structure of primary and motile cilia. (A) Schematic illustration of a primary cilium. CCP: clathrin-coated pits, CCV: clathrin-coated vesicle. (B) Electron microscope picture of a motile cilium. Sources: Ke and Yang, 2014; <http://cytochemistry.net/cell-biology/cilia.htm>.

The unique molecule composition in ciliary membranes as well as in the cilia compartment emphasizes the diverse but also very specialized functions of this structure. Beyond its structural role, the axoneme harbours another important function, in transporting ciliary proteins to the cilia tip and retrogradely transferring activated signalling molecules from the cilia tip towards the nucleus to influence gene expression. This bidirectional transport, so called intraflagellar transport (IFT), is mediated by the motor proteins kinesin and dynein, while kinesins drive the anterograde transport facilitating the entry of proteins in the cilium, dyneins serve as the retrograde motor responsible for the protein exit (Fig. 6). The interaction among these motor proteins and the IFT proteins occurs in the transition zone, a subdomain that is located between the axoneme and the basal body in the proximal region of the cilium and that is essential for controlling the

ciliary protein trafficking¹⁴². The gating of ciliary proteins is tightly regulated in this region by another set of molecules including importin- β 2 and RanGTP, recognizing ciliary localization sequences¹⁴³.

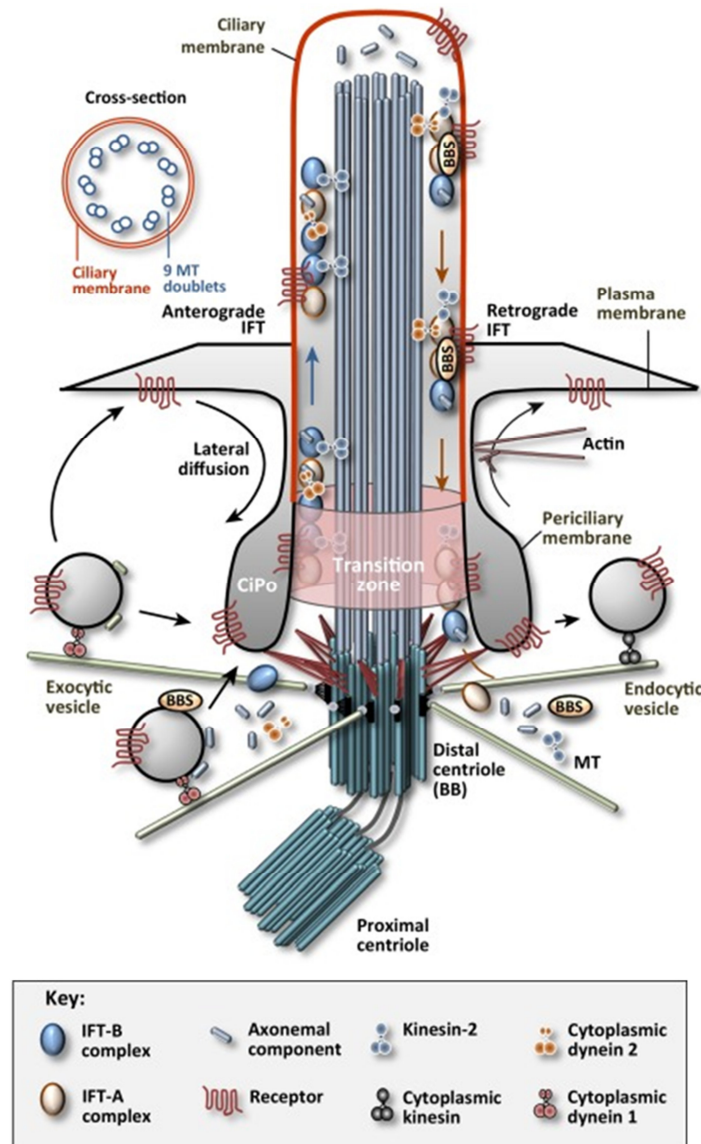


Figure 6: Trafficking in the primary cilium. Transport processes that control delivery of proteins to and from the ciliary membrane for cilia assembly and disassembly as well as signalling. Source: Pedersen, 2016.

One of the best examples of ciliary protein trafficking is the SHH signalling, the major signalling pathway located in primary cilia. Upon activation, rearrangement of the receptors PTC and SMO are essential for the resulting translocation of GLI proteins from the cilium tip to the nucleus to activate or repress specific genes¹⁴⁴. The protein delivery towards the cilium is mediated by directed vesicle transport. Specific sorting and direction of these vesicles is guaranteed by a group of proteins called small GTPases, includ-

ing several Ras-related in brain (RAB) proteins¹⁴⁵. These proteins are activated by their molecular counterparts, guanine exchange factors (GEFs), that act as a molecular switch through replacement of Guanosine diphosphate (GDP) with Guanosine triphosphate (GTP)¹⁴⁶.

Functional differences of primary and motile cilia

The principal difference between the two types of cilia, besides the structural aspect, is their function and occurrence. Beating motile cilia are found solely on a few highly specialized tissues, such as the embryonic node or the adult pulmonary epithelium, and they appear in higher numbers per cell. On nodal cells, cilia generate the extracellular fluid flow (so called “nodal flow”) during embryo development, which is important for the left-right patterning and is achieved by a clockwise rotation that induces leftward flow. Disruption of this flow causes randomization of the organ situs. How the asymmetric patterning is initiated by the nodal flow is still under discussion. Two hypotheses exist suggesting either the involvement of ion channels on neighbored primary cilia, which would sense and proceed the leftward flow into the cell defining the cell fate¹⁴⁷ or the gradient of extracellular morphogens, which would be transported to the left side of the embryo and induce laterality signal transduction cascades¹⁴⁸. In adult tissues, the predominant role of motile cilia is to remove particles, as in the respiratory tract, or mobilize cells, as in the reproductive systems and in highly specialized structures of the brain^{149,150}. Recently, motile cilia were found in the middle ear epithelium as well, but their function has not been discovered yet¹⁵¹. Moreover, there has been some evidence that motile cilia can also exhibit sensory functions¹⁵².

Opposite thereto, nearly all embryonic and adult tissues, including stem cells and cardiac tissue, have sensory primary cilia. Each cell harbours only one primary cilium. During development and cell growth, this type of cilia represents an indispensable signalling centre not only by sensing extracellular chemical and mechanical changes through several receptors and channels expressed on the ciliary surface, but also by integrating key signalling transduction components. Among them are Platelet-derived growth factor (PDGF), SHH, TGF β and Ca²⁺ signalling pathways, which are temporally coordinated dependent on the cell type¹⁴⁴. Mutations in cilia-related genes therefore result in several congenital malformations. In adult tissues, primary cilia are still necessary for cell cycle control or maintenance of the differentiated state. However, disruption of ciliary signal-

ling in adult tissues does not lead to such dramatic phenotypes seen in the embryo¹⁵³. Often, though, it leads to uncontrolled cell division and the development of cancer^{154–161}.

Ciliogenesis and cell cycle

Especially during ciliogenesis, the process during which the cilium is built, numerous molecules need to be transported towards the membrane. This process is tightly coupled to the cell cycle. Cilia assembly is started in the G_1 phase of the cell cycle; the cilium is maintained during the G_1 and a quiescent G_0 phases; just before cell division, the structure is disassembled and the mother centriole is moved towards the cell centre to enable cytokinesis^{162,163} (Fig. 7).

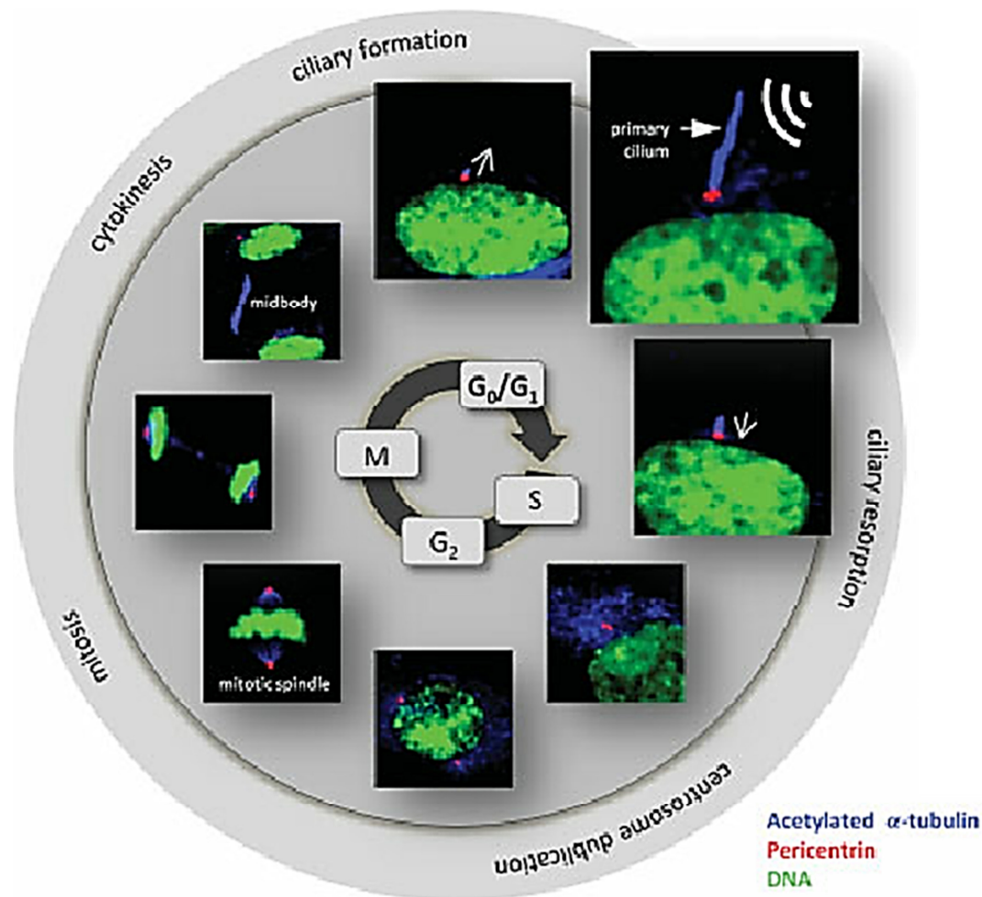


Figure 7: Ciliogenesis and cell cycle. Cilia formation and centriole location throughout the different phases of the cell cycle. Source: Christensen, 2012.

The inverse relationship between cilium and cell cytogenesis has been further underlined by the discovery of Aurora A, a mitotic kinase located close to the centrosomes and the mitotic spindle, which negatively regulates ciliogenesis in dividing cells by me-

diating centrosome maturation and cell cycle re-entry from G_0 to G_1 phase¹⁶⁴. The expression of another protein, Nuclear distribution protein nude homolog 1 (NDE1), that is located at the mother centriole and interacts with ciliary dyneins, is reversely correlated with cilia formation and its depletion leads to elongated cilia along with a delay in G_1 to S phase transition¹⁶⁵. Similar interactions are seen for the dynein protein T-complex testis-specific protein 1 (TCTEX1), whereby its phosphorylation not only accelerates the G_1 to S transition but also regulates cilia length, thereby determining if the cells remain in a proliferative state or start differentiating in neural progenitors during the development of the murine neocortex¹⁶⁶. Another interesting finding is that upon stimulation of the ciliary SHH pathway, transcription of several cell cycle genes such as cyclin D and E is activated¹⁶⁷. Recently, a novel molecular link between cilia disassembly and cell cycle progression was discovered. Hereby, cell cycle progression was induced by a growth factor-induced block of actin polymerization in the cilium¹⁶⁸.

Primary cilia in cardiac development and disease

Since primary cilia are not only coordinating the signal transduction of many pathways defining cell fate but are also highly synchronized with the cell cycle, they seem to balance proliferation and differentiation processes during morphogenesis of several tissues in a highly regulated spatiotemporal manner. A misbalance of proliferation and differentiation results in many congenital diseases affecting kidney, brain and heart development among others¹⁶⁹.

During cardiogenesis, both types of cilia are expressed in a distinct temporal window thereby influencing different aspects of heart formation. First steps in cardiac development are regulated by motile as well as primary cilia in the embryonic node, mainly establishing the left right-axis of the heart during gastrulation¹⁷⁰⁻¹⁷². Therefore, anomalies during this stage lead to abnormal looping as well as defects in the remodelling of the primitive heart tube into heart chambers¹⁷³. Moreover, abnormal nodal motile cilia may cause disturbed fluid flow, which is described as one theory of the onset of HLHS. Supportive data exist showing that fluid shear stress is required for maturation of the heart chambers and changes can cause CHD¹⁷⁴.

Later on, during specific periods of cardiac development so called cardiac primary cilia are found on these cells. They ensure correct differentiation, maturation and morphogenesis of the developing myocardium by stringently coordinating multiple signal

transduction networks¹⁷⁵. Signalling of the SHH pathway for instance is active in primary cilia of the mouse embryonic heart as well as in cardiomyocytes derived from stem cells *in vitro*. Additionally, a link between ciliary proteins and ventricle septation could be shown^{176–178}. Consequently, patients carrying genetic variants in signalling components of the SHH pathway frequently suffer from CHD¹⁷⁹. Another pathway essential for proper cilia function and, simultaneously, for correct heart formation is TGF β . Disruption of TGF β receptor signalling leads to cardiac malformations as well as heterotaxia. TGF β receptors are located in vesicles or early endosomes and associated to the cilium through activation of SMAD2/3 that is situated in the ciliary pocket where, upon activation, they co-localize and accumulate at the base of the cilium. Moreover, TGF β receptor ligands are able to induce cardiac differentiation^{180–182}. Finally, PDGF receptor α (PDGFR α) is specifically found on ciliary membranes as well in several tissues including the heart¹⁸³. Already in mouse embryonic heart ventricles PDGFR α is co-localized with sensory cilia, suggesting a role of the signalling cascade in cardiogenesis. Alterations of this pathway *in vitro* lead to disrupted differentiation of cardiac structures, while mice lacking PDGFR α show severe heart malformations and die prenatally^{184,185}. Other important cardiac developmental pathways such as WNT and NOTCH have been controversially discussed concerning their role in ciliary signalling. Even though components of these signalling cascades are localized in ciliary membranes and interruption leads to defective ciliogenesis, knocking out crucial parts of the primary cilia does not lead to altered WNT signalling in mouse embryos for instance^{186–188}.

Besides the cilia-mediated signalling networks, also ciliogenesis itself is essential for cardiogenesis. If cilia are not formed appropriately and therefore the IFT is defective, the cardiac differentiation and morphogenesis is interrupted. Consequently, mutations in ciliary structural genes result in cardiac malformations¹⁸⁹. *In vitro* studies in mouse embryonic stem cells (mESCs) demonstrated the importance of ciliary structural components in cardiomyocyte differentiation by the observation of a differentiation block upon knockdown of IFT-related genes¹⁷⁶. Another process important to guarantee proper cilia function and thus flawless cardiogenesis is vesicular transport, which is required for the shuttle of proteins towards and away from cilium. Interruption of ciliary-related endo- and exocytosis is associated with CHD as well¹⁹⁰. Supporting this postulated crucial role of cilia in proper cardiogenesis, Li *et al.* found a high number of cilia-related genes in-

volved in the onset of CHD in mice performing a global genetic mutagenesis analysis¹⁹¹.

1.2.4. Regulation of cardiogenesis by autophagy

However, congenital heart disorders are diverse and thus the question remains of how cilia malfunctioning lead to different types of cardiac malformations and why exclusively particular cardiac cell types are affected, representing a key element of this thesis. Interestingly, recent publications suggest a direct interplay of cilia and cell cycle with autophagy. This process has been described to play a role in cell type specific progression of differentiation and is highly regulated in a spatiotemporal manner¹⁹².

The process of autophagy

At the latest when the Nobel Prize in Medicine in 2016 was announced for the scientists who discovered the process of “autophagy” (Greek: “self-eating”) and its role in diseases, this hitherto rather understudied process became more popular and many researchers started to investigate its role in several processes under healthy and diseased conditions. Until today, autophagy could be shown to be involved in several steps of embryonic development along with its role in the homeostasis of many adult tissues, but most of its functions are most likely not even discovered yet.

Autophagy displays a conserved process that is required in most cells at basal levels to remove damaged proteins and organelles from the cells, thereby assuring their homeostasis. Moreover, it is required for the clearance and recycling of the protein set of a cell in response to cellular fate changes or stress. Disturbed autophagy would therefore lead to accumulation of unwanted or unused proteins as well as cellular differentiation or homeostasis defects¹⁹³. It can be distinguished into selective and non-selective autophagy as well as micro- and macroautophagy. Microautophagy is understood as direct lysosomal enclosure of cytoplasmic cargo, while macroautophagy includes a step in which autophagosomes are formed around target molecules and subsequently fuse with lysosomes for degradation. Macroautophagy is the main process and in focus of this thesis and hereafter referred to as “autophagy“.

Autophagy is induced by intracellular stress, such as ER stress, by extracellular stress, including pathogen infections, hypoxia, and oxidative stress, or by depletion of growth

factors causing starvation that is combated through macromolecule retrieval *via* autophagy¹⁹⁴. In mammalian cells, the ER stress response that mediates autophagy induction is mainly translated by unfolded protein response (UPR) signalling, including inositol-requiring enzyme 1 (IRE1), Activating transcription factor 6 (ATF6) and Protein Kinase RNA-like ER Kinase (PERK) that activate transcription of target genes and simultaneously process the autophagy protein Microtubule-associated protein 1A/1B-light chain 3 (LC3)^{195–197}. Moreover, increased Ca^{2+} release upon ER stress results in the activation of AMP-activated protein kinase (AMPK) that can also be associated to autophagy induction¹⁹⁸. Hypoxia-induced autophagy is mainly mediated by the Hypoxia-inducible factor 1 (HIF1) pathway along with the AMPK- mechanistic Target of Rapamycin (mTOR) signalling¹⁹⁹. The link between oxidative stress in form of ROS formation and autophagy stimulation might be activation of the liver kinase B1 (LKB1)-AMPK signalling cascade by Reactive oxygen species (ROS)-activated Poly(ADP-ribose)-Polymerase 1 (PARP-1)²⁰⁰. The nutrient status is sensed by the two signalling cascades TOR and RAS/PKA^{201,202}. In contrast to this stress-induced activation, autophagy up-regulation after pathogen invasion is mainly mediated by specific toll-like receptors (TLRs)²⁰³ (Fig. 8).

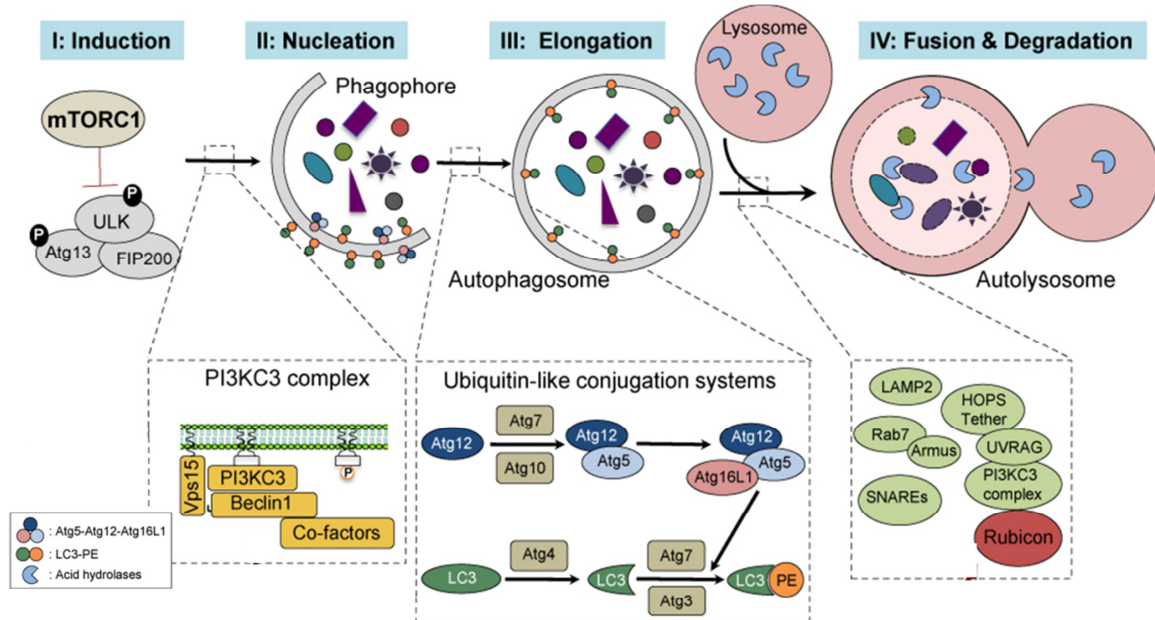


Figure 8: Autophagy process: Autophagosome formation and the involved signalling pathways leading to autophagy induction and progression. Source: Yang, 2015.

Upon autophagy initiation, double-membrane phagophores are formed, eventually out of the ER, Golgi apparatus or endosomes^{204,205} following polymerization of autophagy-

related (ATG) proteins. In the next step, the maturation of these phagophores to autophagosomes is mediated through the processing of cytosolic LC3-I to LC3-II by conjugation of phosphatidylethanolamine and subsequent insertion in the phagophoric membrane. Then, either a bulk of random protein or ubiquitinated target proteins, captured by adaptor proteins that are recruited to LC3^{206,207}, such as ATGs^{208,209} or nucleoporin p62 (also known as sequestosome-1 (SQSMT1)), are enclosed in the autophagosome (Fig. 8). In the final step, the autophagosome fuses with the lysosome to consequently degrade the proteins through lysosomal enzymes²¹⁰ (Fig. 8).

Hence, ATG proteins represent the core machinery of autophagy and different sets of ATG proteins are involved in every aforementioned step. Besides this protein set, other important proteins families are crucial during the autophagic process. These include parts of the secretory and endocytic network as well as cytoskeleton components, mostly microtubules, which mediate the processes of autophagosome transport, fusion and autophagic clearance among others. Transport of autophagosomes as well as the clearance of protein aggregates is mainly regulated by microtubules and their motor protein dynein^{211–213}, the main part of the ciliary transport system as mentioned above. Additionally, autophagosome-lysosome fusion requires small GTPases such as RAB proteins, also involved in the ciliary vesicular transport²¹⁴. Interestingly, the main autophagy induction pathway, mTOR signalling, could further be activated by fluid flow-induced ciliary Ca²⁺ signalling after bending of the primary cilia. This leads to AMPK activation by LKB1 that is located at the basal body of the cilium, thereby regulating cell size and cellular homeostasis among others²¹⁵.

Autophagy and its interplay with cilia

The overlapping components of autophagy and cilia suggest a tight connection of those two regulatory units. Indeed, the base of the cilium represents the predominant site for autophagosome formation, induced by ciliary SHH signalling^{216,217} and subsequent recruitment of ATG proteins. In turn, cilia formation is controlled through autophagy by processing certain proteins necessary for ciliogenesis^{218–220}. Moreover, ciliogenesis as well as autophagy are both induced by nutrient deprivation; environmental changes are sensed by cilia and lead to autophagy activation, following cilia length modulation for instance. These processes are mainly mediated by SHH and mTOR signalling. The reciprocal interplay between ciliogenesis and autophagy is very complex and not fully

understood yet (Fig. 9). A good example for this complicated interaction is illustrated by the degradation of the ciliary proteins IFT20 and OFD1 during autophagy, which in turn affects cilia length depending on environmental changes. Interestingly, while the degradation of IFT20 appears during basal autophagy and favours cilia disassembly, OFD1 degradation occurs early during serum starvation and leads to increased cilia assembly, since this protein is a negative regulator of cilia formation. However, later during serum starvation, IFT20 is degraded again leading to subsequent disassembly of the cilium. This emphasizes the important role of this close interaction of primary cilia and autophagy for cellular homeostasis^{220,221}.

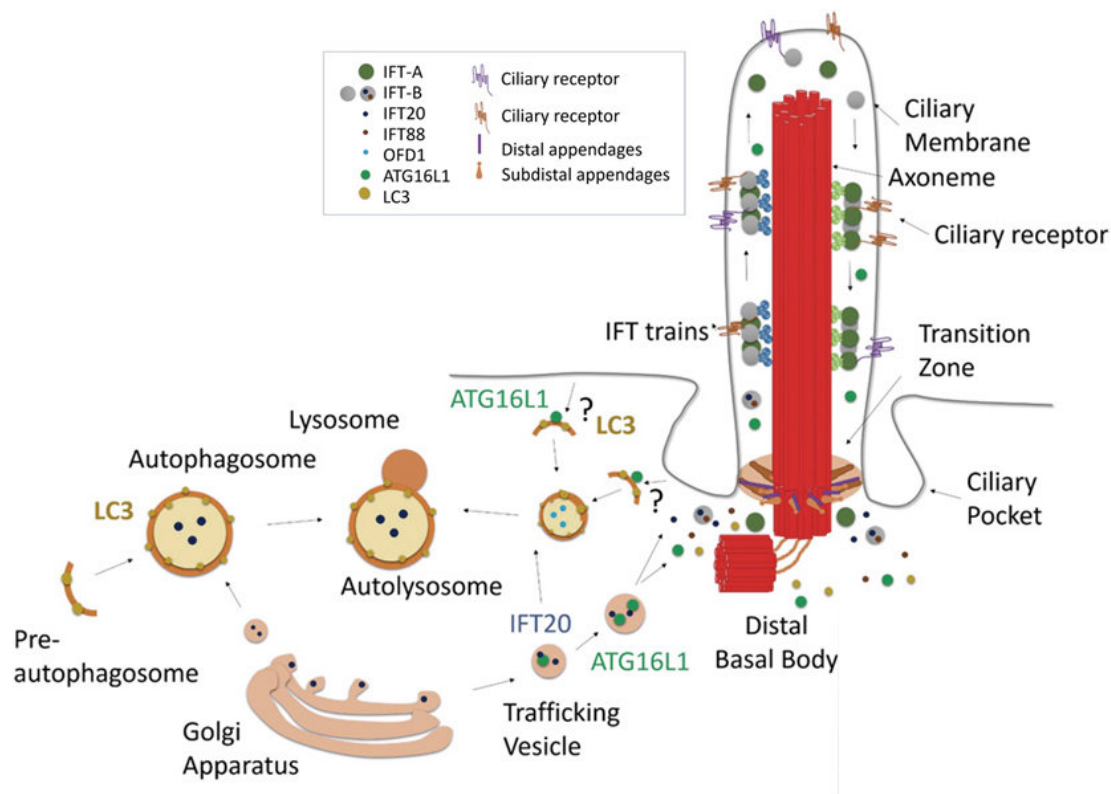


Figure 9: Interaction between autophagy and cilia. Influence of ciliary proteins on several processes in the cell including autophagy. Source: Pampliega, 2016.

Autophagy and the cell cycle

Finally, there is accumulating evidence of a correlation between autophagy and cell cycle regulation, especially since the cell cycle entry depends strictly on the presence of nutrients and mitogens and is strongly affected by stress. Autophagy is mainly active during the G₁ and S phase of the cell cycle; though, it can be detected during all phases to a certain extent, speaking against a cell-cycle dependent induction of autophagy^{222,223}. Due to its function in cellular homeostasis, autophagy activity in the interphase of the

cell cycle helps to remove unwanted or defective structures after cell division. Moreover, it prevents the accumulation of midbodies in the cell after division. Pluripotent and cancer cells exhibit lower autophagic activity, leading to an accumulation of midbodies that, in an unknown way, seem to maintain the undifferentiated state²²⁴. However, a significant autophagy reduction has been reported in the M phase of the cell cycle dependent on Cyclin-dependent kinase (CDK) 1 activity which is then reactivated in the G₁ phase, most likely to protect the cells from uncoordinated degradation of fragmented cellular components and chromosomes^{225,226}. Cell cycle arrest is correlated with stress-induced autophagy by CDK1 activity that is able to induce this process via LKB1–AMPK signalling. Additionally, p53, a tumour suppressor protein that rapidly reacts to cellular changes orchestrating appropriate cell cycle responses, has been connected to stress-induced autophagy regulation. While activated nuclear p53 stimulates autophagy through the activation of AMPK and the inhibition of mTOR, inactive cytosolic p53 inhibits autophagy^{227,228}. Inhibition of autophagy by mTOR activity can also favour complete senescence of cells²²⁹, but interestingly, counteracting senescence under stress-free conditions by autophagy upregulation might be a trigger for stem cell maintenance^{230,231}.

Autophagy in (cardiac) development and disease

Due to its strong interplay with the ciliary machinery and the cell cycle, it is not surprising that autophagy is also connected to embryonic development. Gene knockout studies of autophagy-related proteins in mice show embryonic lethality²³², interestingly again in a spatiotemporal manner, since the silencing of different genes lead to lethality at different stages of development. This highlights the importance of autophagy during several distinct developmental steps, starting already at the 2-cell stage, in supplying the embryo with nutrients and removing maternal proteins²³³. At neonatal stages, autophagy is required under nutrient supply stress before breastfeeding²³⁴. Most likely, various different cell types and tissues involve autophagic steps in their individual specification, since reasons for embryonic lethality upon autophagy manipulation are mainly anomalies in distinct embryonic tissue formation, apoptotic events and differentiation defects^{235–238}. Jang and colleagues recently demonstrated that autophagy controls very early embryonic germ layer decisions between neuroectodermal and mesendodermal fate. This study shows an intriguing link between autophagy, cilia and cell cycle, postu-

lating that this fate decision is regulated by the so called “Primary Cilium-Autophagy-Nrf2” (PAN) axis. Hereby, the authors could show that specification of embryonic stem cells towards neuroectoderm is dependent on a prolonged G₁ phase leading to increased ciliation. This enrichment of ciliated cells results in increased autophagy and expressional changes in contrast to the simultaneously arising mesendoderm that did not show these modifications at this stage¹⁹².

So far, most studies indicating a role of autophagy in embryogenesis have focused on neuronal development and haematopoiesis. However, by knocking out FAK family kinase-interacting protein of 200 kDa (FIP200) in mice, autophagosome formation is interrupted and embryos die at E13.5-E16.5 exhibiting heart and liver defects. FIP200 is an interaction partner of the mammalian ATG1-analogue UNC-51-Like Kinase-1 (ULK1) that is involved in proliferation, apoptosis and migration among others²³⁹. Moreover, in zebrafish that constitutively express GFP-LC3 as an autophagy marker, autophagy could be detected during embryonic development in several tissues including the myocardium. Morpholino knockdown of autophagy genes lead to higher lethality in general along with structural heart defects affecting looping, chamber and valve formation as well as altered cardiac gene expression and increased cell death²⁴⁰. Interestingly, FGF signalling could be strongly connected to autophagy in terms of cardiac development. Here, autophagy is blocked by FGF receptor activity leading to a differentiation stop in cardiac progenitors, thereby regulating the differentiation velocity²⁴¹. FGF receptor signalling has been shown to be important for proliferation, differentiation and migration by inhibiting autophagy in several other cell types as well, resulting in differentiation progression or suppression, respectively. In P19CL6 cells, autophagic activity could be detected during differentiation into cardiomyocytes and upon autophagy blockage, cardiogenesis is inhibited by activated NOTCH and WNT signalling²⁴². In general, for WNT signalling, two different autophagy regulations were discovered. On the one hand, WNT inhibitors could activate autophagy by mTOR-dependent mechanisms but on the other hand, WNT signalling was reduced by autophagy postulating a feedback mechanism²⁴³.

Additional pathways essential for proper embryogenesis such as SHH and TGF β signalling are regulated by autophagy as well, while here the connection to cardiogenesis is still under investigation. The function of the SHH pathway in autophagy regulation seems to be cell-type depended. For instance, SHH signalling inhibits autophagosome

formation under specific conditions in neuronal stem cells, while it activates autophagy in hippocampal neurons, illustrating different functions of SHH during neuronal development²⁴⁴. TGF β signalling induces autophagy in many carcinoma cell lines and leads to an upregulation of autophagy genes, thereby mediating cell cycle arrest and growth inhibition^{245,246}. These controversial findings again suggest a feedback loop and spatio-temporal regulation within specific developmental stages^{241,247}.

1.3. Congenital heart disease modelling

To understand the cause of cardiac malformations as well as the impact of single gene variants, suitable *in vivo* and *in vitro* systems are required to study the role of the beforehand described pathways and mechanisms in the disease pathology.

1.3.1. *In vivo* cardiac disease modelling

The generation and analysis of various animal models have revealed crucial steps and signalling pathways during cardiogenesis, which can now help to identify affected cellular signalling components and structures in CHD. Additionally, potentially causative genes discovered through genetic studies of large cohorts of patients born with cardiac malformations can be verified by generating knockout models. Due to a high conservation of cardiac organization, cardiovascular development as well as physiological features of the heart between mice and humans, these animals represent a suitable model system for investigating CHD.

Nowadays, several knockout mouse models exhibiting a CHD phenotype have been established, including tissue- and time-specific knockouts. With advanced technologies such as Clustered Regularly Interspaced Short Palindromic Repeats (CRISPR/Cas) genome editing, even specific mutations can be introduced to the genome to evaluate the impact of specific variants in cardiovascular malformations. Cardiac malformations caused by monogenic variants, mostly as part of syndromic cases, have been modelled by complete as well as tissue-specific knockouts. An example is the DiGeorge syndrome, where a complete knockout mouse of a discovered candidate gene, *TBX1*, was generated. The phenotype of *Tbx1* null mice shows a defective aortic arch and a persistent truncus arteriosus (PTA), resembling the phenotype described in patients^{248–250}.

Tissues-specific knockout of *Tbx1* revealed the requirement of TBX1 in SHF cells for the formation of the pharyngeal arch and the OFT²⁵¹. Other syndromes exhibiting congenital heart defects and being modelled in mice include Noonan syndrome and Marfan syndrome. The Noonan syndrome displays several cardiac malformations, with genetic variants in the *protein tyrosine phosphatase nonreceptor type 11 (PTNP11)* gene encoding Src homology-2 domain containing protein (SHP2) being the most prevalent cause. Expression studies of the mutant protein in mice could recapitulate the clinical phenotype, exhibiting valve and septal defects²⁵². Marfan syndrome, however, is characterized by a haploinsufficiency of the *Fibrillin-1 (FBNI)* gene, leading to altered TGF β signalling and disorganized microfibrillar structures^{253–255}. Knocking out this gene in mice results in a similar phenotype, though with different severities that could be rescued by overexpression of the wildtype allele²⁵⁶ as well as by the administration of an angiotensin II receptor blocker. The drug is now tested in clinical studies as a potential treatment for Marfan syndrome^{257,258}, highlighting the importance of mice models for identification of new drug targets. Further possibilities for investigating cardiac congenital malformations are conditional mutagenesis in mice or ablation of specific cardiac precursor populations that also lead to heart defects, such as SHF-mediated heart tube abnormalities or cardiac septation defects resembling Tetralogy of Fallot (TOF) or DORV¹⁰⁴.

Researchers also tried to model complex congenital cardiac diseases such as HLHS by generating knockout mice or manipulating mechanisms thought to be influential for the onset of the disease. Although some of the structural anomalies of the disease could be recapitulated, the complete clinical picture of HLHS could not be displayed in these model systems yet. Interruption of the blood flow in mice embryos, aimed at mimicking the “flow theory”, only led to a defective formation of the branchial arch²⁵⁹. Genetic approaches of knocking out *NOTCH1* to imitate complex congenital heart defects also led to an incomplete picture in which the mice show a ventricular septal defect, abnormalities in the patterning of the aortic arch as well as pulmonary artery stenosis, however solely in specific genetic backgrounds²⁶⁰. This speaks for a genetic component in the “flow theory”. Hereby, specific mutations directly or indirectly lead to decreased blood flow in the developing left ventricle causing malformations^{261,262}.

1.3.2. *In vitro* cardiac disease modelling using hiPSCs

Nevertheless, to model complex CHD, in which more than one gene is involved, other systems might be more useful or new techniques are required, which enable efficient mutation introductions in several candidate genes in parallel. Another restriction of the usage of animal models to recapitulate cardiogenesis and congenital heart defects is that specific steps in heart development differ fundamentally between species²⁶³ plus very early steps of cardiac progenitor formation and specification are difficult to study in living animals. The access to human cardiac material is very limited and it is nearly impossible to examine human cardiac development *in vivo*. An alternative is represented by human embryonic stem cells, differentiated *in vitro* towards cardiomyocytes. However, major hurdles such as limited access and strict ethical restrictions have hampered a widespread use of hESCs. A decade ago, researchers managed to reprogram terminally differentiated human tissue-specific cells back to pluripotent stem cell like cells^{264,265}. These so called “human induced pluripotent stem cells (hiPSCs)” raised a completely new alternative to hESCs, hiPSCs can be differentiated towards myocytes *via* cardiac progenitors and cardiogenesis and heart defects can be studied *in vitro*. Moreover, patient-specific hiPSCs possess the whole genetic background of the patient, thus being more suitable for modelling complex diseases.

1.3.2.1. Reprogramming of somatic cells to hiPSCs and cardiac differentiation

The successful generation of hiPSCs by the research group led by Yamanaka in 2007 marked a milestone in the field of regenerative medicine and completely changed the way to look at the development of human disease. In his pioneering work, Yamanaka was able to reprogram mouse somatic cells towards pluripotent stem cell-like cells by overexpressing four transcription factors important for the maintenance of a pluripotent state, namely Octamer-binding transcription factor 4 (OCT4), Sex determining region Y box 2 (SOX2), Kruppel-like factor 4 (KLF4) and myelocytomatosis viral oncogene homolog (c-MYC). The obtained iPSCs shared similar characteristics with ESCs regarding self-renewal capacity, pluripotency and the ability to form all three germ layers both *in vivo* by teratoma formation after transplantation in immune deficient mice as well as *in vitro* by spontaneous embryonic body (EB) formation²⁶⁶. Shortly afterwards, Yamanaka and others succeeded to reprogram human adult fibroblasts, creating a highly

valuable new option to approach human disease modelling^{264,265}. To date, a wide spectrum of somatic cells could be reprogrammed with this technology including keratinocytes²⁶⁷, astrocytes²⁶⁸ peripheral blood mononuclear cells (PBMCs)^{269,270} or T-lymphocytes²⁷¹ among others.

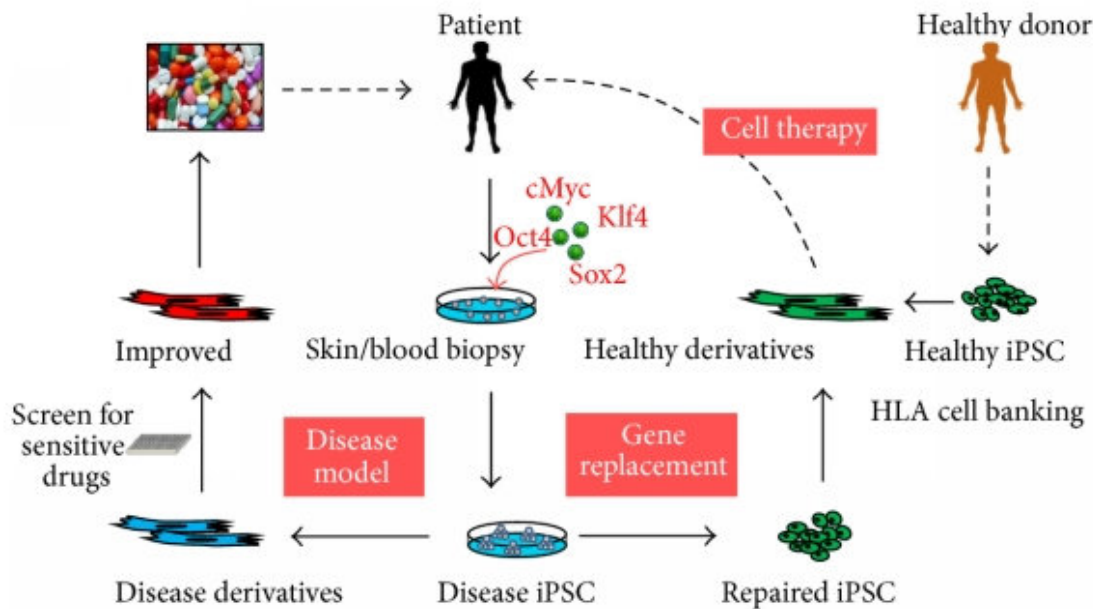


Figure 10: Application fields for hiPSCs. Research application of hiPSCs in disease modelling as well as in clinical interventions concerning cell therapy including gene replacement strategies. Source: Wang, 2014.

Initially, retroviruses carrying the reprogramming factors were used, causing irreversible integrations of the sequences into the targeted genome. In terms of future clinical applications in cell therapy, random genomic integrations are unfavourable, since they might cause altered gene expression of important genes or activation of pro-oncogenes. Therefore, latest approaches aimed to achieve non-integrative delivery of the factors using adenoviruses²⁷² or Ribonucleic acid (RNA) viruses such as Sendai virus²⁷³ that can replicate in the host cell without entering the nucleus. Moreover, other delivery methods including non-viral vectors²⁷⁴ or direct delivery of proteins²⁷⁵, mRNA^{276,277}, microRNA (miRNA)^{278,279} or the addition of small molecules^{280,281} by transfection have been successfully applied. These cells can be subsequently used for disease modelling, tissue replacement therapies as well as toxicology and drug screening (Fig. 10).

For the purpose of disease modelling, material from patients with different disorders can be reprogrammed gaining patient-specific hiPSCs, which provide the opportunity to study the role of specific mutations in the onset of disorders as well as testing specific

drugs on patient-specific tissues such as cardiomyocytes. Another therapeutic approach, as a consequence of the identification of causative mutations, would be genetic correction of this mutation and subsequent application of the corrected cells back to the patient to combat the disease²⁸².

In the recent years, numerous protocols have been published to differentiate hiPSCs towards many types of tissues including cardiomyocytes and neural cells. This possibility opened an entirely new chapter not only in investigating developmental disorders, but also in the field of personalized medicine.

1.3.2.2. Cardiac differentiation protocols

Until now, multiple disorders have been studied using patient specific hiPSCs carrying disease-causing mutations, including many cardiac disorders²⁸³. Several protocols have been successfully published to efficiently generate cardiovascular progenitors, cardiomyocytes as well as more specific cardiac subtypes including atrial²⁸⁴ nodal²⁸⁵ and epicardial cells²⁸⁶. One common technique to generate cardiomyocytes is spontaneous differentiation of hiPSCs resulting in the formation of EBs, adapted from protocols developed for hESCs. Hereby, cells are cultured in suspension and under high serum conditions (20%), but the efficiency of cardiomyocyte formation is very low with maximum 10%²⁸⁷. Further adaptations of the original protocol in order to reach a higher efficiency include the supply of additional growth factors such as BMP4, basic FGF (bFGF), ACTIVIN A, VEGF, dickkopf-related protein 1 (DKK1), stem cell factor (SCF) or WNT3a by applying different types of media like StemPro®-34 or STEMdiff™ APEL™ medium to the cells for enhanced proliferation of cardiac progenitors^{288–294} or insulin growth factors (IGF) for enhanced cardiomyocyte proliferation²⁹⁵. Moreover, controlling the size of the EBs leads to an increased efficiency. This can be reached by the so called spin EB method, where the cells are centrifuged to control the aggregate size, adapted from hESC differentiation²⁹⁶. Culturing of hiPSCs on microwells with a defined size²⁹⁷ as well as micropatterned matrices²⁹⁸ helps also to regulate the size of the forming EBs. Another possibility is co-culture with mouse-endodermal-like cells (END-2), in serum-deprived and ascorbic acid supplemented medium, developed in hESC culture^{299,300}, or END-2 conditioned medium³⁰¹.

However nowadays, most established cardiac differentiation protocols are directed, signified by the defined addition of small molecules or factors, and hiPSCs are often cultured in monolayers on matrices such as Matrigel®. Those supplemented factors, includ-

ing ACTIVIN A, BMP4, WNT3a and bFGF, could improve the differentiation efficiency up to 30%^{302,303}. Additionally, cells can also be cultured with the matrix sandwich differentiation method where a monolayer of hiPSCs plated on Matrigel[®] is subsequently covered by the same matrix³⁰⁴. An improvement of the efficiency was yielded by small molecule activation and the sequential manipulation of the canonical WNT pathway³⁰⁵. Hereby, WNT signalling is initially activated by CHIR99021, a GSK3 β inhibitor, to induce mesoderm formation, followed by WNT inhibition by IWR1 or related substances to direct the differentiation towards the myocytic lineage³⁰⁵⁻³⁰⁷. A drawback of this method, manipulating important developmental signalling pathways for the generation of functional myocytes, might be that these factors could interfere with studying the disease.

Since these efficient cardiac differentiation protocols show increased cell death due to strong selection in the initial phases in favour to achieve highly pure cardiomyocyte populations, early cardiac progenitor stages are nearly impossible to analyse. Therefore, researchers have developed more defined protocols to specifically generate cardiovascular precursors. A promising protocol published is developed by Cao *et al.*, with which they achieved homogeneous populations exhibiting cardiac progenitor characteristics by applying BMP4, ascorbic acid and CHIR99021 to hiPSCs³⁰⁸. More recently, Birket *et al.* developed a protocol that generates cardiovascular progenitors from hiPSCs by the addition of the IGF-1 and SMO agonist (SAG)³⁰⁹.

1.3.2.3. Cardiac disease modelling using patient-specific hiPSCs

Applying those protocols on beforehand generated patient-specific hiPSCs, research groups could investigate molecular mechanisms of cardiac diseases. In the beginning, research has been primarily focused on monogenic diseases with clearly distinguished phenotypes. Monogenic disorders of two classes of cardiac diseases, namely arrhythmias and cardiomyopathies, have been successfully modelled using patient-specific hiPSCs, whereby arrhythmias represent diseases that are tendentially more easily to display in the iPSC system since they illustrate channelopathies with clear electrophysiological readouts.

Monogenic cardiac disorders: Arrhythmias

The first monogenic cardiac disease modelled with patient-specific hiPSCs was the Long-QT syndrome (LQTS)³¹⁰. The LQTS exhibits prolongation or delay of the QT

interval on an electrocardiogram (ECG) illustrating the repolarization of the ventricles and often results in polymorphic ventricular tachycardia, syncope and sudden cardiac death at an early age. Genetic analysis of numerous patients revealed more than 500 mutations in 13 genes being causative for the disease. Those genes encode cardiac ion channels with the most prevalent mutations in potassium channels. There are three main types of LQTS described, LQT1 with mutations in the *Potassium voltage-gated channel (KCN) Q1* gene, LQT2 with variants in the *KCNH2* gene, and LQT3 carrying mutations in the *sodium voltage-gated channel alpha subunit 5 (SCN5A)* gene^{311–313}.

The first LQT iPSC-based model was generated for LQT1: patient-specific hiPSCs of two patients carrying a dominant missense mutation in *KCNQ1* were differentiated into cardiomyocytes and characteristic phenotypes, such as prolonged action potential duration and an impaired function of *KCNQ1* channels, along with increased arrhythmic response to catecholamine, could be detected³¹⁴. Shortly after, LQT2 was modelled with similar success. LQT2 hiPSC-derived cardiomyocytes exhibit prolonged QT intervals, as measured by classical patch clamp methods or extracellular field potential measurements^{315–320}. In this disease model, a rescue of the LQT2 phenotype could also be reached by genetic correction of the *KCNH2* mutation. Thus, for the first time, a single mutation could be successfully assigned to the disease in a human disease model³¹⁹. LQT3 syndrome is characterized by a gain of function mutation in a sodium channel encoding gene resulting in increased sodium flux in the depolarisation phase and consequently in prolonged action potential duration (APD)^{321,322}. Comparing the electrophysiological properties of the LQT3 hiPSC-derived cardiomyocytes those of healthy related controls, increased sodium channel activity and prolonged APDs could be measured in diseased cardiomyocytes. Moreover, the effect of pharmacological substances modulating specific ion channel functions was evaluated on the individual patient myocytes, indicating the potential of patient-specific hiPSCs as a new tool for patient-specific drug screening^{321,323}.

Another arrhythmia that was modelled in the hiPSC system is catecholaminergic polymorphic ventricular tachycardia (CPVT), a disease that leads to the development of stress-induced ventricular tachyarrhythmia and syncope, which can result in sudden cardiac death in young patients. Two types of CPVTs have been described; CPVT1, which is autosomal dominant inherited and characterized by causative mutations in the *cardiac ryanodine receptor 2 (RYR2)* gene, a calcium channel on the sarcoplasmic re-

ticulum (SR)³²⁴; and CPVT2, which is autosomal recessive and linked to mutations in *calsequestrin 2* (*CASQ2*), a calcium binding protein inside the SR^{325,326}. Hence, alterations in calcium are the molecular cause of this severe phenotype. CPVT1 patient iPSC-derived cardiomyocytes showed abnormal calcium signalling. Moreover, induction of stress by stimulating adrenergic receptors lead to arrhythmias and altered impulse formations, whereby either early afterdepolarizations (EADs) or late afterdepolarizations (DADs) were detected in respect to the individual genetic background of the patients. Interestingly, electron microscopic analysis of patient iPSC-derived cardiomyocytes revealed ultrastructural differences of the SR along with an immature phenotype³²⁷. The calcium flux irregularities could be restored by treatment with substances that prevent the release of calcium from the SR³²⁸ or by antiarrhythmic medications^{329,330}.

Monogenic cardiac disorders: Cardiomyopathies

The second group of monogenic cardiac diseases that was studied using patient-specific hiPSCs are cardiomyopathies, representing a more complex class to display in the iPSC system compared to channelopathies, since the phenotypic readout is more difficult to obtain.

Familial hypertrophic cardiomyopathy (HCM), characterized by highly hypertrophic left myocardium that increases the risk of cardiac complications such as arrhythmias and heart failure with increasing age, is one example of a classical cardiomyopathy³³¹. Mutations in 11 genes that encode proteins of the cardiac sarcomere have already been described to be causative in this disease. Tissue samples of patients suffering from this disorder have been reprogrammed to investigate the role of *MYH7* variants in the onset of the disease. Myocytes generated from *MYH7*-mutated hiPSCs showed typical hypertrophic features, including cellular expansion and multinucleation as well as molecular phenotypes such as altered calcium signalling and defects in nuclear factor of activated T-cells (NFAT) translocation, Atrial natriuretic peptide (ANF) expression, calcineurin activation and dysregulated β - to α -myosin ratio³³². But until now, a link between molecular defects and the phenotypic manifestation is not completely uncovered.

A more complex cardiomyopathy that was in focus of hiPSC disease modelling in the recent years is dilated cardiomyopathy (DCM). The genetic contribution to this disease is 30-35% and genes affected encode cardiac structural proteins including *Lamin A/C* (*LMNA*), *Desmin* (*DES*), *cardiac Troponin* (*cTNT*) and *Titin* (*TTN*). Patient-specific

hiPSCs carrying mutations in these genes have been generated^{333–337}, which exhibit several molecular and structural defects resembling the disease phenotype. Due to the high number of causing genes with different functions, a complete picture of the disease could not be created yet. An advanced approach to cure DCM by performing antisense-mediated skipping of the *TTN* diseased exon on iPSC-derived myocytes was also tested³³⁶.

Finally, arrhythmogenic right ventricular cardiomyopathy (ARVC), an arrhythmic disorder characterized by fibrofatty replacement of cardiomyocytes, has been also studied using patient-specific hiPSCs. This autosomal dominant disorder is predominantly caused by mutations the *plakophilin-2 (PKP2)* gene, encoding a structural part of the cardiac desmosome. In patient iPSC-derived myocytes, reduced expression of PKP2 and its interaction partner plakoglobin could be observed, in conjunction with impaired nuclear translocation of plakoglobin and reduced WNT signalling. Moreover, the structure of the myocytes appears to be less organized, desmosomes show an abnormal shape and fat droplets were accumulated^{338,339}. Peroxisome proliferator-activated receptor- γ (PPAR- γ) activity seems to be involved in the onset of the disease and PPAR- γ inhibitors could prevent the reinforced lipogenesis³⁴⁰. However, so far no research group has been able to uncover the molecular mechanisms leading to the clinical phenotype, emphasizing the difficulties of modelling more complex diseases.

Complex cardiac disorders

Even more challenging is the modelling of complex multigenic diseases including CHDs. The phenotypic readouts are diverse and blurred. Moreover, due to complex interplays between several possible disease-causing genetic variants carried by the patient as well as additional risk factors influencing the outcome of the disease, it is difficult to discover targets for future therapies.

Few research groups tried to understand the origin of complex CHDs such as TOF and HLHS by generating patient-specific hiPSCs. First approaches to model HLHS revealed mainly transcriptional differences of cardiomyocytes when compared to unrelated healthy controls. Especially, expression of crucial developmental genes such as NOTCH1 pathway components^{341–344}, as well as early cardiac markers including MESP1, NKX2.5, TBX2, HAND1/2 and GATA4 was dysregulated or delayed. Interestingly, Bohlmeier *et al.* could show persisting expression of embryonic genes, such as

atrial myosin light chain 2 (MLC2a), indicative of a premature state of HLHS cardiomyocytes^{342,345}. Another finding that is consistent among those studies was an impaired formation of cardiomyocytes and decreased expression of specific cardiac marker genes such as cTNT, while other cardiac marker genes were significantly upregulated together with rather disorganized myofilaments and shifted contributions to the emerging atrial and ventricular lineages^{341,342}. Tomita-Mitchell *et al.* observed an increased MYH7/MYH6 ratio along with an abnormal expression of contractility genes³⁴⁶. In mice there is a change of MYH expression from MYH7 to MYH6 during cardiogenesis, thus, this results could illustrate an interrupted maturation of HLHS myocytes³⁴⁷. In contrast, Jiang *et al.* discovered an upregulation of MYH6 levels and a decreased expression of MYH7 in diseased HLHS hiPSC-derived myocytes and interpreted this result as predominant atria vs ventricular formation³⁴². Hrstka *et al.* succeeded to rescue the reduced myocyte formation in counteracting the dysregulated NOTCH1 expression with nitric oxide (NO), known to be required for efficient NOTCH signalling, thus suggesting a pathway that could be targeted in HLHS therapy. Their work strengthened the role of NOTCH signalling in the onset of HLHS and claim that this pathway is important in fate decisions during cardiogenesis³⁴⁴. Another possibly affected mechanism described is intracellular calcium release that seems to take place not only through the RYR receptor but also through alternative routes such as inositol trisphosphate (IP₃) receptors³⁴².

All the transcriptional abnormalities described so far in HLHS hiPSC-models give a good first insight on the disease mechanism but do not unequivocally explain the dramatic misguided development seen in the heart of HLHS patients. An extended analysis of crucial developmental processes such as ciliogenesis and autophagy in early cardiogenesis in response or leading to those transcriptional differences might help enormously to explain the onset of this disorder. Moreover, these altered mechanisms might reflect the convergence of different mutations and environmental risk factors in this single superordinate resulting defect. The main focus of this PhD thesis was to use patient-specific hiPSCs to decipher the molecular and cellular principle underlying HLHS development.

2. Methods

2.1. Reprogramming of human fibroblasts to hiPSCs

Primary skin fibroblasts (PSF) of two unrelated patients born with hypoplastic left heart syndrome were reprogrammed into patient-specific hiPSCs. For this, the cells were infected with Sendai viruses (SeV) containing vectors that encode the transcription factors OCT4, SOX2, KLF4 and c-Myc (CytoTune™ iPS Sendai Reprogramming Kit, Thermo Fisher Scientific). For infection, an MOI of 3 of each CytoTune™ SeV was used. The medium containing SeV was replaced after 24 hours and the infected cells were subsequently cultured in fibroblast medium consisting of DMEM/F-12 (Invitrogen), 10% FBS (Invitrogen), 2 mM L-glutamine (Invitrogen), 100 µM MEM non-essential amino acids (NEAA) (Invitrogen) and 50 U/ml penicillin and 50 µg/ml streptomycin (Invitrogen) for 4 days before transferring them onto irradiated mouse embryonic fibroblasts after trypsinization. On this feeder layer, the cells were cultured in hESC medium (DMEM/F-12 supplemented with 20% knockout serum replacement (KSR, Invitrogen), 2 mM L-glutamine, 0.1 mM MEM NEAA, 0.1 mM β-mercaptoethanol, 50 U/ml penicillin, 50 µg/ml streptomycin and 10 ng/ml human b-FGF (R&D)) until colonies with typical morphological features of hiPSCs came up. These colonies were picked mechanically by cutting them into smaller pieces and further cultured on Geltrex™ reduced growth factor Basement Membrane Matrix-coated cell culture dishes (Invitrogen) in Essential 8™ medium (E8) (Life Technologies). Karyotyping of iPSCs was performed at the Institute of Human Genetics of the Technical University of Munich. To confirm the presence of the *de novo* mutations 50 ng genomic DNA was isolated using the Genomic DNA Purification Kit (Gentra Systems) and Sanger sequenced.

To confirm the loss of SeV transgenes, we performed a RT-PCR for the transcripts of the transduced transgenes. Subsequently, quantitative real-time PCR (qRT-PCR) and immunostaining of pluripotency genes was carried out to assess the pluripotency state of the reprogrammed cells compared to RNA isolated from the original PSFs. To test the differentiation capacity as another indicator of pluripotency, cells were spontaneously differentiated into embryonic bodies and expression of markers of all three germ layers was analysed at day 21 of differentiation by qRT-PCR. Detailed methods are described in the corresponding chapters.

2.2. Cell culture

2.2.1. hiPSC cell culture

hiPSCs were cultured on Geltrex™ reduced growth factor Basement Membrane Matrix-coated cell culture dishes (Invitrogen) in Essential 8™ medium (E8) (Life Technologies), supplemented with 50 U/ml penicillin and 50 µg/ml streptomycin, either as single cells or colonies. Medium was changed daily in both culture conditions. Single cells were splitted every 3-4 days in respect to their confluency, according to the following steps: cells were washed twice with PBS^{-/-} (Invitrogen) and incubated with 1mL EDTA single cell splitting solution (500 mL PBS^{-/-}, 0.9 g NaCl (Sigma-Aldrich), 500 µL 0.5M EDTA (Invitrogen)) for eight minutes at room temperature, and collected with 4 mL E8 prior centrifugation at 296xg for five minutes. Subsequently, cells were resuspended in E8 medium supplemented with 10 µM thiazovivin (Sigma-Aldrich) for improving cell survival and plated at the desired density. Colonies were splitted every 5-7 days according to size and differentiation state. Differentiated areas were scratched away manually under a light microscope (5x magnification), the cells were washed twice with PBS^{-/-} and 1x Dispase was added to the cells for five minutes at 37°C. The plate was washed twice with DMEM/-F12, detached colonies were scraped from the plate using a 13 mm cell scraper (TTP) and mechanically broken into the appropriate size, passed through a 40 µM cell strainer (Corning) and afterwards plated on Geltrex™-coated plates in E8 containing 10 µM thiazovivin. Medium was changed 24 hours after splitting in order to remove thiazovivin.

To freeze single cell hiPSCs, the cells were washed twice with PBS^{-/-} and incubated with EDTA solution for eight minutes at room temperature. Afterwards, cells were collected in 4 mL E8 and centrifuged at 296x g for five minutes. The supernatant was discarded and cells were resuspended in hiPSC single cell freezing medium (45% DMEM/F-12 (Invitrogen), 5% DMSO (Invitrogen), 10% Ethylene Glycol (Sigma-Aldrich), 50% FBS (Sigma-Aldrich)). Cells were stored in cryotubes at -80°C in freezing containers containing isopropanol for 24 hours and subsequently transferred to liquid nitrogen for long term storage.

For freezing of hiPSC colonies, the plates were washed twice with PBS^{-/-} and incubated with 1x Dispase for five minutes at 37°C. Afterwards, the cells were washed twice with DMEM/F-12, scraped off the surface with a 13 mm cell scraper and collected by cen-

trifugation at 296x g for five minutes. After centrifugation, the supernatant was discarded, cells were resuspended in 1x mFreSR (Stemcell Technologies) and transferred to cryotubes. The cryotubes were stored for 24 hours in freezing containers at -80°C before transferring them to liquid nitrogen.

2.2.2. Directed differentiation of hiPSCs into cardiovascular progenitors (CVPCs)

For directed cardiovascular progenitor differentiation of patient and control hiPSCs, cells were washed twice with PBS^{-/-} and collected using Accutase® (Thermo Fisher). Subsequently, cells were plated on the desired culture dishes or chamber slides respectively coated with Geltrex™. Cells were kept in CVPC-induction medium (CIM), containing DMEM/-F12, 1x B27 supplement (without vitamin A), 2 mM L-glutamine, 100 U/ml penicillin, 100 µg/ml streptomycin and 400 µM 1-thioglycerol (Sigma-Aldrich) supplemented with 50 µg/mL ascorbic acid (Sigma), 25 ng/mL recombinant human BMP4 (R&D) and 5 µM CHIR99021 (Axon) together with 24 hours supplementation with 10 µM ROCK inhibitor Y27632 (Merck Millipore) to improve cell survival. These culture conditions were maintained for three days according to the protocol of Cao *et al.*³⁰⁸. For cilia structure and pathway analysis, cells were seeded in a density of 8.75×10^4 cells/cm² to achieve 100% confluency after one day and thus obtaining a high number of cells in G₀ phase of the cell cycle where cilia are formed. All other experiments were performed on cells seeded with a density of 5×10^4 cells/cm². For proliferation analysis, 10 µM of the thymidine analogue 5-ethynyl-2'-deoxyuridine (EdU) was added for 2 hours before further processing. Autophagy induction was carried out by the addition of 10 µg/mL brefeldin A for six hours, for autophagy inhibition 100 µM or 200 µM chloroquine (CQ) was incubated for 12 hours. Proteins were collected upon stimulation for protein expression analysis.

2.2.3. Directed differentiation of hiPSCs into cardiomyocytes

Cardiomyocytes were generated from hiPSCs by applying a modified version of the protocol published by BurrIDGE *et al.* in 2014. For this, hiPSCs were plated as colonies on a 12-well plate and cultured in E8 medium. After reaching 80-100% confluency, cardiomyocyte differentiation medium 1 (CDM1) containing RPMI 1640, 1x B27

(without insulin) supplemented with 6 μM CHIR99021 was applied. Two days after induction, medium was changed to CDM1 supplemented with 5 μM IWR1 (Calbiochem). At day four of cardiomyocyte differentiation medium was changed to CDM1 without factors and cells were maintained under these conditions with a medium change performed every second day. First beating foci were detected at around day 7 after induction of differentiation.

2.2.4. Spontaneous differentiation of hiPSCs into EBs

To rule out an influence of those small molecules on marker gene expression and myocyte formation, undirected spontaneous cardiac differentiation was performed. Hereby, hiPSC colonies were rinsed twice with PBS^{-/-} before incubating them with 1x Dispase for five minutes at 37°C. After incubation, the cells were collected in a 15 mL tube and centrifuged for collection. Subsequently, the supernatant was removed and cells were carefully resuspended in hiPSC mouse embryonic feeder cell (MEF) conditioned medium (DMEM/F-12 (Invitrogen), 20% KSR, 2 mM L-glutamine, 100 μM MEM NEAA, 50 U/ml penicillin, 50 $\mu\text{g/ml}$ streptomycin, 0.1 mM β -mercaptoethanol) supplemented with 10 μM ROCK inhibitor Y27632 and 10 ng/mL b-FGF (Invitrogen) to plate them on non-adherent polyhema-coated cell culture dishes to induce EB formation. After three days, medium was changed to EB20 medium (DMEM/F-12, 20% FBS, 2 mM L-glutamine, 0.1 mM MEM NEAA, 50 U/ml penicillin and 50 $\mu\text{g/ml}$ streptomycin), supplemented with 50 $\mu\text{g/ml}$ freshly added ascorbic acid. Hereby, floating EBs were pelleted by sedimentation in a 15 mL tube and, after subsequent careful aspiration of the medium, resuspended in EB20 medium. In the same way, a medium change was carried out five days after induction. After seven days, the floating EBs were collected in a 15 mL tube, resuspended in fresh EB20 medium and plated on adherent gelatine-coated 4-well cell culture plates (Thermo scientific) at 20-30 EBs per well. Medium was changed every second day to fresh EB20 medium containing 50 $\mu\text{g/ml}$ ascorbic acid and first beating foci were observed at around day 10 after induction.

2.2.5. mESC cell culture

Isl1-Cre-RosaYFP mESCs were cultured on irradiated mouse embryonic fibroblasts - coated culture dishes in mESC medium consisting of DMEM, 15% FBS, 2mM L-

glutamine, 0.1 mM MEM-NEAA, 1mM sodium pyruvate, 50 U/ml penicillin, 50µg/ml streptomycin and 0.1 mM β-mercaptoethanol, supplemented with 10ng/mL Leukemia Inhibitory Factor Protein (LIF) (Merck Millipore). For passaging, cells were washed twice with PBS^{-/-} and incubated with 0.05 M trypsin for five minutes at 37°C. Subsequently, trypsin was inactivated with ESC medium and the cells were mechanically broken into single cells and collected by centrifugation at 296xg for five minutes, followed by resuspension in mESC medium and replating on irradiated mouse embryonic fibroblasts-coated culture dishes in the desired ratio.

2.2.6. Spontaneous differentiation of mESCs into EBs

Cardiomyocyte formation was induced by spontaneous embryonic body (EB) formation. For this, the mESCs were collected with 0.05 M trypsin and 66.6×10^5 cells were added to a polyhema-coated cell culture dish in mESC medium without LIF. For cardiovascular progenitor analysis, five days old EBs were harvested and washed with PBS^{-/-}, following treatment with 0.05 M trypsin and separation of the EBs into single cells by pipetting. The cells were spun down at 296x g for five minutes resuspended in 1% FBS in PBS^{-/-} and filtered for cell sorting.

2.3. Cloning

2.3.1. Human DENND5B expression vector

For the generation of an expression vector of DENN Domain Containing 5B (DENND5B), pcDNA3.1(+) was used as a backbone (Thermo Fisher) which enables high level expression of target sequences in mammalian cells. The plasmid contains a human cytomegalovirus immediate-early (CMV) promoter, large multiple cloning sites (MCS) and a neomycin resistance cassette.

PCR on cDNA of control human EBs was performed with primers flanking the human *DENND5B* coding region (primer sequences listed under 2.9) and the PCR product of a size of 3825 bp was purified using the QIAquick Gel Extraction Kit for DNA extraction from agarose gels (Qiagen). Subsequently, the sequence was subcloned into the pCR-Blunt-II-TOPO vector (Thermo Fisher). Then, the plasmid was transformed into TOP10

competent cells of the Zero Blunt® PCR Cloning Kit (Thermo Fisher). Transformed cells were plated on LB agar with 25 µg/mL kanamycin for antibiotic selection and incubated overnight at 37°C. Next day, colonies were picked and cultured for 8 hours at 37°C at 250 rpm. Finally, plasmids were isolated and amplified using the QIAprep Spin Miniprep Kit (Qiagen). Control digests were carried out using the restriction enzymes *XhoI* and *AgeI* to select the plasmids harbouring the fragment and sequenced with specific primers (found under 3.9) to verify the correct sequence. Sanger sequencing of the fragment was performed by Eurofins MWG Operon.

In a second step, pCR-Blunt-II-TOPO-hDENND5B plasmid was digested with the restriction enzymes *KpnI* and *XhoI* and the hDENND5B fragment was purified using the QIAquick Gel Extraction Kit. At the same time, the pcDNA3.1(+) vector was digested with *KpnI* and *XhoI* and dephosphorylated. The resulting product was purified with the QIAquick Gel Extraction Kit and both fragments ligated using the T4 DNA ligase at 16°C overnight (Fig. 11). The ligation product was transformed in TOP10 competent cells and the transformed cells were seeded on LB agar plates containing 100 µg/mL ampicillin. Subsequently, colonies were picked following culture of those colonies for 8 hours at 37°C at 250 rpm before plasmid isolation and amplification using the Miniprep Kit from Qiagen. Finally, a control digest with the enzymes *KpnI* and *XhoI* was conducted.

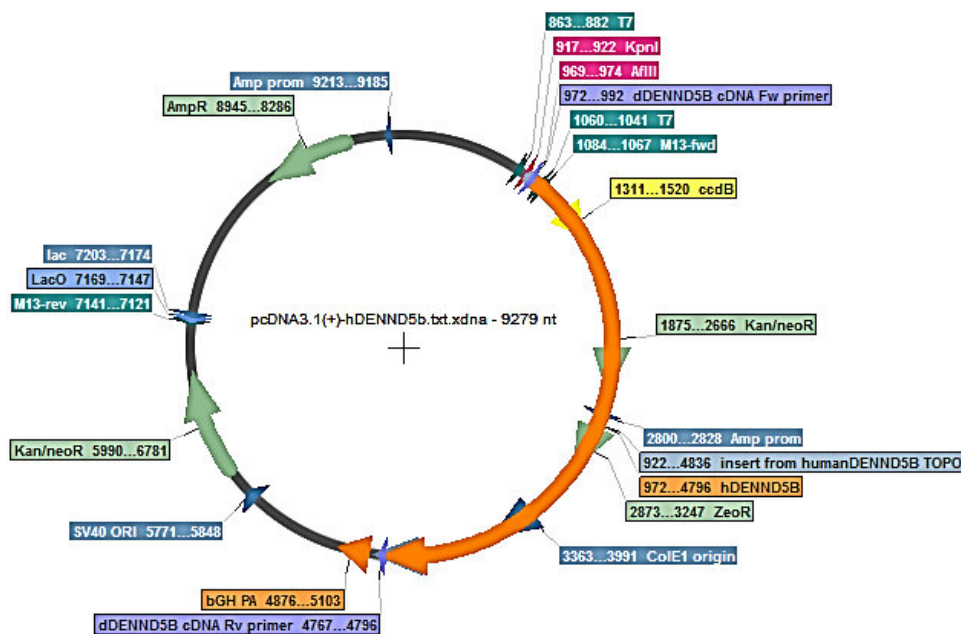


Figure 11: Restriction map of pcDNA3.1(+)-hDENND5B.

2.3.2. PiggyBac™ NKX2.5 Enhancer

The PiggyBac™ transposon-transposase system is a genome editing tool that efficiently inserts multiple copies of a target sequence into the DNA of cells of interest. Hereby, the transposase, encoded on a co-transfected plasmid, recognises specific inverted terminal repeat sequences (ITRs) flanking the target sequence that was beforehand cloned into the transposon vector. It excises the target fragment and integrates it into TTAA sites in the genome of the target cell³⁴⁸.

The backbone used for the generation of the PiggyBac™ NKX2.5 Enhancer construct was the transposon vector PB007 (Transposagen) that consists of a large MCS, flanked by insulators to protect the insert from gene silencing and genomic position effects. The NKX2.5-Enhancer sequence was cloned from human genomic DNA into pCR2.1-TOPO by our collaborator group AG Krane at the German Heart Centre Munich (Fig. 12).

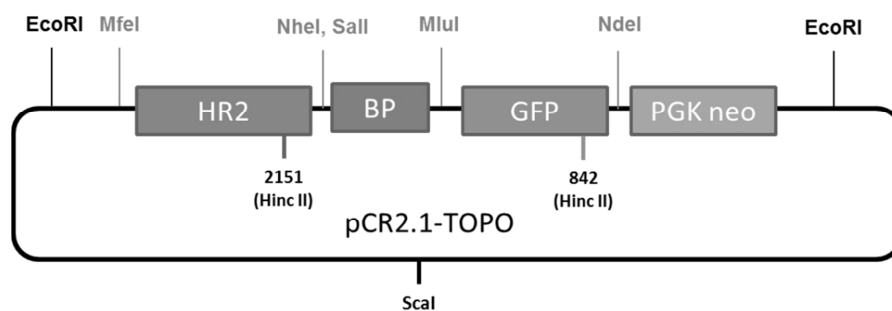


Figure 12: NKX2.5-Enhancer construct. HR2: homology region 2, BP: base promoter, PGK neo: neomycin resistance cassette.

The enhancer construct was digested with *EcoRI* and *Scal* and the resulting 4.9 kb product was purified using the QIAquick Gel Extraction Kit. After blunting the ends of the product with T4 DNA polymerase (New England Biolabs), the construct was purified with the QIAquick PCR Purification Kit before it was ligated into the PiggyBac™ backbone PB007 using the T4 DNA ligase at 16°C overnight (Fig.13). The plasmid PB007 was beforehand digested with *ApaI* and dephosphorylated. Subsequently, the construct was transformed in TOP10 competent cells that were plated on LB agarose dishes supplemented with 100 µg/mL ampicillin for antibiotic selection. Formed colonies were picked and cultured shaking at 37°C for 8 hours. Finally, the plasmid was

isolated and amplified using the QIAprep Spin Miniprep Kit. To evaluate the cloning, a control digest and sequencing was performed.

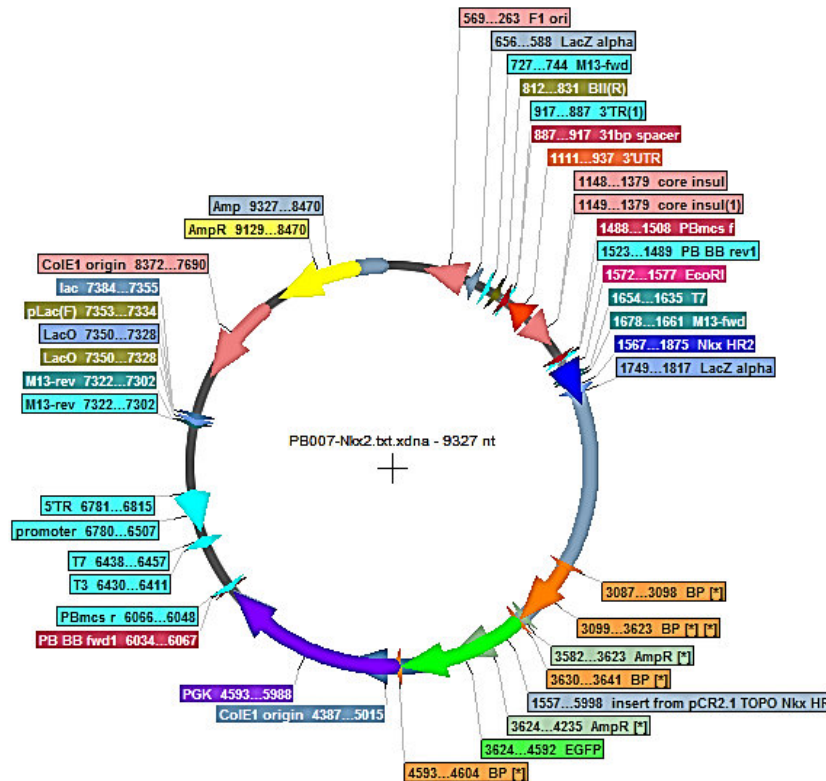


Figure 13: Restriction map of PB007-Nkx2.5.

2.4. Transfection generating stable cell lines

The generation of stably transfected NKX2.5 Enhancer lines was performed by transfection with FuGENE HD Transfection Reagent (Promega). For this, hiPSCs were plated as single cells on Geltrex™ coated plates. After reaching 60-80% confluency medium was changed, transfection reagents were warmed up to room temperature and 100 μ L Opti-MEM™ (Invitrogen) was mixed with 500 ng PB007-NKX2.5 plasmid and 1500 ng Super PiggyBac™ Transposase PB200PA-1 plasmid (System Biosciences Inc.) to add 2 μ g total amount of DNA in a 1.5 mL Eppendorf tube. 6 μ L of the FuGENE HD Transfection Reagent was added to the tube. The samples were gently mixed and incubated for 30-60 minutes at room temperature allowing to form transfection complexes prior to the dropwise addition to the cells. After 24 hours, medium was changed back to E8 and antibiotic selection with 400 μ g/mL neomycin G418 (Life technologies) was

conducted for seven days by a daily medium change to gain stable transfected hiPSC lines.

2.4.1. Clonal selection

For clonal selection of stably transfected NKX2.5-Enhancer hiPSC lines, cells were collected with Accutase® and counted. The dilution of the cell suspension to achieve a seeding of 5-10 cells per well of a 48-well plate was calculated and the cells were plated down on Geltrex™-coated cell culture plates with an addition of thiazovivin for the first 24 hours. After 7-10 days, the plated isolated single cells grew into colonies that were separately picked and plated in individual wells of a 12-well plate for each clone. The clones were further passaged onto 3.5cm cell culture dishes before analysing the transposon integration copy number.

2.5. Immunofluorescence

After applying different stimuli, cells were fixed with 4% paraformaldehyde (PFA) for 15 minutes at room temperature. In case of performing the click it EdU reaction using the Click-iT® Plus EdU Imaging kit from life technologies, the fixed cells were washed with 3% BSA in PBS^{-/-}. Afterwards, cells were permeabilized with 0.5% Triton™ X-100 for 20 minutes at room temperature following the EdU detecting reaction. In the meantime, the click it plus reaction mix was prepared according to the user manual. Cells were washed twice with 3% BSA and the reaction cocktail was applied to the cells for 30 minutes at room temperature, protected from light. After incubation, the cells were washed twice with 3% BSA. For subsequent antibody staining, different permeabilization and blocking conditions were used depending on the antibodies used.

For pluripotency and SeV staining, cells were permeabilized and blocked with 10% goat serum, 0.1% Triton™ X-100 in PBS^{Ca2+/Mg2+} for one hour at 37°C and the primary antibodies rabbit polyclonal human NANOG (Abcam) (1:500) and mouse monoclonal TRA1-81-Alexa-Flour-488 conjugated (BD Pharmingen) (1:20) were used. For SeV staining, rabbit polyclonal anti-Sendai Virus (MBL) (1:1000) primary antibody was applied to the cells in 1% goat serum, 0.1% saponin and 0.1% Triton™ X-100 in PBS^{Ca2+/Mg2+}. For apoptosis staining, 10% BSA in PBS^{Ca2+/Mg2+} was added for blocking for

90 minutes at room temperature following incubation with anti-cleaved Caspase 3 (clCasp3) (Cell Signaling) (1:400) in 1% goat serum, 0.1% saponin and 0.1% Triton™ X-100 in PBS^{Ca2+/Mg2+}. For cardiac progenitor marker and cardiomyocytes staining, unspecific binding sites were blocked and cells permeabilized using 10% goat serum, 0.1% saponin and 0.1% Triton™ X-100 in PBS^{Ca2+/Mg2+} followed by anti-ISL1 (Developmental Studies Hybridoma Bank) (1:100), anti-NKX2.5 (H-114, Santa Cruz Biotechnology) (1:100), anti-cTNT (Cell signalling) (1:500) or anti- α -Actinin (Sigma Aldrich) (1:300) antibody staining in 1% goat serum, 0.1% saponin and 0.1% Triton™ X-100 in PBS^{Ca2+/Mg2+}. For visualization of primary cilia, cells were permeabilized with 0.1 M glycine and 0.2% Triton™ X-100 in PBS^{Ca2+/Mg2+}, washed twice with 0.1% Tween®20 in PBS^{Ca2+/Mg2+} (PBST) and subsequently blocking was performed using 10% FBS, 3% goat serum, 0.1% Tween®20 and 0.1% BSA in PBS^{Ca2+/Mg2+}. Afterwards, primary antibodies for acetylated tubulin (Sigma Aldrich) (1:500) and pericentrin (Abcam) (1:1000) in 1% FBS, 0.1% Tween®20 and 0.1% BSA in PBS^{Ca2+/Mg2+} were applied to the cells. All primary antibodies were incubated overnight at four degrees. After incubation, the cells were rinsed three times and fluorophore-conjugated secondary antibodies for the respective species (Alexa Flour® 488, 555, 594 and 647, 1:500, Thermo Fisher) in either 1% goat serum, 0.1% saponin and 0.1% Triton™ X-100 in PBS^{Ca2+/Mg2+} or in 1% FBS, 0.1% Tween®20 and 0.1% BSA in PBS^{Ca2+/Mg2+} were applied for 1-2 hours at room temperature.

For the primary cilia staining, cells were incubated for two hours at room temperature before performing the washing and antibody steps. Cells were washed three times with PBS^{Ca2+/Mg2+} after antibody incubation and Hoechst 33258 dye (1:250) was applied for 20 minutes following two washes with PBST and one wash with PBS^{Ca2+/Mg2+} before embedding the chamber slides with DAKO fluorescence mounting medium. Images of the fluorescence slides were taken using a DMI6000-AF6000 Leica epifluorescence microscope. Cilia number and length analysis was performed on a Leica SP5 confocal microscope by our collaborator Felizitas Schmidt of the group of Prof. Heiko Lickert.

2.6. Flow cytometry

cTNT staining was performed to monitor cardiac differentiation over time. Therefore, cells were harvested using Accutase® and fixed at specific time points during cardiac

differentiation with 4% PFA for 12 minutes. After one washing step with 1% BSA in PBS^{-/-}, cells were simultaneously permeabilized and unspecific binding sites blocked by 10% FBS, 0.1% Triton™ X-100 for one hour at room temperature. The primary antibody against cTNT (1:500) was incubated for one hour at room temperature. Cells were washed once with 0.1% Triton™ X-100 before applying the desired fluorophore-conjugated secondary antibody for one hour at room temperature. After another washing step, cells were resuspended in 1% BSA in PBS^{-/-} and filtered using xx μM filters before measurement.

To analyse cell cycle phase distribution, the DNA-binding properties of the propidium iodide (PI) dye were utilized. Cells were harvested with Accutase®, centrifuged at 296xg and washed twice with PBS^{-/-}. Subsequently, cells were fixed with 70% ethanol for two hours shaking on ice followed by three washing steps and RNase A treatment (200 μg/mL, DNase free) (Qiagen) for 30 minutes at room temperature. Propidium iodide (1 mg/mL) (Sigma Aldrich) was added for 30 minutes at room temperature. To determine the DNA content of each cell, measurement of the propidium iodide (PI) emission at 605 nm was performed. To exclude cell doublets, single cells were identified with forward scatter (FS) versus side scatter (SS) and subsequent pulse shape analysis applying pulse area versus pulse width on the gated single cells. This population is plotted in a PI histogram. The G₁ phase is characterized by lower DNA content and consequently lower PI emission while the G₂/M phase, due to DNA duplication prior to cell division, has twice the amount of DNA and thus a higher PI signal intensity (Fig. 14).

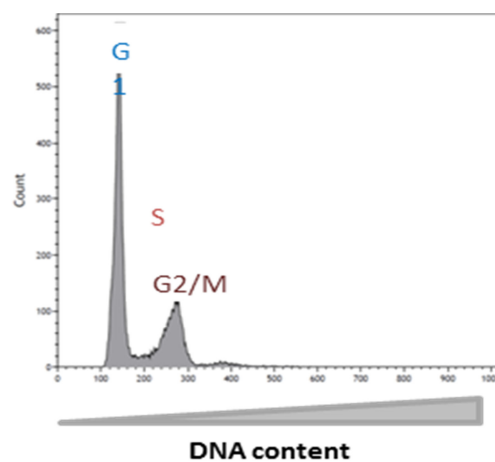


Figure 14: Flow cytometry readout after PI staining.

The number of proliferating cells during cardiac differentiation was measured by incorporation of EdU in the DNA during cell division. Therefore, cells were incubated for two hours with 10 μ M EdU, collected after Accutase™ treatment for five minutes at 37°C and counted. 1×10^7 cells/mL were resuspended in 1% BSA in PBS^{-/-}. Subsequently, cells were fixed and permeabilized and the click it reaction was performed according to the user manual of the Click-iT® EdU Alexa Fluor® 488 Flow Cytometry Assay Kit (Life Technologies). After the reaction, a second blocking step was carried out applying 10% FBS, 0.1% saponin in PBS^{-/-} to the cells for one hour at room temperature following a co-staining for cleaved caspase3 (1:800) for two hours at room temperature. Cells were washed with 0.1% saponin in PBS and the secondary fluorophore-conjugated antibody was added for two hours at room temperature following a washing step with 0.1% saponin in PBS^{-/-}. For measurement, the cells were resuspended in 0.1% saponin in PBS^{-/-} and filtered to achieve a homogenous single cell suspension. All measurements were performed with the Beckman Coulter Gallios 100C/3L. Analysis of the results was done with the Kaluza software.

Fluorescence-activated cell scanning and sorting (FACS) of Isl1-YFP mouse ES cell-derived cardiac progenitors as well as stably transfected NKX2.5 enhancer-GFP human iPSC-derived cardiac progenitors and myocytes was performed by the FACS Sorting Facility of the Microbiology department in the Klinikum rechts der Isar. Cells were washed with PBS^{-/-} and collected with the respective enzyme and resuspended in 1% FCS in PBS^{-/-} following dissociation into single cells by passing through a 35 μ M cell strainer. Cells were stored on ice and the sorting was performed with the Aria FACS machine (Beckman Coulter) at 20000 eps (events per second) at an excitation of 488 nm. The sorted cells were collected in FCS and further processed in respect to the desired experiment.

2.7. RNA isolation, RT-PCR and qRT-PCR

Cells were lysed and total RNA was extracted using the Absolutely RNA Microprep Kit (Agilent) according to the manufacturer's instructions under RNase-free conditions. RNA concentration was measured with a Nanodrop 1000 Spectrophotometer (Thermo Fisher Scientific) and cDNA was synthesized from 1 μ g of the total RNA using the

High-Capacity cDNA Reverse Transcription kit (Applied Biosystems) according to the product manual.

Table 1: RT Master Mix.

Reagent	Volume [μl]
2x Power SYBR Green PCR Master Mix	5.0
Forward Primer [10 μ M]	0.3
Reverse Primer [10 μ M]	0.3
cDNA Template	1.0
Sterile H ₂ O	3.4

The reaction was conducted on a Thermocycler DNA Engine PCR machine (Peltier Thermal Cycler, Bio-Rad) using the following protocol:

Table 2: RT PCR program.

	Temp [$^{\circ}$C]	Time [min]
Stage 1	25	0:10
Stage 2	37	120
	85	0:05

40 cycles of stage 2 were performed for amplification.

Quantitative real-time PCR was performed using the POWER SYBR® Green Master Mix (Applied Biosystems) for human cDNA and TaqMan™ probes for murine cDNA combined with gene-specific designed primer pairs. The expression profile of target genes was detected on an AB Applied Biosystems 7500 Fast Real-Time PCR system machine. The following program was used for the reaction:

Table 3: qRT-PCR program.

	Temp [$^{\circ}$C]	Time [min]
Stage 1	50	00:20
Stage 2	95	10:00
Stage 3	95	00:15
	60	01:00
Stage 4	95	00:15
	60	01:00
	95	00:30
	60	00:15

Stage 3 was performed 40x for amplification before proceeding to stage 4. Relative expression levels compared to *GAPDH* expression was calculated using the $\Delta\Delta C(t)$ method.

2.7.1. qRT-PCR for pluripotency and embryonic germ layer markers and cardiac specific genes

To test whether the generated hiPSC lines are able to differentiate in cells contributing to all three embryonic germ layers, qRT-PCR was performed for specific mesodermal, endodermal and ectodermal markers, on 21 days old EBs. For mesodermal gene expression, primer pairs for *CD31*, *DES*, *ACTA2*, *SCL*, *MYL2* and *CDH4* were used, for the endoderm, *PDX1*, *SOX7* and *AFP* gene expression was evaluated and as endodermal markers, the expression of the genes *KRT14*, *NCAM1*, *TH* and *GABRR2* was tested, all compared to the respective hiPSC line.

The expression analysis of specific cardiac progenitor markers indicating the differentiation capability of the generated hiPSC lines as well as the expression of SHH pathway components was assessed by qRT-PCR as well. Selected target genes were *NANOG*, *TDGF1*, *OCT3/4*, *NKX2.5*, *ISL1*, *TBX20*, *PDGFR α* , *SOX1*, *FOXA2*, *T*, *MESPI* and *GLII*. Amplification of the target genes was conducted using the program depicted in table 3. All primer sequences are listed under 2.9.

2.7.2. qRT-PCR of PiggyBacTM integration numbers

The detection of the number of PiggyBacTM construct integrations was carried out through the PiggyBacTM copy number Kit (#PBC100A-1) from SBI System Biosciences with an adapted reaction profile:

Table 4: qRT-PCR program for PiggyBacTM copy number detection.

	Temp [°C]	Time [min]
Stage 1	50	02:00
Stage 2	95	10:00
Stage 3	95	00:15
	60	01:00
Stage 4	95	00:15
	60	00:15
	95	00:15

Stage 3 was repeated for 40 cycles. To calculate expression levels relative to *GAPDH*, the $\Delta\Delta C(t)$ method was applied. The number of PiggyBac™ transposon insertions per genome in a clonal line was determined by comparing the number of genomes detected by a UCR1 primer mix to the number of transposons present in the genome detected by a PiggyBac™ copy number primer mix according to the manufacturer's instructions.

2.7.3. PCR of Sendai transgenes and endogenous pluripotency marker expression

To prove that the generated hiPSC lines are free of the SeV transgenes, cDNA of the hiPSC lines was compared to samples of the corresponding infected fibroblasts and non-infected fibroblasts. The expression of the endogenous pluripotency markers *KLF4*, *OCT3/4*, *SOX2*, *NANOG*, *REX1* and *TDGF1* was measured to evaluate the pluripotency state of the generated hiPSC lines compared to its corresponding primary skin fibroblasts. FIREPol® DNA Polymerase PCR on 25 ng/μL cDNA of each sample was conducted according to manufacturer's manual (Solis Biodyne). Resulting products were evaluated by gel electrophoresis using a 2% agarose gel in which samples were separated at 300 V for 30 minutes following imaging analysis with the transilluminator Bio-vision 3000 WL (Peqlab). Primer sequences are listed under 2.9.

2.8. Western Blot

2.8.1. Protein sample preparation

Protein expression was analysed by western blot. Upon stimulation, cells were washed twice with PBS^{-/-} and lysed with RIPA buffer freshly supplemented with proteinase inhibitor to the cells on ice and scraping them off the plate with a cell scraper after five minutes of incubation. Cells were collected in a 1.5 mL Eppendorf tube and incubated on ice for another 10 minutes following centrifugation in a pre-cooled centrifuge at 4°C for 15 minutes at 14000xg. The supernatant was collected and shock-frozen in liquid nitrogen before short term storage at -80°C. If continuing with the western blot, proteins need to be kept on ice.

The protein concentration was determined using the Pierce™ BCA Protein Assay kit from Thermo Scientific. Protein lysates and a BSA standard in several concentrations were pipetted on a 96-well flat bottom plate followed by the addition of the colorimetric substrate mixture supplied by the kit. After 15 minutes of incubation at 37°C, the absorbance at 550 nm was measured with a Dynatech MR5000 machine and the protein concentration of the lysates calculated referring to the BSA calibration curve generated. 50 µg protein lysate were used for detection of Gli1. For p62 detection after autophagy induction or inhibition, respectively, 20 µg of the protein lysate were applied on the gel. The desired amount of protein was mixed with 5-fold Laemmli-buffer (100 mM Tris-HCl, 5% SDS, 50% glycerol, 500 mM 2-mercaptoethanol, 0.05% Bromophenol blue) and the samples were heated at 95°C for 15 min before placing them back on ice and performing the electrophoresis.

2.8.2. SDS-PAGE and Blotting

Proteins were separated by their molecular weight by SDS-PAGE (sodium dodecyl sulfate-polyacrylamide gel electrophoresis) applying the method of Laemmli (1970). SDS-polyacrylamide gels consisting of a 5% stacking gel on top of a separation gel were prepared beforehand using the Mini Protean system from Bio-Rad. The cast gels were placed into a gel chamber containing 1x SDS running buffer (containing 144 g Glycine, 20 g SDS and 30.3 g Tris(hydroxymethyl)-aminomethan (TRIS)) and 20 µL of the samples and a protein standard ladder were loaded into the gel. A constant voltage of 90 V was applied to the gel for protein separation.

Table 5: Separation and stacking gel composition.

Separation gel (10 mL)	10%	Stacking gel (10 mL)	5%
ddH ₂ O	7.9 mL	ddH ₂ O	5.5 mL
1.5M TRIS-HCl (pH 8.8)	5 mL	1M TRIS-HCl (pH 6.8)	1 mL
30% (w/v) Polyacrylamide (29:1)	6.7 mL	30% (w/v) Polyacrylamide (29:1)	1.3 mL
20% (w/v) SDS	100 µL	20% (w/v) SDS	40 µL
10% (w/v) APS	200 µL	10% (w/v) APS	80 µL
TEMED	16 µL	TEMED	16 µL

After finishing the run, the gels were removed from the chambers and the blotting of the proteins onto an Amersham Hybond™-N⁺ membrane (GE healthcare) was performed.

Blotting was performed in a wet blotting chamber containing ice-cold 1xblotting buffer (diluted from 10X running buffer: 30.2 g TRIS, 144 g glycine, 10 g SDS in 1 l sterile H₂O, by adding 70% sterile H₂O and 20% methanol) at 100 V for 90 minutes.

2.8.3. Staining and detection

Subsequently, the membrane was removed from the chamber and washed in dH₂O before a Ponceau S staining was done to confirm the successful transfer of the proteins from the gel onto the membrane. The membrane was washed with PBST to remove the dye and blocked with 5% milk powder in PBST for two hours on a shaking platform. Primary antibodies against human Gli1 (Abcam) (1:1000) or p62 (Enzo Life Sciences) (1:2000) as well as actin (1:1000) (serving as a loading control) were applied onto the membrane for detection and incubated overnight at 4°C. After incubation, the membrane was washed with PBST five times for five minutes each, following the application of the HRP-conjugated secondary antibodies concordant with the required species for one hour at room temperature. Afterwards, the washing steps were repeated.

For visualisation of the proteins, the membranes were incubated with enhanced chemiluminescence (ECL) plus reagent from the Amersham™ ECL™ Prime Western Blotting Detection reagent kit (GE Healthcare) for five minutes at room temperature in absence of light. To detect the light transmitted by the substrate, an Amersham Hyperfilm™ ECL film (GE healthcare) was exposed to the membrane for different incubation times, dependent on the signal intensity, inside a dark room. The exposed film was developed in a WB developing machine and subsequent quantification of the scanned film by the ImageJ software was performed.

2.9. List of oligonucleotides

Gene	Species	Sequence
<i>DENND5B</i>	human	Forward 5'-ACAATCGCTGGGTAAGTCGG-3'
		Reverse 5'-ATGCTCAGAATGCTGGCGAA-3'
<i>FGFR1</i>	human	Forward 5'-TCAGATGCTCTCCCCTCCTC-3'
		Reverse 5'-GAGCTACGGGCATACGGTTT-3'
<i>MACF1</i>	human	Forward 5'-TCAGAGTCGCTGATGAACGG-3'
		Reverse 5'-CATTGATGTGCTTGCGGAACC-3'

<i>GAPDH</i>	human	Forward	5'-TCCTCTGACTTCAACAGCGA-3'
		Reverse	5'-GGGTCTTACTCCTTGGAGGC-3'
<i>GLI1</i>	human	Forward	5'-CACAGGCATACAGGATCCCC-3'
		Reverse	5'-TGGATGTGCTCGTGTGAT-3'
<i>GLI2</i>	human	Forward	5'-TCTGCTTCCCCCTTGACAGTA-3'
		Reverse	5'-GCCTAATTTCTGCTCGAATGCAC-3'
<i>ISL1</i>	human	Forward	5'-AAAGTTACCAGCCACCTTGGGA-3'
		Reverse	5'-ATTAGAGCCCGGTCCTCCTT-3'
<i>Isl1</i>	mouse	Forward	5'-GCCTTGCAAAGCGACATAGA-3'
		Reverse	5'-TGCCAGTAGAATTAGAGCCTGG-3'
<i>NANOG</i>	human	Forward	5'-TGCAAGAACTCTCCAACATCCT-3'
		Reverse	5'-ATTGCTATTCTTCGGCCAGTT-3'
<i>NKX2.5</i>	human	Forward	5'-CAAGTGTGCGTCTGCCTTT-3'
		Reverse	5'-TTGTCCGCCTCTGTCTTCTC-3'
<i>PDGFRα</i>	human	Forward	5'-TGGCAGTACCCATGTCTGAA-3'
		Reverse	5'-CCAAGACCGTACAAAAGGC-3'
<i>REX1</i>	human	Forward	5'-ACCAGCACACTAGGCAAACC-3'
		Reverse	5'-TTCTGTTCACACAGGCTCCA-3'
<i>SOX1</i>	human	Forward	5'-TCGCTTTCTCAACACCCTTC-3'
		Reverse	5'-AGGCTGAATTCGGTTCTCATT-3'
<i>TBX20</i>	human	Forward	5'-CCAACAATGAACTGGATCAACA-3'
		Reverse	5'-GCACCCTTGGCTGGTACTT-3'
<i>TDGF1</i>	human	Forward	5'-CCCAAGAAGTGTTCCTGTG-3'
		Reverse	5'-ACGTGCAGACGGTGGTAGTT-3'
<i>TBX5</i>	human	Forward	5'-GGGCAGTGATGACATGGAG-3'
		Reverse	5'-GCTGCTGAAAGGACTGTGGT-3'
<i>Yfp</i>	mouse	Forward	5'-GGGTGTTCTGCTGGTAGTGG-3'
		Reverse	5'-AGCAGAAGAACGGCATCAAG-3'
<i>KLF4 endo</i>	human	Forward	5'-ATAGCCTAAATGATGGTGCTTGG-3'
		Reverse	5'-AACTTTGGCTTCCTTGTTTGG-3'
<i>SOX2 endo</i>	human	Forward	5'-GGGAAATGGGAGGGGTGCAAAGAGG-3'
		Reverse	5'-TTGCGTGAGTGTGGATGGGATTGGTG-3'
<i>OCT4 endo</i>	human	Forward	5'-GACAGGGGGAGGGGAGGAGCTAGG-3'
		Reverse	5'-CTTCCCTCCAACCAGTTGCCCAAAC-3'
<i>CD31</i>	human	Forward	5'-ATGCCGTGGAAGCAGATAC-3'
		Reverse	5'-CTGTTCTTCTCGGAACATGGA-3'
<i>FOXA2</i>	human	Forward	5'-CCGACTGGAGCAGCTACTATG-3'
		Reverse	5'-TGTACGTGTTTCATGCCGTTT-3'
<i>ACTA2</i>	human	Forward	5'-GTGATCACCATCGGAAATGAA-3'
		Reverse	5'-TCATGATGCTGTTGTAGGTGGT-3'
<i>SOX7</i>	human	Forward	5'-TGAACGCCTTCATGGTTTG-3'
		Reverse	5'-AGCGCCTTCCACGACTTT-3'
<i>AFP</i>	human	Forward	5'-GTGCCAAGCTCAGGGTGTAG-3'
		Reverse	5'-CAGCCTCAAGTTGTTCTCTG-3'
<i>KRT14</i>	human	Forward	5'-CACCTCTCCTCCTCCAGTT-3'
		Reverse	5'-ATGACCTTGGTGCGGATTT-3'
<i>TH</i>	human	Forward	5'-TGTACTGGTTCACGGTGGAGT-3'
		Reverse	5'-TCTCAGGCTCCTCAGACAGG-3'
<i>SeV</i>	human	Forward	5'-GGATCACTAGGTGATATCGAGC-3'
		Reverse	5'-ACCAGACAAGAGTTTAAGAGATATGTATC-3'
<i>DENND5B cloning</i>	human	Forward	5'-ATGAGCGGGAGCTGCGCGGCG-3'
		Reverse	5'-TTACACATCCACTCCTTTGATGAGTGATCC-3'

3. Results

3.1. Identification of *de novo* mutations by whole exome sequencing in HLHS trios

Current knowledge about the basis of CHD suggests a polygenetic model combined with environmental circumstances as major regulators for the onset of this pathologic condition. Since only the child is affected by HLHS while the parents do not show a HLHS phenotype, a trio whole exome sequencing analysis was performed including the affected child and the parents to find *de novo* mutations in the child that might play a role in the onset of the disease. Hereby, through sequencing of all expressed genes in a genome in all three subjects, comparative analysis reveals the mutations that are acquired in the child in contrast to those that were inherited by the parents. This analysis was conducted by the Institute of Human Genetics at the Helmholtz Centre Munich (Prof. Thomas Meitinger) discovering a slight increase of *de novo* mutations detected in patients compared to a control group (Fig. 15A). The analysis revealed a distribution of 0 to 5 *de novo* mutations among 78 analysed trios, whereby most of the patients carried 0 or 1 mutations (Fig. 15B). Predicted functional effect of a coding variant was surveyed using the programs Polyphen2 (<http://genetics.bwh.harvard.edu/pph/>), SIFT (<http://sift.jcvi.org/>) and Combined Annotation Dependent Depletion (CADD) (<http://cadd.gs.washington.edu/>).

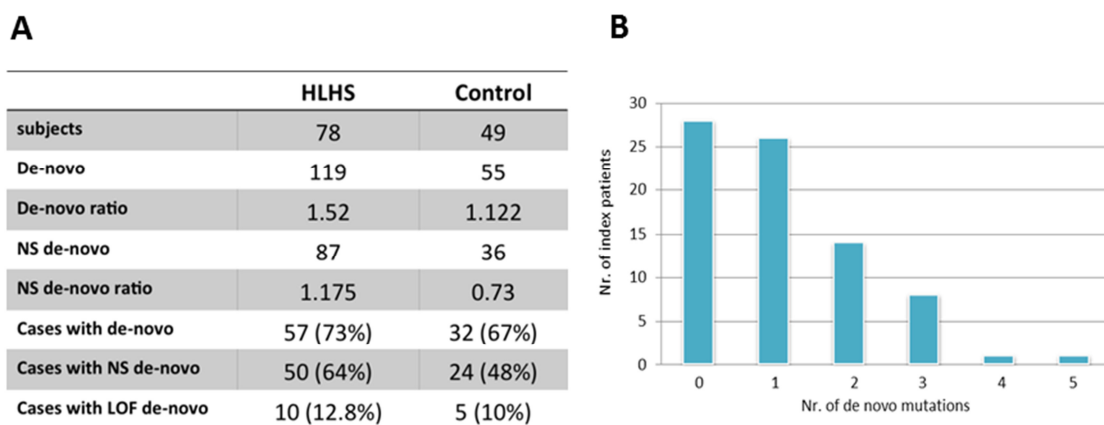


Figure 15: Analysis of *de novo* mutations in HLHS subjects. (A) Occurrence of *de novo* mutations in HLHS patients compared to control subjects (B) Number of non-synonymous *de novo* mutations identified in 78 index patients NS= non synonymous mutations; LOF= loss of function mutations.

Moreover, the study could show that in some cases, the same gene family was found to be mutated in more than one patient (Fig. 16A), suggesting a more likely involvement of these variants in the development of the disease. We had access to fibroblasts for three of the patients carrying one of the mutations that were found in more than one patient thus being able to reprogram these individual cells to hiPSCs to further investigate the role of these mutated proteins in heart development and the occurrence of CHD. One was the *FGFR1* mutation (line 606), where the patient is carrying an additional *Mixed lineage leukemia protein-1 (MLL1)* mutation. The second hiPSC line (line 375) was generated from fibroblasts of a patient displaying a mutation in the *DENND5B* gene, a protein involved in retrograde vesicular trafficking mediated by RAB proteins, as well as two additional *de novo* mutations in *Syntabulin (SYBU)* and *Brain-specific angiogenesis inhibitor 2 (BAI2)* whereas the latter is predicted to be benign. The third HLHS hiPSC line (line 612) represents a patient carrying disease-causing *de novo* variations in the *MACF1* gene, a microtubule-associating factor, and *Myelin Regulatory Factor (MYRF)*, as well as benign mutations in *Absent In Melanoma 1-Like (AIMIL)* and *NADH:Ubiquinone Oxidoreductase Subunit B10 (NDUFB10)* (Fig. 16B). In the following, only the probably damaging *de novo* mutations that were hit twice in the study, namely *DENND5B*, *MACF1* and *FGFR1*, are considered as “lead *de novo* mutations” and investigated further,

A			B			
Sample ID	Gene	Description	iPS line	sex	<i>de novo</i> mutation(s)	gene description
73495/HLHS0013	CYP17A1/CYP2A13	Belongs to the cytochrome P450 family				
70270/69270	DENND4B/DENND5B	DENN domain-containing protein 4B/5B	375	male	DENND5B , BAI2 SYBU	DENN domain-containing protein 5B brain-specific angiogenesis inhibitor 2 syntabulin
73119/HLHS0121	FGFR1/FGFR2	Fibroblast growth factor receptor 1/2				
HLHS0028/73503	GLI1/GLI2	Zinc finger protein involved in Sonic Hedgehog signalling	606	female	FGFR1 , KMT2A	fibroblast growth factor receptor 1 Histone-lysine N-methyltransferase 2A
70315/66111	MACF1/MACF1	Microtubule-actin cross-linking factor 1	612	male	MACF1 , MYRF, AIMIL, NDUFB10	microtubule-actin crosslinking-factor 1 myelin regulating factor absent in melanoma 1-like protein NADH-dehydrogenase ubiquinone
HLHS0163/HLHS0011	ZNF469/ZNF394	Zinc finger protein				
84490/HLHS0091	SLC26A6/SLC9A4	Solute carrier family 26, subfamily A				
70315/84490	MYRF/MYRF	Myelin regulator factor				
HLHS0040/HLHS0124	PTCH1/PTCH2	Protein patched homolog 1. Acts as a receptor for SHH				

Figure 16: Summary of *de novo* mutations of interest. (A) List of gene families found twice in the *de novo* mutation analysis of HLHS patients. (B) *De novo* mutations of patients selected for hiPSC generation.

3.2. Generation of hiPSCs from HLHS patients

Fibroblasts of three HLHS patients were reprogrammed to hiPSCs by Dr. Thomas Brade and Martina Dressen (German Heart Center Munich, AG Krane), applying SeV containing three vectors including the four factors OCT4, SOX2, KLF4, and c-MYC, published by Yamanaka in 2006²⁶⁶. After successful generation of clones exhibiting hiPSC morphology features, these clones were tested positive for the expression of pluripotency markers by immunofluorescence (TRA1-81 and NANOG) and PCR (NANOG, OCT4, SOX2, KLF4 and REX) (Fig. 17A and C). The cells were approved to be SeV free by PCR and the karyotype did not show any abnormalities (Fig. 17D). Subsequent spontaneous differentiation into EBs could confirm the pluripotent state of the reprogrammed cells by upregulated mRNA levels of markers representative for all three germ layers (Fig. 17B).

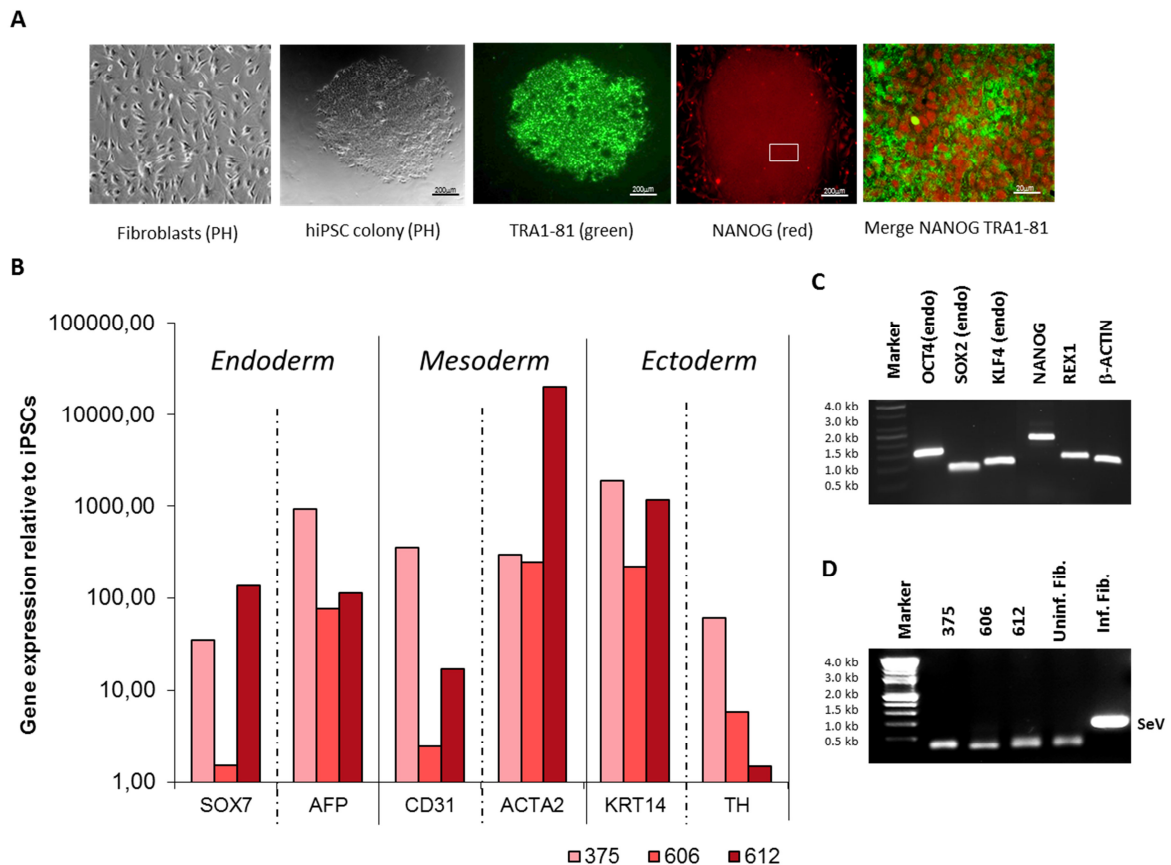


Figure 17: Generation and characterization of virus-free hiPSCs from fibroblasts of HLHS patients. (A) Representative pictures of skin fibroblasts from a HLHS patient and hiPSC colonies on feeders of a HLHS patient in BF and stained with TRA1-81 (green) and NANOG (red). (B) Expression of germ layer markers in patient hiPSC-derived whole EBs d21. (C) Representative picture of pluripotency marker gene expression in HLHS patient hiPSCs. (D) Loss of SeV transgene expression.

3.3. Marker gene expression during cardiac differentiation of HLHS-hiPSCs

Induction of cardiomyocyte formation

Analysing myocyte formation during induced cardiac differentiation (Fig. 18A) in the patient lines compared to control lines performing cTNT staining followed by flow cytometry measurement we observed an upregulation of cTNT after induction of differentiation. Both, control lines and patient lines switched on cTNT expression at day 5-6 (Fig. 18B). Moreover, analysis of the cardiac sarcomeric structure of the patient iPSC-derived myocytes performing an immunostaining for cTNT and α -actinin revealed a non-disrupted sarcomeric organization in all patient lines if compared to control cardiomyocytes.

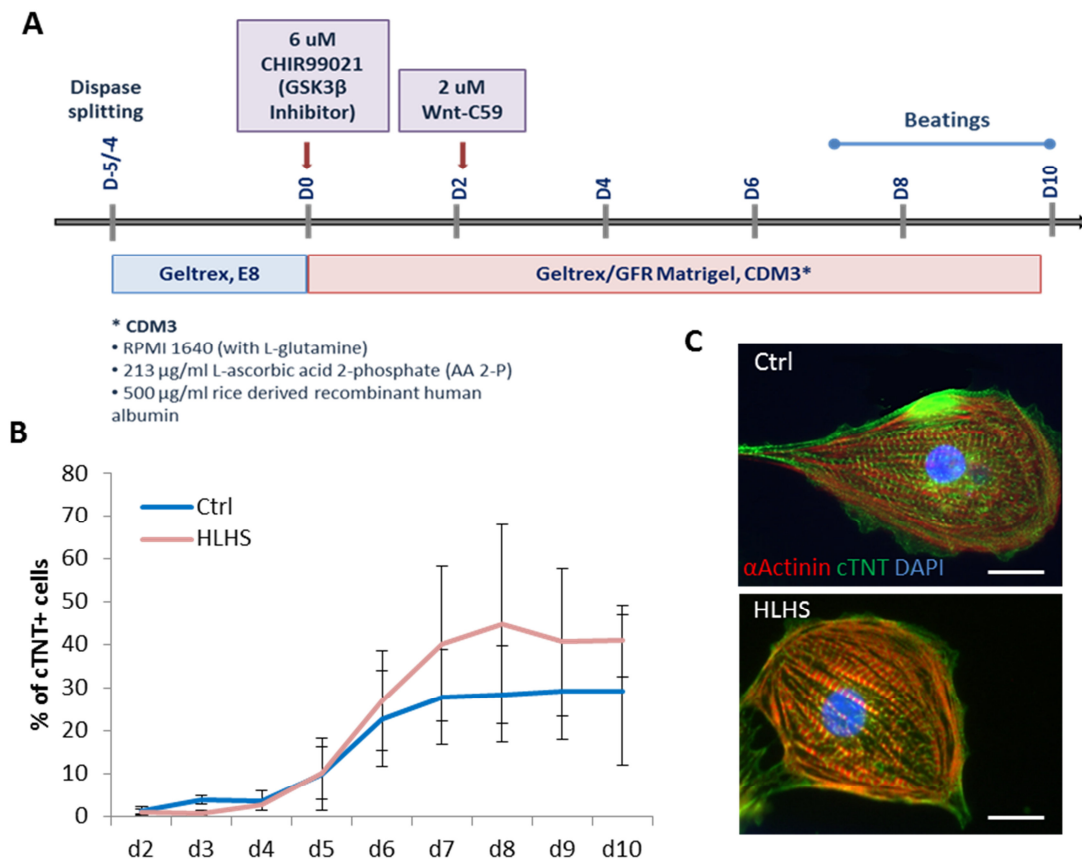


Figure 18: Comparison of cardiomyocyte differentiation between patient and control lines. (A) Differentiation protocol adapted from the protocol published by Josef Wu³⁴⁹ (B) Flow cytometry analysis of cTNT expression during cardiac differentiation of patient and control lines. (C) Representative pictures of control- and patient iPSC-derived cardiomyocytes, stained with α -Actinin (red), cTNT (green) and DAPI (blue). Scale bars: 25 μ M.

Subsequently, an expression analysis of key cardiac progenitor markers at several time points during directed and undirected cardiac differentiation was conducted to further analyse the capability of the patient lines to form appropriate cardiomyocytes. The results, shown in Figure 19, revealed a statistically significant decrease in expression of *NKX2.5* at day 6 of cardiac differentiation and a completely abolished expression of *TBX5*, while there is no significant difference detected for *ISL1* and *TBX20* (Fig. 19).

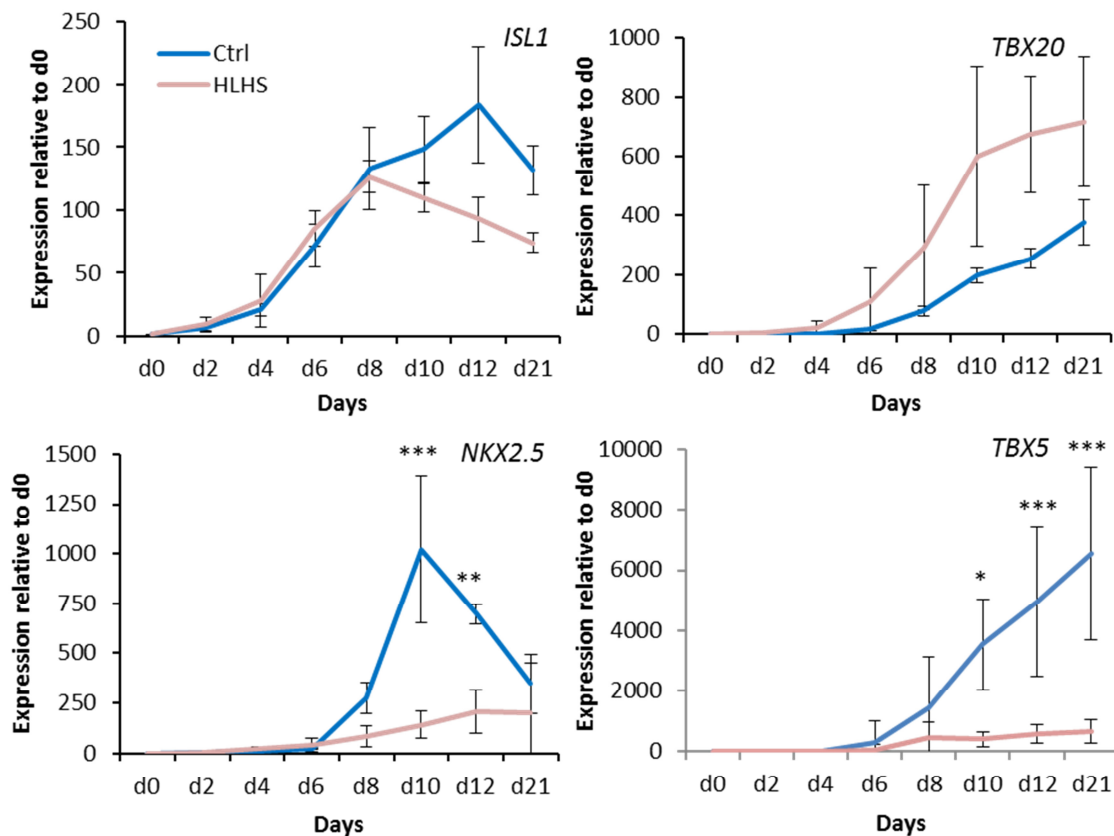


Figure 19: Analysis of spontaneous differentiation ability of patient hiPSC lines compared to control hiPSC lines. qRT-PCR analysis of cardiac progenitor markers during spontaneous differentiation. $n \geq 3$. *NKX2.5* d10: $p=0.001$, d12: $p=0.003$. *TBX5* d10: $p=0.02$, d12: $p=0.0007$, d21: $p=0.002$ * p value ≤ 0.05 ; ** p value ≤ 0.01 ; *** p value ≤ 0.01 .

Induction of cardiovascular progenitor (CVPC) formation

The transcriptional differences are observed in cardiac progenitor markers and they occur already at the progenitor stage, suggesting alterations of earlier stages of cardiogenesis leading to expression changes and a possible differentiation delay. But due to high cell death rates within the first days of cardiac differentiation induction, earlier progenitor stages cannot be evaluated in terms of the detected expression alterations. To investigate these early cardiac stages, we generated CVPCs of the patient lines as well as control lines using the protocol published by Cao *et al.* in 2014 (Fig. 20A and B)³⁰⁸. We

could confirm that application of the protocol lead to cells expressing key markers of the mesodermal and cardiovascular lineage (Fig. 20C and 21). Expression of pluripotency markers decreased during differentiation and there is no indication of endodermal or ectodermal lineage induction observed by the lack of marker gene expression of these two germ layers. Additionally, we were able to induce CVPC formation in our patient lines as well (Fig. 22).

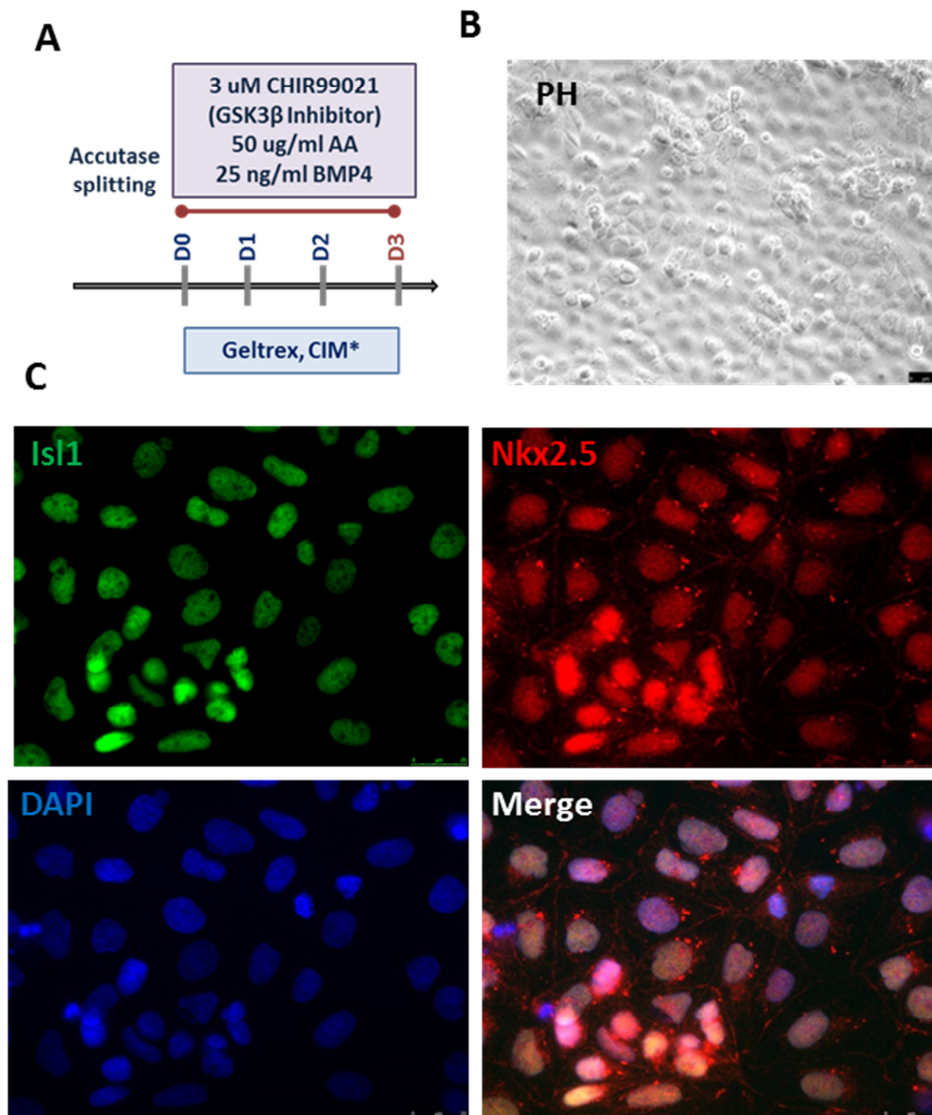


Figure 20: hiPSCs induction to CVPCs. (A) Outline of the protocol. (B) Phase contrast image of CVPCs after 3 days of differentiation. Scale bar=50 μ m. (C) Immunofluorescence analysis of the cardiac progenitor markers ISL1 and NKX2.5 at day 3 of CVPC induction in a control hiPSC line. Scale bars = 25 μ m.

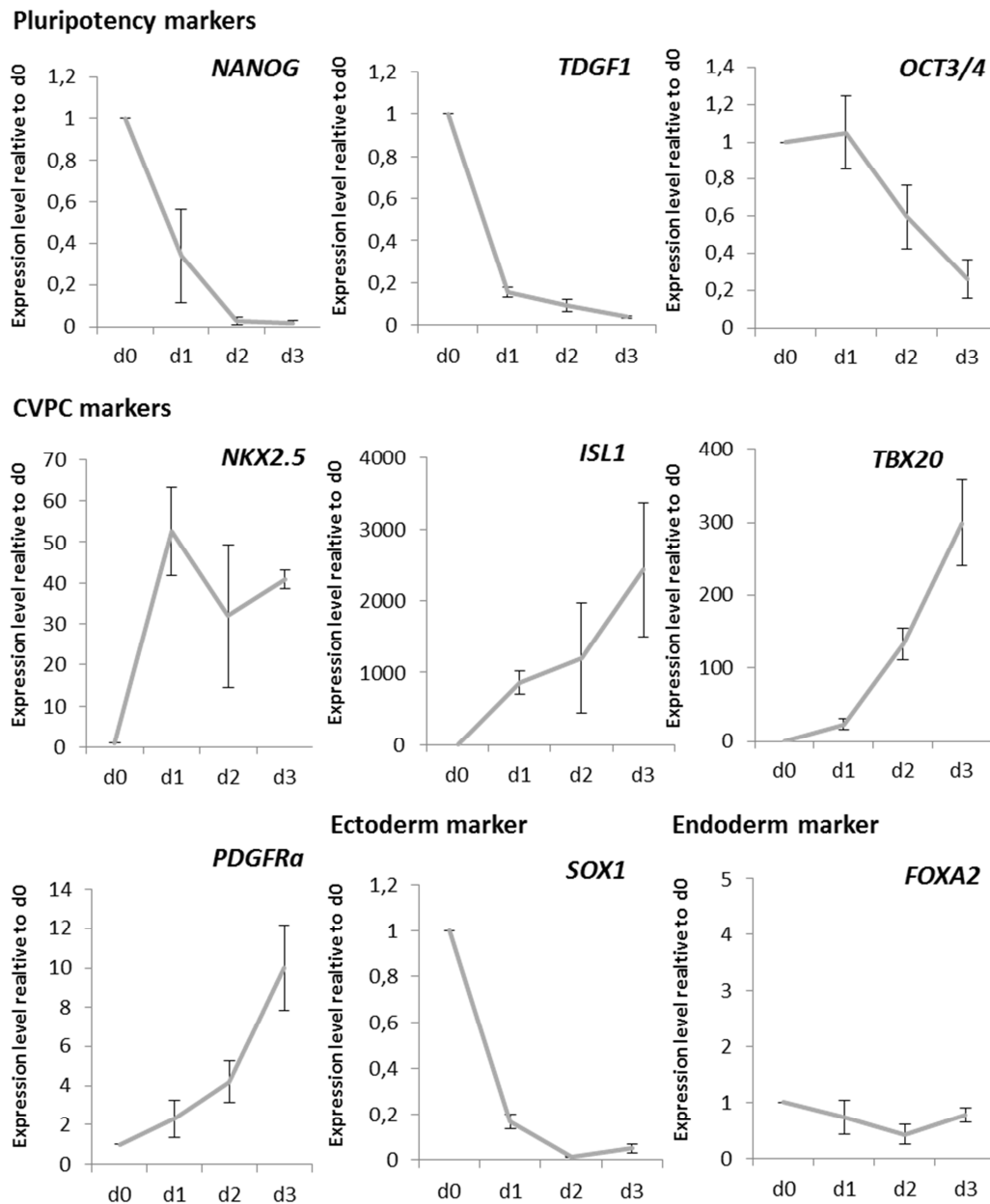


Figure 21: Characterization of CVPCs. qPCR analysis of pluripotency markers, mesoderm markers, cardiac progenitor markers as well as an ectodermal and an endodermal marker during differentiation towards CVPCs for a control hiPSC line. n = 3.

Examining marker gene expression in the three patient lines during CVPT differentiation, we found that genes such as *TBX5* and *NKX2.5*, indicating CVPC formation, showed significantly lower expression levels in all three patient iPSC lines 3 days after CVPC induction compared to control lines. However, expression levels of other CVPC markers including *PDGFRα*, *TBX20* and *ISL1* did not reveal any significant differences (Fig. 22). This indicates that CVPCs are formed, but not all markers are expressed in the

CVPCs derived from the patient hiPSCs. In the following, we investigated which molecular mechanisms might be responsible for the expression differences and whether we could further strengthen our hypothesis from the *ex vivo* data of a possible differentiation delay.

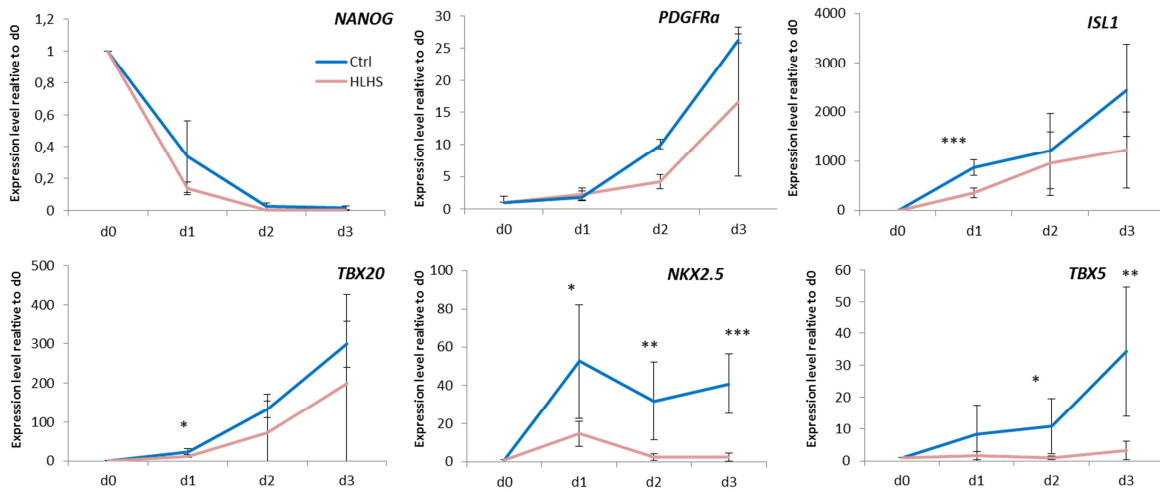


Figure 22: Analysis of CVPC differentiation ability of patient hiPSC lines compared to a control hiPSC line. qRT-PCR analysis of a pluripotency marker, mesoderm markers and cardiac progenitor markers during CVPC induction. $n = 3$. ISL1 d1: $p=0.0005$. TBX20 d1: $p=0.02$. NKX2.5 d1: $p=0.02$; d2: $p=0.009$; d3: $p=0.0004$. TBX5 d2: $p=0.04$; d3: $p=0.01$ * p value ≤ 0.05 ; ** p value ≤ 0.01 ; *** p value ≤ 0.01 .

3.4. Proliferation analysis during cardiac differentiation of HLHS-hiPSCs

Changing proliferation rates are an indicator of ongoing differentiation: the more cells proliferate, the more immature they are since they need to divide before specialization into a particular tissue³⁵⁰. Therefore, proliferation helps to understand whether the cardiac markers are simply not described but the cell fate of the forming CVPCs is unaltered or if they are formed at later stages suggesting a delay. Thus, we studied the proliferation in CVPCs derived from the patient hiPSCs compared to control lines by incorporation of EdU during DNA replication before cell division³⁵¹. Patient-derived hiPSCs as well as control lines were differentiated towards CVPCs and the number of proliferating cells was assessed from day 0 to day 3 of differentiation performing flow cytometry and immunostaining. While there was no difference detected at the pluripotency state (~50%) as well as during the first day of differentiation observing a slight decrease of proliferating cells (~48%), day 2 after induction showed a much higher proliferation

in the patient lines (~35%) while in the control lines an ongoing reduction of the number of dividing cells was observed (~20%). At day 3, the proliferation rate of patient lines was also reduced to the same extent as the control lines (~20%) suggesting a delay in differentiation in these lines (Fig. 23A, B and D).

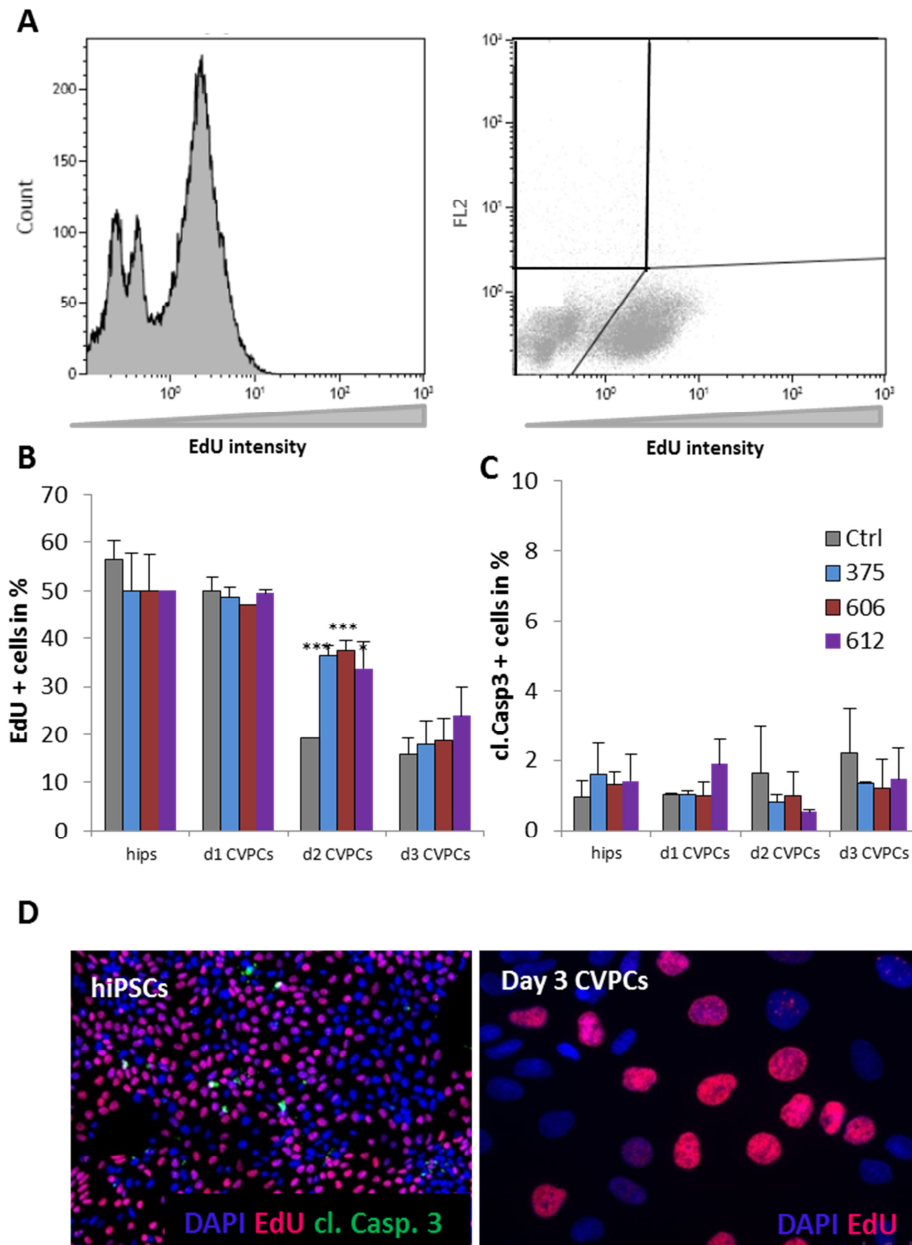


Figure 23: Proliferation analysis of HLHS patient lines compared to control lines during application of the three day CVPC differentiation protocol. Incorporation of EdU for two hours before analysis using the click-iT® EdU Assay. **(A)** Representative flow cytometry plot of cells after EdU incorporation. **(B)** Percentage of EdU⁺ cells after CVPC induction. **(C)** Percentage of cleaved caspase 3⁺ cells during CVPC differentiation. **(D)** Representative picture of cells incubated with EdU (red) and stained for cleaved caspase 3 (green) and DAPI (blue). n=3. Day 2 CVPCs: p=0.006 for 375, p=0.0007 for 606 and p=0.038 for 612. * p value ≤ 0.05; ** p value ≤ 0.01; *** p value ≤ 0.01

3.5. Apoptosis analysis during cardiac differentiation of HLHS-hiPSCs

To rule out the possibility that increased cell death is the cause of the changes in proliferation, apoptosis was evaluated during CVPC differentiation using a cleaved caspase 3 antibody for flow cytometry as well as immunofluorescence staining. No differences between patient and control lines were observed neither on hiPSC stage nor on cells differentiated for 3 days towards cardiac precursors (~1-2%) (Fig. 23C and D).

3.6. Cell cycle analysis during cardiac differentiation of HLHS-hiPSCs

We further evaluated the cell cycle distribution during CVPC differentiation aiming to support the observed proliferation phenotype. The cell cycle length, especially the length of the G₁ phase, is an indicator of the progression of differentiation of hiPSCs towards more specialized tissues. A longer G₁ phase is representing naïve cells in a pluripotency stage which is prolonged during differentiation³⁵². Hence, we applied a PI dye on patient and control hiPSCs being induced to form cardiac precursors for 0 up to 3 days. PI binds to DNA and thus, the DNA content of the cells can be quantified by flow cytometry thereby defining the cell cycle stage of the cells³⁵³. As expected, all lines show the same pattern of cell cycle distribution at the pluripotency stage with around 30% of the cells in the G₁ phase. At day 1 after induction, the control lines as well as 612 and 606 patient iPSC lines exhibited a reduced number of cells in the G₁ phase of around 15% while the 375 line did not show any change in numbers. Upon further differentiation, all patient lines retain the low number of cells in the G₁ phase while the control lines showed the expected increase of cells in the G₁ phase to ~60% and this difference in cell number in the G₁ phase is statistically highly significant. However, all three patient lines were able to reach this level at day 3 of CVPT differentiation only, whereas the control lines do not increase numbers of cells in G₁ phase any further at day 3, supporting the hypothesis of a prolonged differentiation into CVPCs again (Fig. 24).

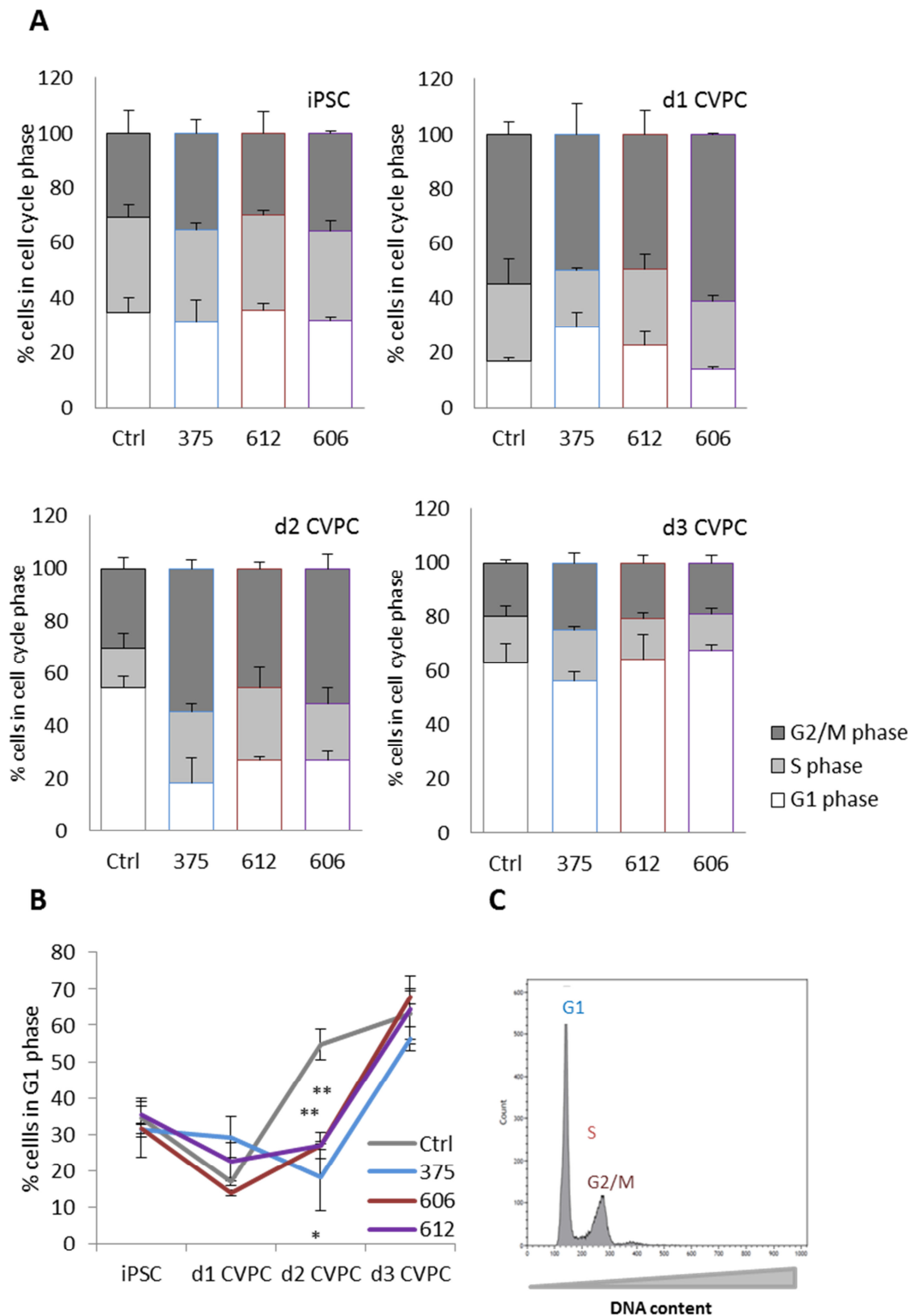


Figure 24: Validation of cell cycle phase distribution using PI DNA staining. (A) Analysis of HLHS patient and control lines stained with PI during CVPC differentiation by flow cytometry. (B) Percentage of cells in G₁ phase after CVPC induction. n=3. Day 2 CVPCs, G₁ phase: p=0.02 for 375, p=0.004 for 606 and p=0.007 for 612. * p value ≤ 0.05; ** p value ≤ 0.01; *** p value ≤ 0.001. (C) Representative flow cytometry plot of cells after PI staining.

3.7. Ciliogenesis analysis in HLHS-hiPSC-derived CVPCs

The obtained results raised the question of a mechanistic link between the discovered transcriptional differences and proliferation as well as cell cycle progression defects indicating a differentiation delay. As described in the introduction, recent publications could demonstrate a direct interaction of the cell cycle and differentiation capacity with ciliogenesis and autophagy which raised our interest in investigating possible alterations in these cellular processes.

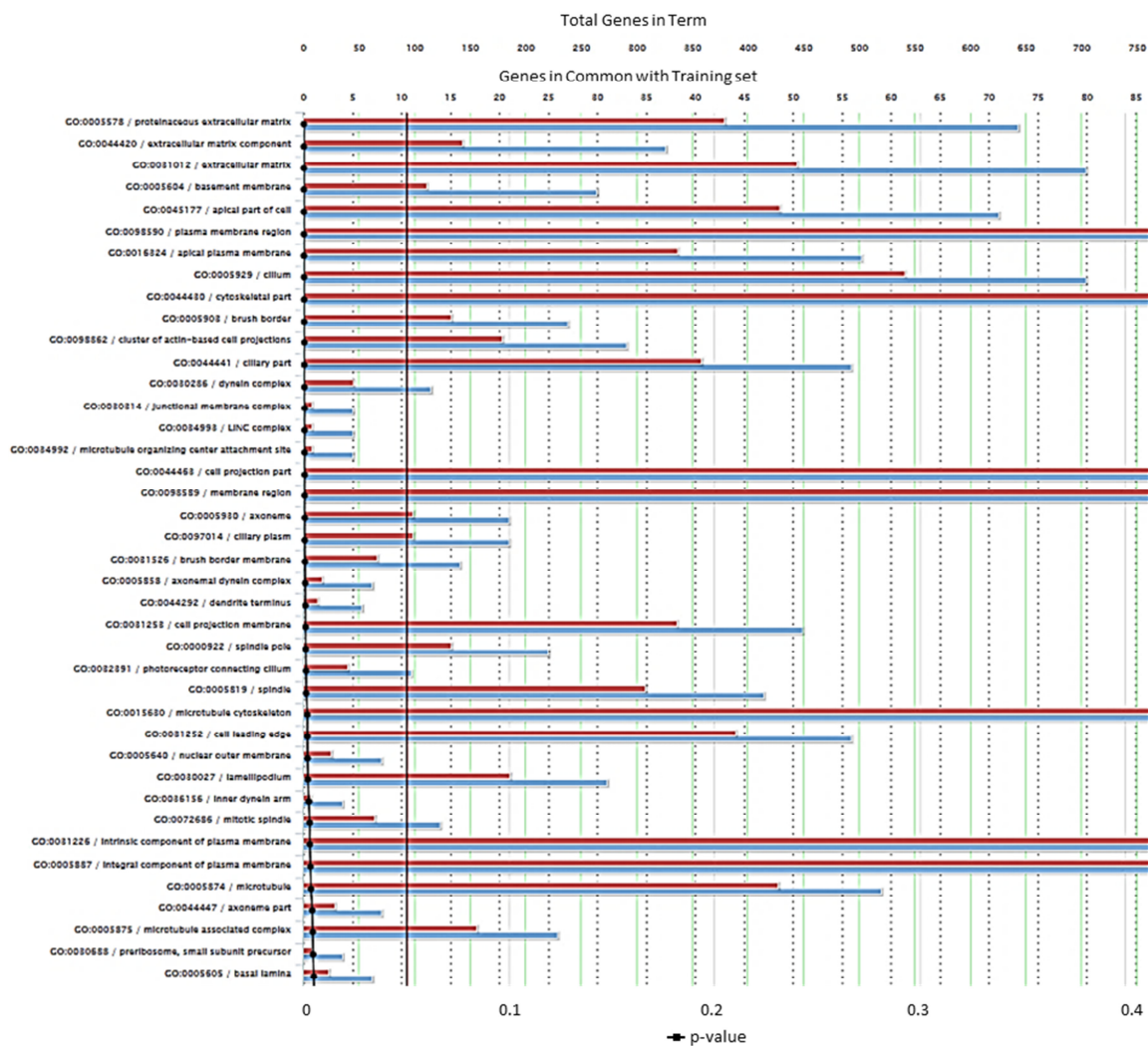


Figure 25: Enrichment analysis of parental inherited variants of the reprogrammed patient lines. TopGene Suite. GO term: Cellular component. Most significant hits ranked for p-values. Selected cut-off for p-value: 0.05.

To find a possible link of these two defects, we more deeply reviewed the results obtained in the *de novo* analysis (chapter 3.2). Interestingly, several cilia-related genes were found in the *de novo* analysis of the HLHS trios. Moreover, further consideration

of parental inherited variants of all three reprogrammed patients revealed a significantly enriched number of mutations in cilia-related genes (Fig. 25). These findings supported our hypothesis of an involvement of the ciliary signalling centre in the observed phenotype.

To compare the structure and function of the ciliary compartment of the patient hiPSC lines with control lines, we first performed expression profiling of GLI, part of the main signalling pathway SHH that is located in the cilium at day 3 of progenitor differentiation. The mRNA expression levels of GLI1 and GLI2 were significantly downregulated in the patient-specific iPSC lines 606 and 612 while the line 375 showed a significant upregulation of GLI1 and GLI2 expression compared to control lines (Fig. 26A). Protein expression analysis confirmed the opposite effect of GLI1 expression seen in the 375 and 606 line with around 2-fold increased protein levels for 375 while the 606 line showed reduced GLI1 protein levels by up to half. The 612 line instead exhibited an 1.5-fold increased expression (Fig. 26B and C).

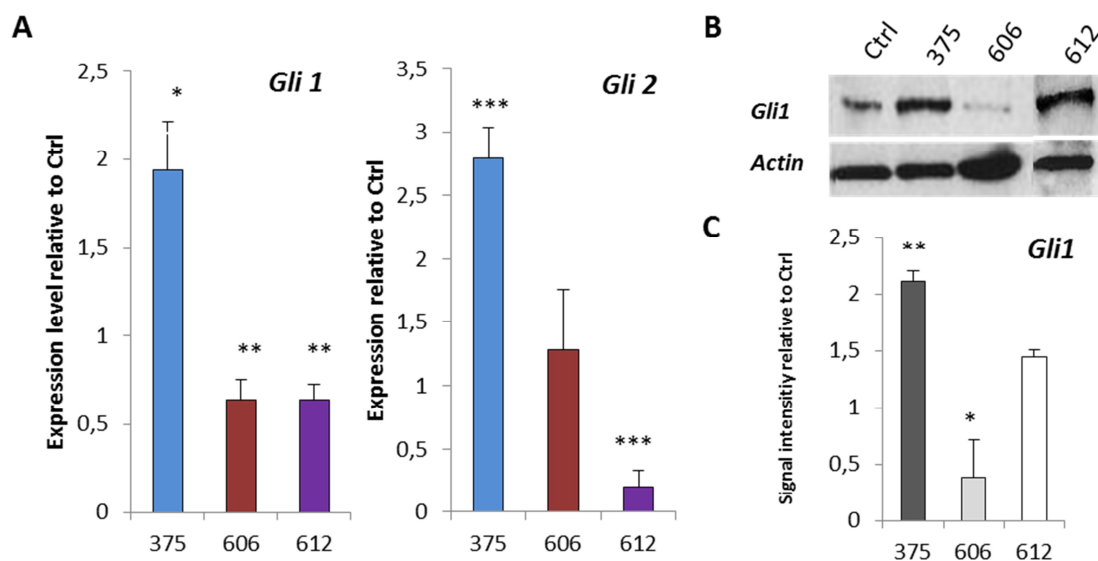


Figure 26: Expression of GLI proteins in the HLHS patient lines at day 3 of CVPC differentiation. (A) mRNA expression of GLI1 and GLI2. GLI1: n=2, p-values p=0.03 for 375; p=0.02 for 606; p=0.005 for 612. GLI2: n=3, p=0.0002 for 375, p=0.0005 for 606, p=0.49 for 612 (B) Protein expression of GLI1, Representative western blot picture and (C) statistical analysis of the signal intensity using ImageJ, normalized to actin. n=2. p=0.008 for 375, p=0.04 for 606 and p= 0.067 for 612. * p value ≤ 0.05 ; ** p value ≤ 0.01 ; ***p-value ≤ 0.001 .

Subsequent structural analysis of cilia was conducted by immunofluorescence staining for acetylated tubulin and pericentrin in day three CVPCs derived from patient as well as control hiPSC lines (Fig. 27A and B). The cells were seeded in high density to direct

cells in the G_0 phase of the cell cycle and thereby stimulating ciliogenesis. Confocal imaging evaluation of the cells was performed at the Institute of Diabetes and Regeneration Research at the Helmholtz institute in Munich by Felizitas Schmidt (AG Prof. Heiko Lickert). Hereby, the CVPCs to be analysed were chosen from regions of the slide that showed the same cell confluency (30-40%) to guarantee similar conditions (Fig. 27C). We could observe a reduced number of ciliated cells in the 606 hiPSC line (~10%) while the 375 and 612 patient hiPSC lines showed a higher number of cells forming cilia (~60%) compared to control iPSC lines (~30%) (Fig. 28D). While 606 and 375 show the same direction seen in the expression data of *GLI1*, the 612 line showed alterations that go in different directions (Fig. 26). The cilia length quantification followed the same trend observed in the cilia number analysis, where the 606 hiPSC line exhibited shorter cilia while the CVPCs derived from the 375 and 612 hiPSC lines had longer cilia, even though these differences could not be proved to be statistically significant (Fig. 27E).

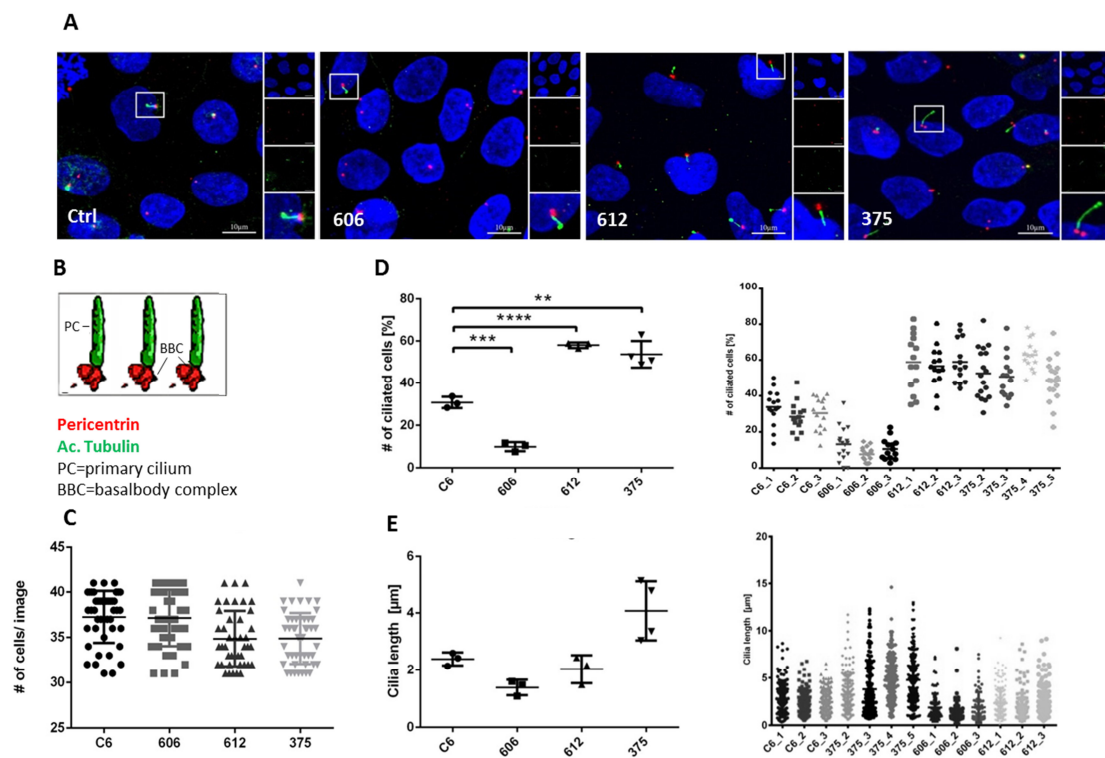


Figure 27: Cilia number and length analysis in d3 CVPCs of HLHS patient lines vs control. (A) Example fluorescence pictures of cilia stainings using acetylated tubulin and pericentrin d3 CVPCs of the HLHS patient lines and the control line. (B) Outline of the staining strategy (C) Cell density distribution of cells analysed. (D) Cilia numbers of 3 days induced CVPCs of HLHS patient and control lines. $n = 3$ per cell line. ~500-600 cells per sample (= 1500-1800 cells per cell line) (E) Cilia length in μm of CVPCs 3 days after inductions of HLHS patient and control lines. $n = 3$ per cell line. * p value ≤ 0.05 ; ** p value ≤ 0.01 ; *** p value ≤ 0.001 . Confocal z-stack images.

3.8. Autophagy analysis in HLHS-hiPSC-derived CVPCs

Due to the close interplay between ciliogenesis and autophagy regulation and the fact that the process of autophagy acts as a key regulator in differentiation progression of precursor cells during embryonic development described in the introduction part, we investigated next whether the observed cilia phenotype could lead to autophagy dysregulation and consequently to a differentiation defect of the CVPCs derived from the HLHS patient-specific hiPSCs. Autophagy induction can be measured by the quantification of p62 protein levels. The role of p62 is to link polyubiquitinated proteins to the autophagy machinery. Therefore, the protein binds to LC3 after autophagy induction and is internalized during autophagosome formation following degradation upon fusion of the autophagosome with a lysosome²¹⁰. Consequently, the amount of detectable p62 protein decreases during autophagy. We tested several autophagy activators for their ability to induce autophagy in the patient-specific hiPSC lines compared to control hiPSCs. The strongest autophagy stimulation was achieved by the substance Brefeldin A, a lactone antiviral that is known as an autophagy inducer (Fig. 29C)³⁵⁴. Contrarily, in all patient-specific hiPSC lines the detected p62 protein levels were much higher compared to the control suggesting a defect in autophagy induction in these lines (Fig. 28).

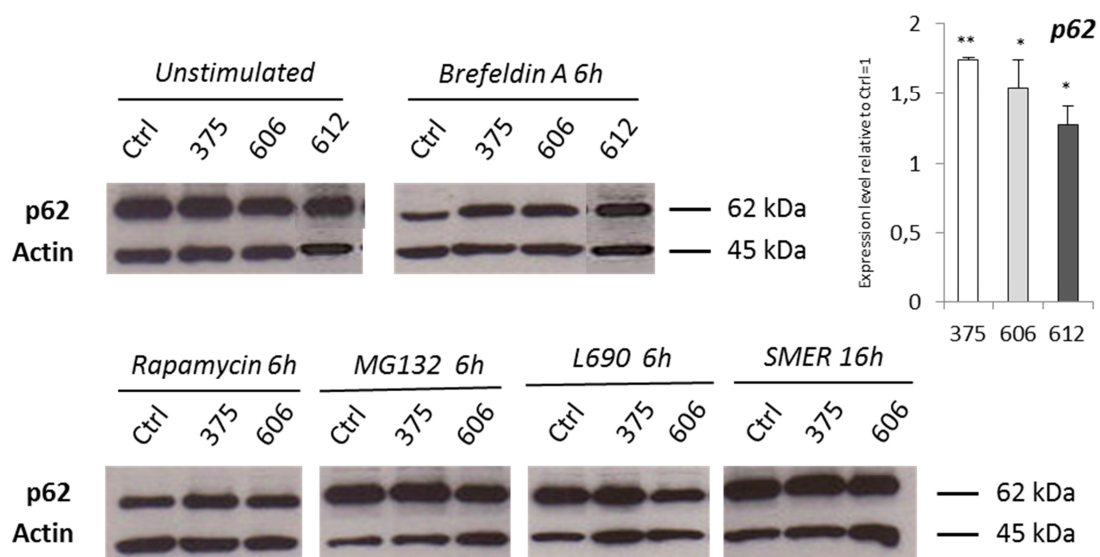


Figure 28: Analysis of autophagic response in patient compared to control lines (A) Autophagy induction in day 3 CVPCs of HLHS patient and control lines applying different activators. **(B)** Statistical analysis of Brefeldin A stimulation. $n=2$, $p=0.006$ for 375; $p=0.05$ for 606; $p=0.043$ for 612. * p value ≤ 0.05 ; ** p value ≤ 0.01 ; *** p value ≤ 0.01 .

3.9. Induction of the HLHS phenotype by autophagy inhibition in control hiPSCs

Linking the observed autophagy defect to the cell cycle progression delay as well as the transcriptional expression alterations, we inhibited autophagy in control hiPSCs via addition of the autophagy inhibitor CQ, an antimalarial drug³⁵⁵, 1.5 days after CVPC induction. In this way, we tried to mimic the transcriptional and cell cycle phenotype seen in patient-derived CVPCs (Fig. 29C).

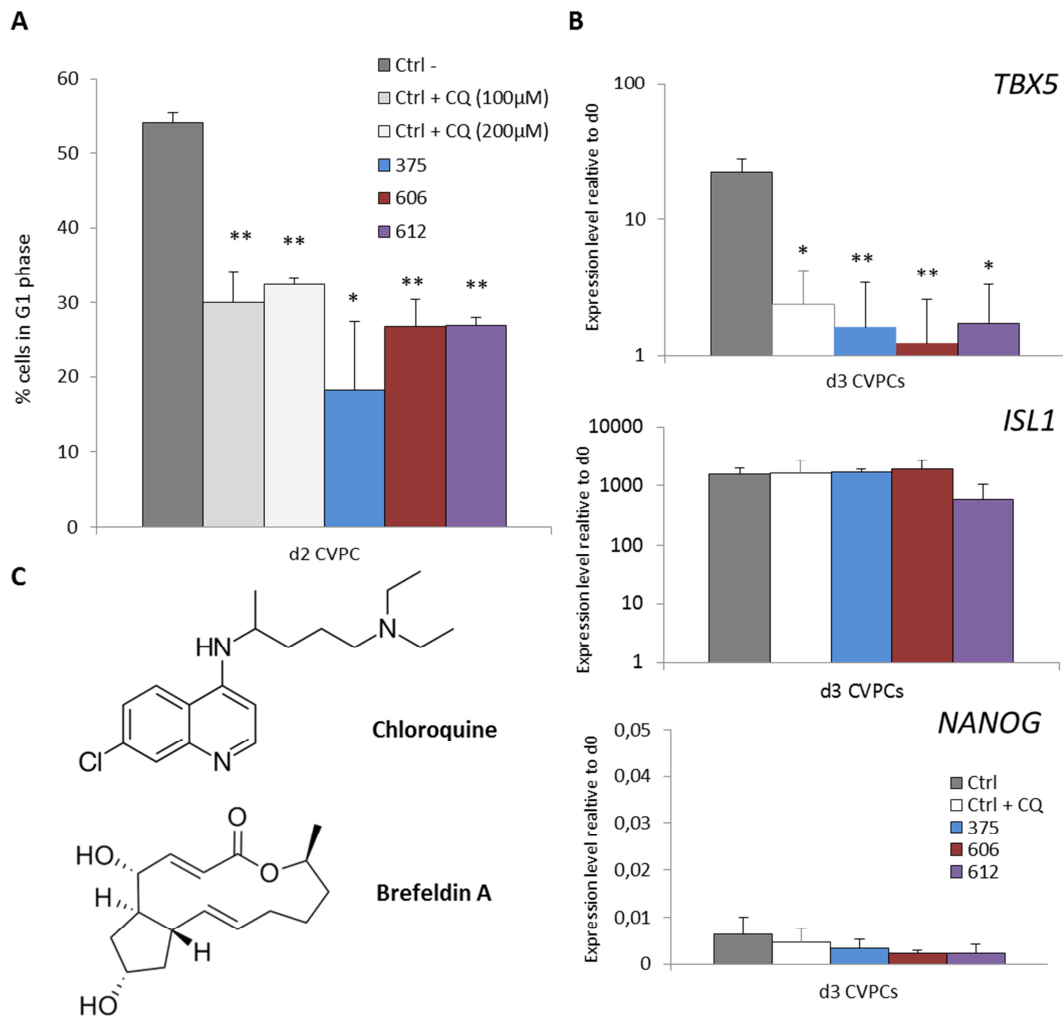


Figure 29: Phenotype induction in control hiPSC lines through autophagy inhibition by CQ. (A) Number of cells in G₁ phase at day2 of CVPC differentiation upon autophagy inhibition by chloroquine (100μM or 200μM). CQ incubation was started 1.5 days after CVPC induction for 12 hours. Results were compared to patient and control numbers. p=0.02 for 375; p=0.004 for 606; p=0.007 for 612, p=0.017 for Ctrl + CQ (100 μM); p=0.003 for Ctrl + CQ (200 μM). (B) Expression of TBX5, ISL1 and NANOG at day 3 of CVPC differentiation after autophagy inhibition by 100 μM CQ. CQ incubation for 12 hours at day 1.5 of CVPC induction. n=2. TBX5: p=0.003 for 375; p=0.002 for 606; p=0.03 for 612, p=0.016 for Ctrl + CQ. * p value ≤ 0.05; ** p value ≤ 0.01; *** p value ≤ 0.01. (C) Structural formula of autophagy inhibitor Chloroquine and autophagy inducer Brefeldin A.

Upon stimulation of 1.5 days induced CVPCs with CQ for 12 hours, the number of cells in the G₁ phase control lines could be significantly reduced to around 30% at day 2 after induction, reaching the levels seen in the patient lines (Fig. 29A). Additionally, the inhibition lead to a reduction of *TBX5* transcription to patient levels while *ISL1* and *NANOG* expression remains unaltered (Fig. 29B).

3.10. Analysis of disease-causing *de novo* mutations of interest

In the next step, we analysed whether the observed phenotype in terms of cardiac malformation and ciliogenesis defects can be linked to the “lead” *de novo* mutations of each line, which occurred in more than one patient. First, we investigated if and in which cardiac progenitor population the mutations are expressed. Therefore, we used a mESC system that marks FHF progenitors during cardiac differentiation through Nkx2.5 enhancer activity linked to YFP expression. We compared the expression of all *de novo* mutations to the SHF population, marked by Isl1-Cre and to cardiomyocytes.

Expression analysis of mutated genes in murine FHF and SHF progenitors

A microarray analysis of the mES cell lines differentiated towards cardiac progenitor cells by undirected differentiation using the EB formation method was performed by IMG^M Laboratories using the platform *Illumina MouseRef-8 v2.0* (in collaboration with the AG Krane at the German Heart Centre Munich). In this array we compared Isl1-Cre-YFP mES cells after 5 days of cardiac differentiation with mouse ES cells stably transfected with GFP under the control of an Nkx2.5 enhancer specific for first heart field cells in mice that were differentiated for five days into cardiac progenitors as well (Fig. 30A). The expression of key genes such as ISL1 and the marker protein YFP were tested by qRT-PCR as a quality control (Fig. 30B).

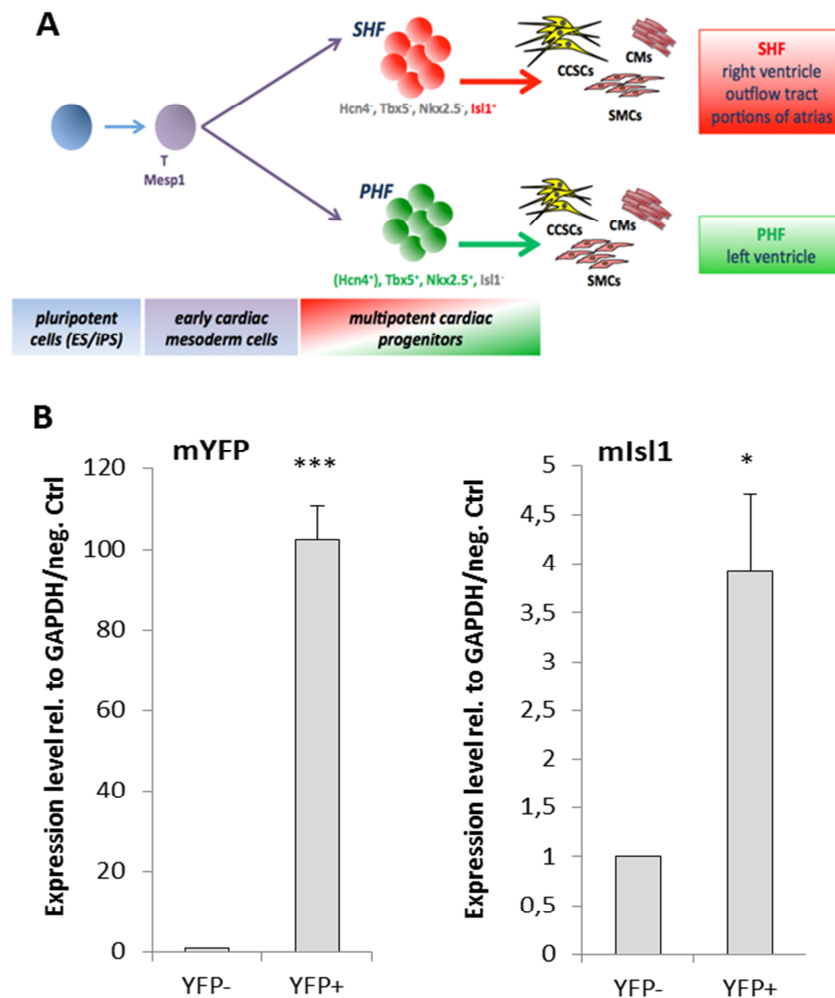


Figure 30: Preparation of mES cells for cardiac progenitor analysis in a microarray. (A) Scheme of the development of the cardiac progenitor cell populations SHF and PHF sorted by FACS. FHF population marked by GFP, generated from a mES cell Nkx2.5 enhancer line. SHF population marked by YFP, generated from mES cells marked by Isl1 Rosa YFP **(B)** Expression analysis of YFP and Isl1 in day 5 cardiac progenitors of the Isl1 Rosa YFP mES cell line relative to GAPDH, compared to mES cells of this line. n=3. p=0.00006 for YFP expression differences, p=0,006 for Isl1 expression differences. * p value \leq 0.05; ** p value \leq 0.01; *** p value \leq 0.01.

The results of the array were analysed regarding the TOP25% genes that show increased expression in the cardiac progenitor cells and cardiomyocytes compared to negative population (Fig. 31A). We found that most of the genes (20) that were *de novo* mutated in the child affected by HLHS were expressed in all three examined populations, while 14 genes were expressed in the progenitor populations, 9 of them in both FHF and SHF, 4 solely in the FHF and 1 only in the SHF. Considering the inherited mutations, so called “rare variants”, again most of the variants were expressed in all three populations (2262), followed by the complete cardiac progenitor population (394). In isolated cardiomyocytes, a high number of the rare variants were expressed as well (Fig. 31B and C).

The lead *de novo* mutations DENND5B and FGFR1 were expressed in mESC-derived FHF progenitors as well, while MACF1 expression was detected to higher levels in the negative population, assumed to consist mainly of SHF cells (Fig. 31D).

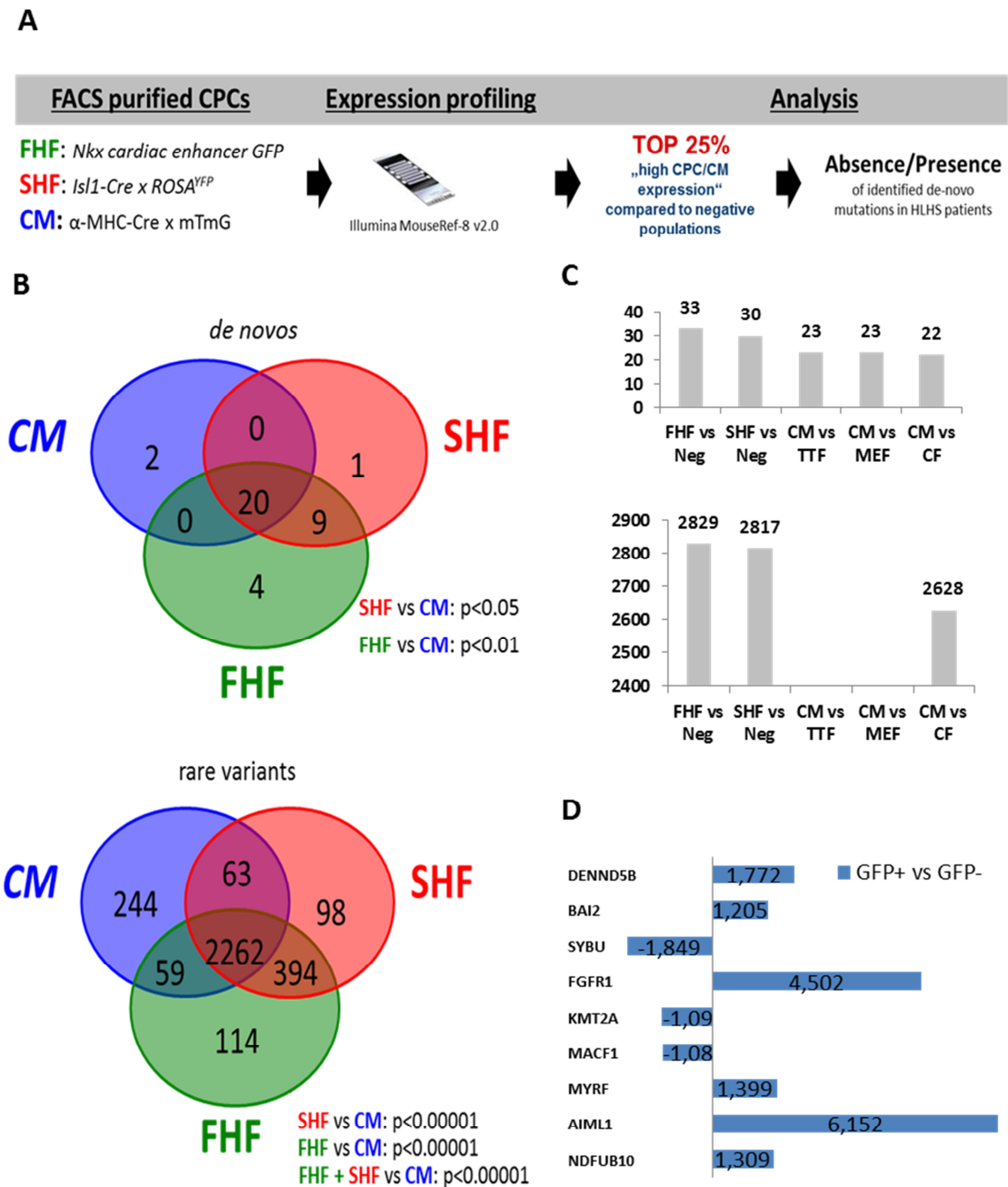


Figure 31: Expression of *de novo* mutations and rare variants in mouse cardiac progenitor cells. (A) Outline of the assay. (B) Distribution of *de novo* and rare variants. (C) Overall frequency of *de novo* mutations and rare variants in progenitor cells and cardiomyocytes. (D) Expression of *de novo* mutated genes of HLHS cell lines in GFP/YFP⁺ murine progenitors compared to a negative population. n=3.

mRNA expression analysis

To further identify a potential contribution of the lead *de novo* mutations in the manifestation of the disease, we analysed the expression levels of these proteins in control lines in respect to the lines carrying the respective mutation. We found no differences in mRNA expression of the mutated proteins at the pluripotent stage as well as in 3 days old CVPCs (Fig. 32)

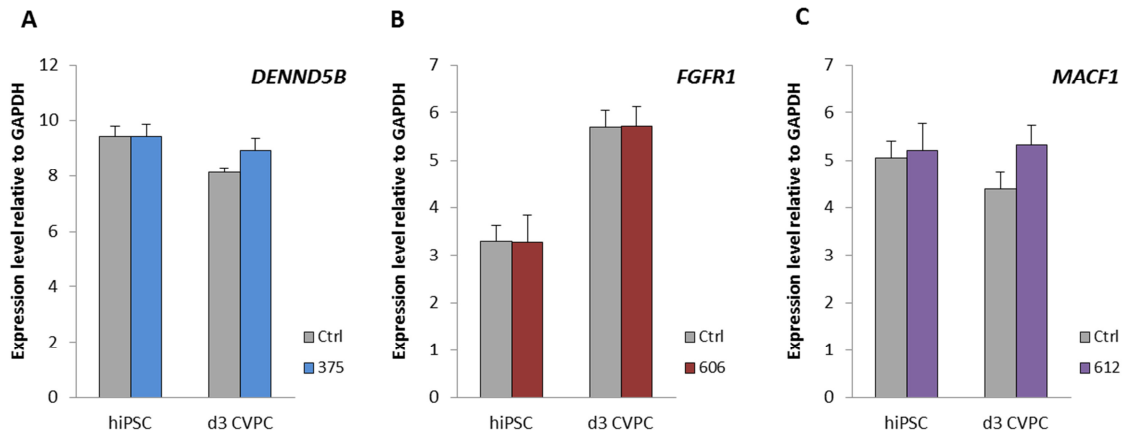


Figure 32: qRT-PCR analysis of mutated genes in patient hiPSC lines compared to control. (A) DENND5B mRNA expression in hiPSCs and d3 CVPCs of the patient line 375 vs. a control line. (B) mRNA expression of FGFR1 in hiPSCs and d3 CVPCs of the patient line 606 vs a control line. n=3. (C) mRNA expression of MACF1 in hiPSCs and d3 CVPCs of the patient line 612 vs. a control line.

3.11. Molecular and functional analysis of DENND5B

It has already been described that FGFR1 and MACF1 play a role in heart development^{356,357}. In contrast, nothing is known about physiological functions of the GEF DENND5B. Therefore, we focused on DENND5B to further elucidate the role of *de novo* mutations in the onset of HLHS. We could show that DENND5B is expressed in mESC-derived FHF progenitors (Fig. 31). Evaluating the functional activity of the mutated DENND5B protein (Fig. 33A and B) we found significant alterations in RAB39 binding ability of the mutated DENND5B. The GDP release and GTP hydrolysis assays as direct readouts of RAB protein binding activity was performed at the Department of Biochemistry at the University of Oxford in the group of Prof. Francis Barr. Hereby, the DENND5B was incubated with different Rab proteins in presence or absence of guanine nucleotide exchange factors (GEFs) that mediate the GDP release and GTP hydrolysis. Upon stimulation with WT and mutated DENND5B, the mutated

DENND5B, the mutated GEF exhibited a decreased ability to hydrolyse GTP (Fig. 33C). Moreover, GDP was released from the Rab proteins to a different extend. While the wildtype DENND5B showed an increased GDP release if incubated with Rab 39a and b, incubation with the mutated DENND5B lead to a significantly reduced release of GDP (Fig. 33D).

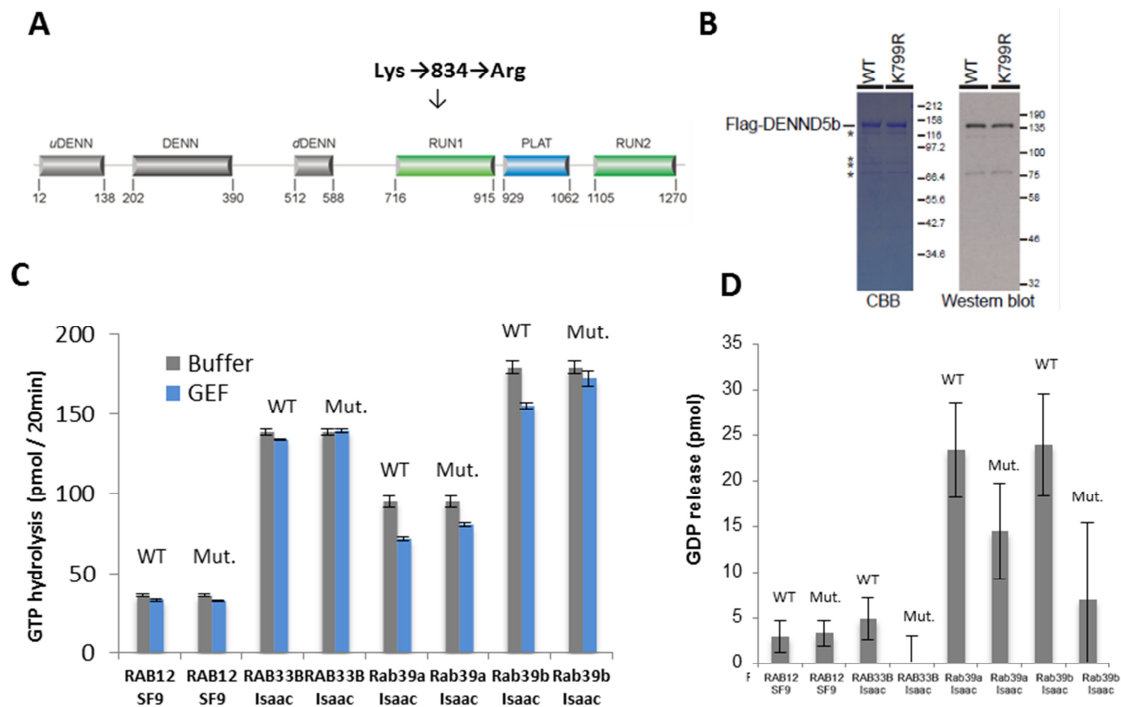


Figure 33: Impaired binding of Rab39 to the mutated DENND5B Protein. (A) Scheme of domains in the DENND5B protein including the mutation site carried by the patient iPSC line and RAB binding sites. (B) Mass spectrometry and western blotting was performed to exclude the presence of additional proteins with potential Rab GEF activity (C) GTP hydrolysis of different Rabs upon incubation with WT and mutated DENND5B (D) GDP release after WT DENND5B and mutated DENND5B (GEF) binding to different Rabs. n=3.

Heart development after in vivo morpholino knockdown of Dennd5b in Xenopus

To further elucidate the functional consequences of the *DENND5B* loss of function mutation in cardiogenesis, we investigated the heart development *in vivo* in *Xenopus laevis* after *Dennd5b* morpholino oligonucleotide mediated knockdown, a model organism which has been proved as a reliable system for studying early cardiac development before. The experiments were performed at the Institute of Biochemistry and Molecular Biology of the University of Ulm (Prof Michael Kühl).

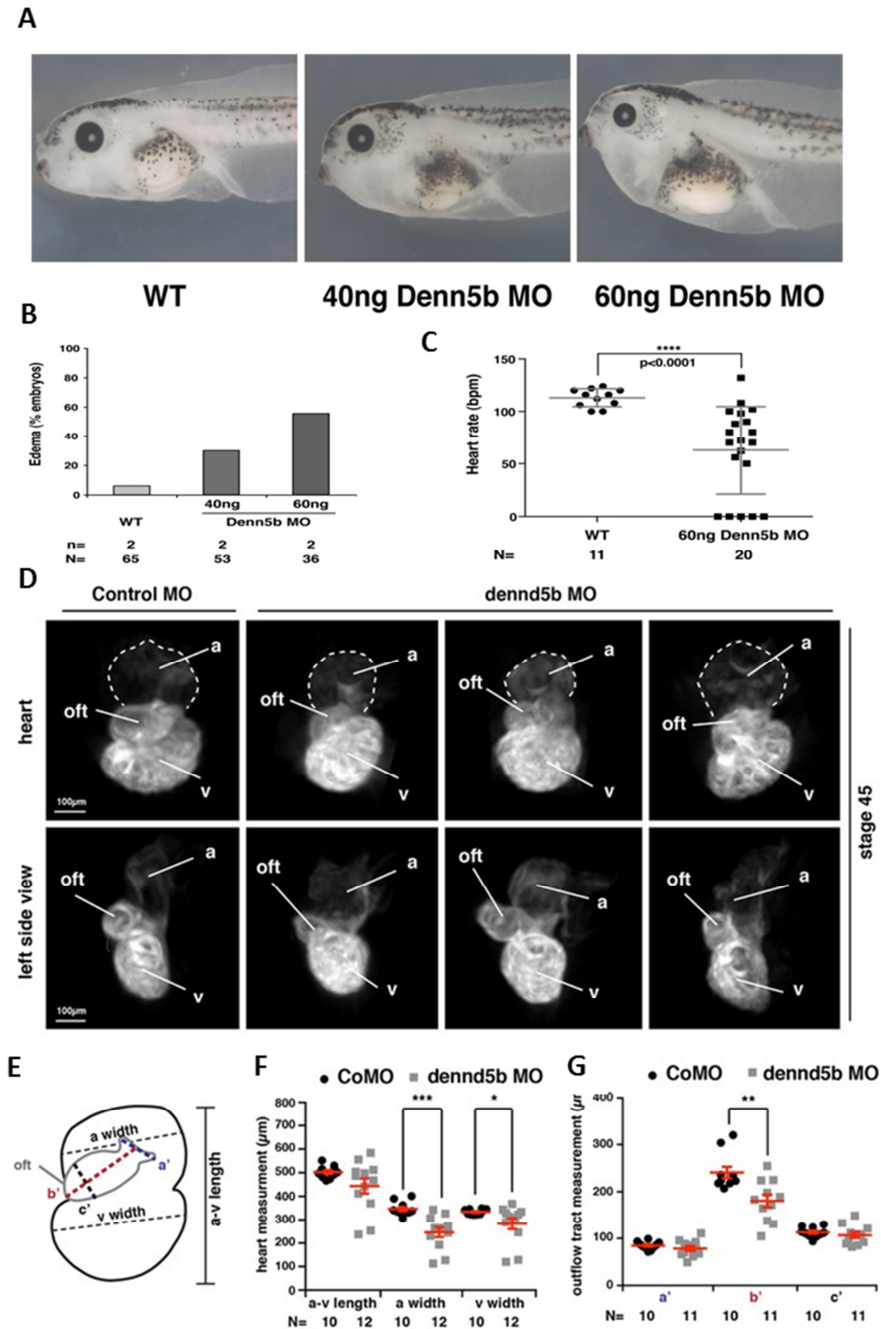


Figure 34: Functional and structural defects in the heart of *Xenopus laevis* after Dennd5b knockdown. (A) Representative picture of oedema formation in *Xenopus laevis* after an increasing dose of Dennd5b morpholino injection. (B) Dose-dependent number of embryos showing oedema after knockdown of Dennd5b. (C) Heart rate of embryos injected with 60ng Dennd5b morpholino. n=2 with N embryos analysed per experiment. (D) Morphology of the heart of *Xenopus laevis* after Dennd5b morpholino injection. (E) Illustration of length and width measurement parameters of the heart and outflow tract. (F) Heart size parameters of Dennd5b morpholino knockdown compared to control morpholino injection. (G) Comparison of outflow tract length and width of Dennd5b mutants and embryos injected with a control morpholino. a= atrium, v= ventricle, oft= outflow tract, CoMo= Control morpholino. * p value ≤ 0.05 ; ** p value ≤ 0.01 ; *** p value ≤ 0.01 .

We could show that a *Dennd5b* morpholino knockdown in *Xenopus laevis* lead to dose-dependent increasing numbers of embryos showing oedema formation compared to wildtype embryos and the manifestation of this phenotype was more severe upon injection of a higher dosage of the morpholino (Fig. 34A and B). Moreover, the heart rate was reduced (Fig. 34C). Both results represent an impaired heart function after *Dennd5b* knockdown. Examining the heart structure of these embryos, we could observe a striking phenotype with a severely underdeveloped ventricle and drastically reduced heart size in a dose-dependent manner (Fig. 34D and F). Additionally, the outflow tract length and width was reduced after injection of an increasing dosage of *Dennd5b* morpholino (Fig. 34G). The heart phenotype could be reversed by the additional injection of the wildtype *Dennd5b* to the *Dennd5b* morpholino mutants.

Analysis of ciliogenesis after in vivo morpholino knockdown of Dennd5b

Additionally, the function of DENND5B in ciliogenesis and cilia function was investigated to confirm the cilia phenotype seen in the HLHS hiPSC patient lines. Therefore, a *Dennd5b* morpholino knockdown in zebrafish was performed by Teresa Casar Tena at the Institute of Biochemistry and Molecular Biology of the University of Ulm (AG Kühl), a well-established model system for cilia-related phenotype illustrations in the group of Prof. Michael Kühl. We found that a loss of *Dennd5b* interferes with heart looping, visualized by *in situ* hybridization for cardiac myosin light chain 2 (*cmlc2*) as a myocytic marker. Not only was the heart phenotype of *Xenopus laevis* confirmed by the observation of a significantly enriched number of embryos displaying no loop (~15%) or L-loop (~20%) of the heart compared wildtype embryos, but also indicate the results a possible defect in cilia function (Fig. 35A). Immunostaining of acetylated tubulin to visualize cilia in the Kupffer's vesicle illustrated a similar number of cilia but a reduced length. Also *Gli1* expression, a downstream target of the SHH pathway, was decreased by 50%, which can be directly correlated to cilia length and function (Fig. 35B-E).

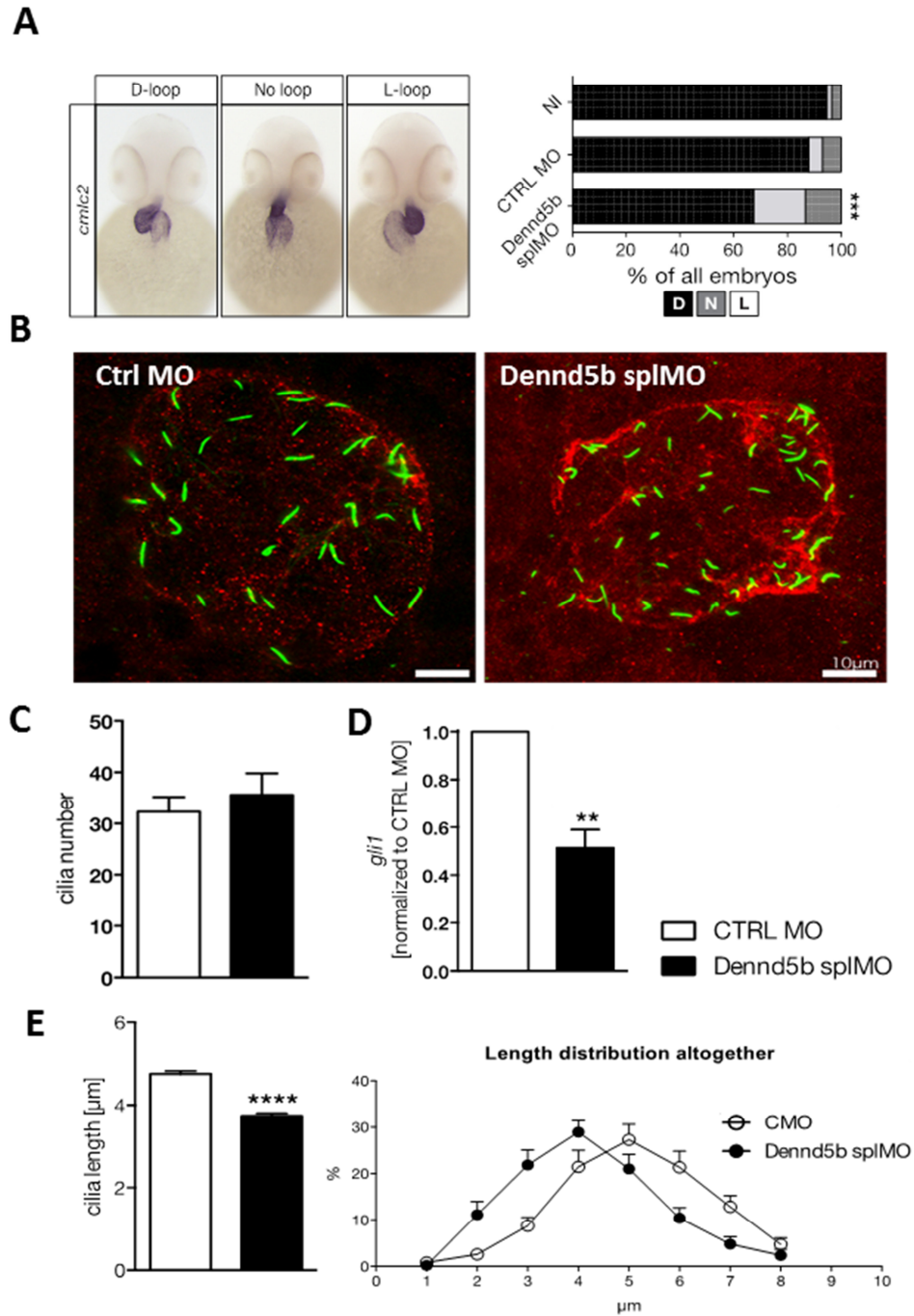


Figure 35: *In situ* analysis of heart phenotypes connected to cilia function after Dennd5b morpholino knockdown (Dennd5b splMO) in zebrafish. (A) Heart looping visualized by *cmlc2* staining in zebrafish embryos injected with Dennd5b morpholino. $n=4$ experiments with 114-120 embryos in total. $p=0.0002$ All experiments compared to control morpholino injection (CTRL MO) and no injection (NI). Two tailed Fisher's exact test. (B) Cilia analysis in Kupffer's vesicle of zebrafish after Dennd5b morpholino knockdown. Cilia staining for acetylated tubulin (green) in zebrafish injected with control morpholino or Dennd5b morpholino. (C) Number of cilia counted in the Kupffer's vesicle upon morpholino knockdown compared to control embryos. (D) Gli1 expression after Dennd5b morpholino injection compared to embryos injected with control morpholinos. (E) Cilia length analysis and length distribution after morpholino knockdown compared to control embryos. * p value ≤ 0.05 ; ** p value ≤ 0.01 ; *** p value ≤ 0.001 ; **** p value ≤ 0.0001 .

3.12. Generation and evaluation of NKX2.5 Enhancer-GFP hiPSC lines for identification of cardiac subpopulations

The NKX2.5 Enhancer construct (Fig. 13) was used for the generation of NKX2.5 enhancer hiPSCs lines to visualize a specific subpopulation of cardiac progenitors that could be assigned to FHF cells in the murine system due to the high homology between the mouse and human enhancer sequence. Therefore, the construct was transfected into control and patient hiPSCs following antibiotic selection. Upon cardiac differentiation, the control line showed NKX2.5 Enhancer GFP signal, first detected at day 6 of differentiation which stayed on until day 10 when the cells were collected for further analysis (Fig. 37). Very weak signal could also be detected in 3 day old CVPCs

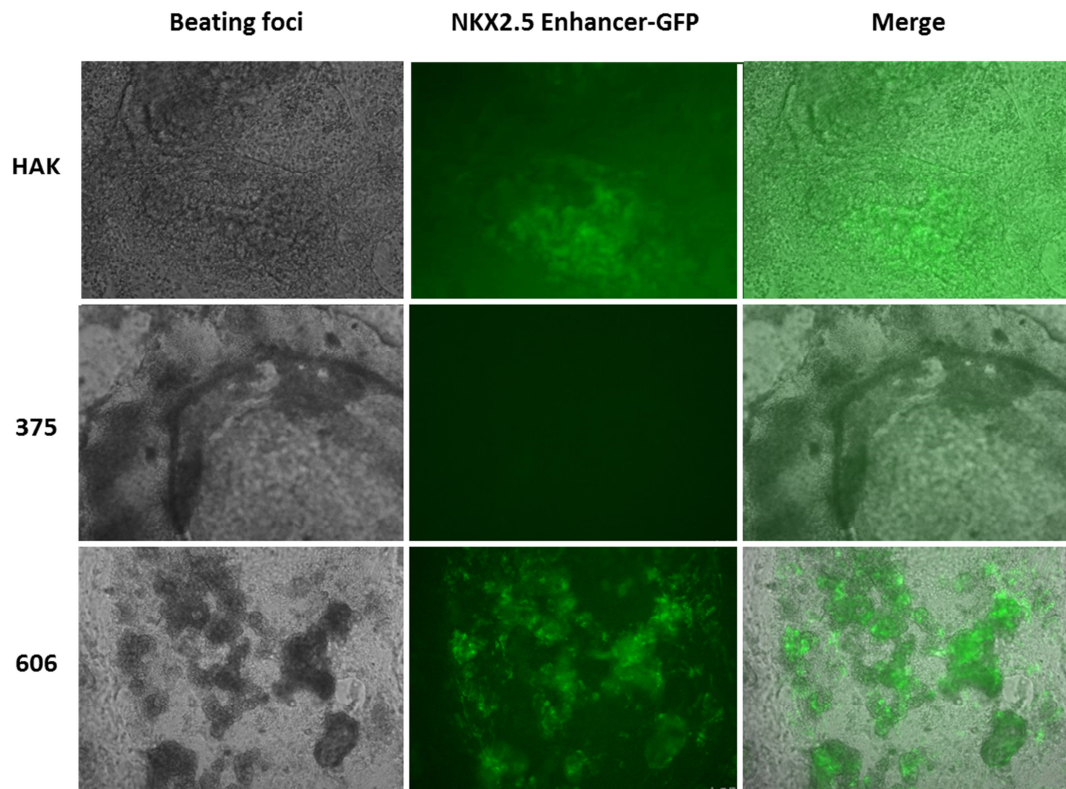


Figure 37: Analysis of NKX2.5 Enhancer expression. NKX2.5 Enhancer signal in 7 days old cardiomyocytes after cardiac differentiation of control and patient hiPSCs stably transfected with the NKX2.5 enhancer construct. Scale bar: 100 μ M.

Flow cytometry analysis of the lines 3 days after CVPC induction revealed an arising population (Fig. 38).

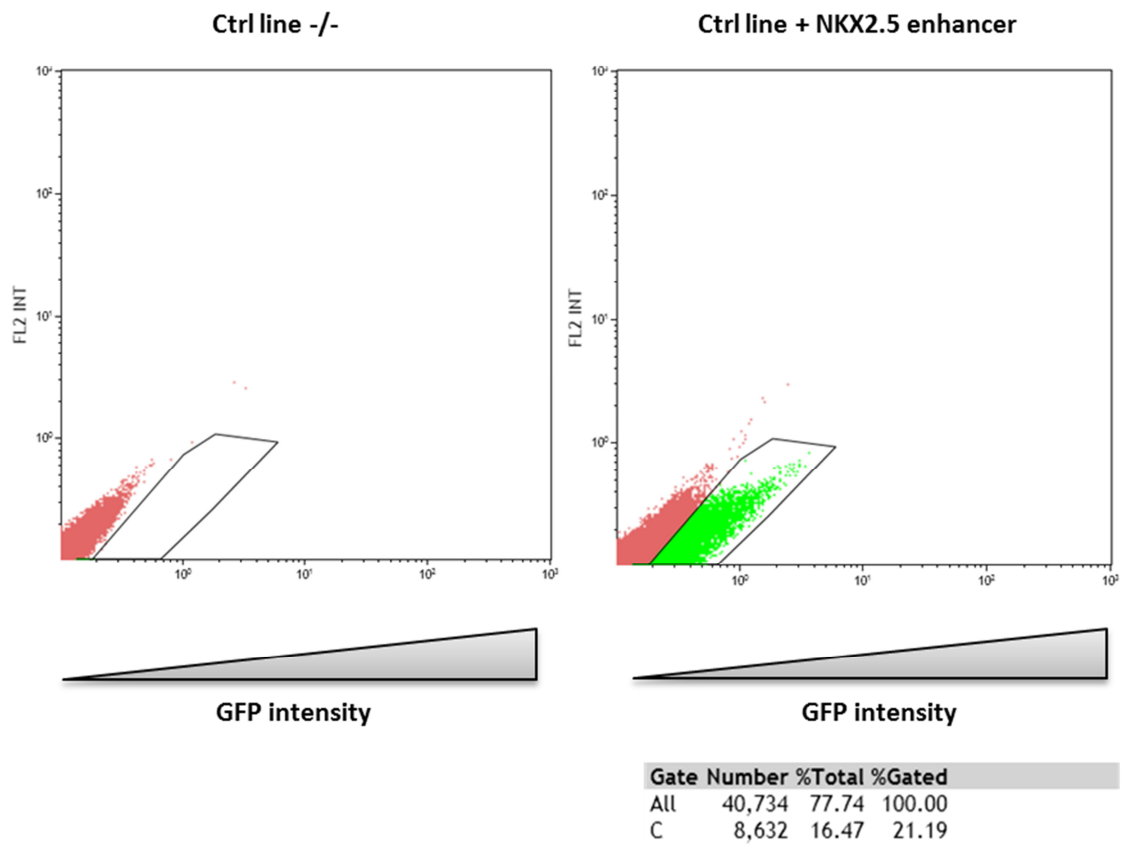


Figure 38: Representative FACS analysis of day 3 CVPCs, stably transfected with the NKX2.5 Enhancer-GFP construct.

4. Discussion

The study of 3 different HLHS patient-specific hiPSC lines along with cardiac HLHS patient material revealed a common delay in cardiac differentiation, mainly described by proteomics and transcriptome analysis, that could be assigned to alterations in cardiac progenitor population formation and function. Hereby, an intriguing link between ciliary malfunctioning, cell cycle progression delay, and autophagy induction failure could explain the molecular basis of the cardiac differentiation defect. Since major phenotypic aspects of HLHS were recapitulated in the hiPSC system, a genetic component in this congenital malformation is suggestive. Additionally, *in vivo* data gained from *Xenopus* and zebrafish morpholino knockdown analysis unravelled a new gene, DENND5B, which was target a of *de novo* mutation in one of the patients, to be crucial in cardiogenesis and cilia function as well as autophagy, thus highlighting a potential contribution of *de novo* mutations to the onset of HLHS.

4.1. Challenges in modelling complex cardiac disease as CHD

The best source of material to study diseases is the patient itself. Comparison of patient-derived diseased tissues to healthy controls has been pivotal in the understanding of the origin of numerous diseases. However, for organs that are difficult to access, e.g. the heart, it is nearly impossible to obtain patient material. We were lucky enough to have access to post-natal cardiac tissue of HLHS patients. Our collaboration partner Prof. Lutz Hein compared this patient material to cardiac tissue of “healthy” aborts of the same stages performing RNASeq analysis. Preliminary results showed a prolonged expression profile of early cardiac genes as well as reduced expression of late cardiac genes in HLHS patient material suggesting a delayed cardiac differentiation. The transcriptional profile appears to stay in a foetal stage. These results stand in line with an already published expression profiling of the atrial septum of HLHS patients conducted by gene-chip microarray analysis. In this study, significant differences between patients and healthy controls in the expression of factors controlling heart development and growth were detected. More in detail, altered gene expression levels of chromatin remodelers along with cell cycle regulators unrevealed a block in cell cycle progression,

most likely resulting in a delay in differentiation and a maturation defect in HLHS myocytes³⁵⁸. In another study, tissue samples of the right ventricle of HLHS patients were compared to those from patients born with a truncus arteriosus; differences in gene expression of proliferation and apoptosis markers as well as extra-cellular matrix components and the cardiac transcription factor NKX2.5 were detected, indicating immaturity and an imbalance in myocyte homeostasis³⁵⁹.

Analysis of patient tissue has, however, in some cases also limitations. For cardiac tissue specifically, not only the number of patients from whom material is available is restricted but also no dynamics of disease initiation and progression can be captured, since the tissue collected represents solely a snapshot of the heart in that particular stage. Moreover, for CHD, evaluation of early stages of cardiogenesis, when morphogenetic defects are expected to occur, is most relevant; but cardiac material from early-embryonic-stage aborts is very challenging to gain. To overcome these obstacles, one way is to generate patient-derived hiPSCs that can subsequently be differentiated towards cardiac structures. This would solve the problem of limited material access since these pluripotent cells are reprogrammed out of easily accessible patient material such as blood or fibroblasts. Additionally, the cardiac development can be monitored over time, including very early stages of cardiogenesis. Especially, the possibility to gain patient-specific hiPSCs created a new chance to model diseases in a human *in vitro* system within a patient-specific genetic background. This opportunity is extremely important for complex genetic disorders such as HLHS, where not a single gene variant can be assigned to the phenotype and classical disease model systems, such as knockout animals, fail to faithfully recapitulate the clinical human phenotype.

The aim of this study was therefore to model HLHS, a congenital cardiac disorder, using patient-specific hiPSCs and thereby uncovering novel molecular mechanisms that can be assigned to the onset of complex genetic diseases such as CHD.

We were able to successfully reprogram fibroblasts of three HLHS patients and subsequently differentiate those hiPSCs into cardiac progenitors as well as beating cardiomyocytes. We compared different stages of cardiac development, aiming to find out if the expressional differences seen in the HLHS cardiac tissue samples, suggesting a differentiation delay, can be recapitulated in the hiPSC system. Thereby, we also tried to understand to which stage of development and cell type this defect can be assigned. While for many adult cardiac disorders hiPSCs disease modelling is restricted by the incomplete

maturation of the formed myocytes³⁶⁰, for our purpose hiPSCs are the ideal system since early developmental stages can be investigated.

Dynamic analysis of directed cardiac progenitor as well as myocardial differentiation over time displayed a consistent dysregulation of the transcription factors TBX5 and NKX2.5 (Fig.19 and 22). These results are in line with other studies investigating transcriptional alterations in HLHS hiPSC-induced cardiomyocytes, which found expressional differences of chamber-specific regulatory genes^{341,342,346}. Transcriptional differences of crucial cardiac progenitor markers have also been described in other CHDs such as Holt-Oram syndrome^{361,362}. To exclude the possibility of an influence of the factors applied to the cells to direct the differentiation, the cells were subsequently differentiated towards cardiomyocytes using the EB differentiation protocol that spontaneously induce cardiomyocyte formation without addition of factors. The cardiomyocyte yield applying this protocol is low and therefore it is not the preferred method. Spontaneous EB differentiation of the hiPSCs revealed similar transcriptional differences in the patient hiPSC-derived cardiomyocytes, suggesting no influence or rescue of the factors applied to the cells during directed differentiation. To sum up this transcriptional analysis, the differentiation delay could be recapitulated in the hiPSC system and, interestingly, it is evident even in cardiac progenitor populations. Thus, for the first time, we have been able to assign the transcriptional phenotype to earlier stages of cardiac development by applying a specific cardiac progenitor differentiation protocol. Hereby we gained insight of early fate decisions of progenitor cells, suggesting defective specification of cardiac precursors as the main driver for the onset of HLHS. Whether the observed transcriptional differences reflect abnormalities within a specific group of progenitor cells (e.g. a delayed specification) or complete absence of specific cardiac progenitor populations remains an open question and is discussed in chapter 5.3. The current work further aimed to address how these transcriptional variations are caused. We tried to evaluate if mutated genes in HLHS patients contribute to the defective gene expression. The documented differences in cardiogenesis between patient and control hiPSCs indeed strongly suggest a genetic component in the disease etiology.

Role of de novo mutations in HLHS (Genetic inheritance model)

So far, no clear genetic inheritance model could be assigned to CHDs including HLHS, although the studies performed direct strongly towards a complex genetic disease as

described in the introduction. Along with the findings that our patient-specific hiPSC cells do have intrinsic alterations leading to a clearly defined cardiac transcriptional phenotype, the *de novo* mutation analysis performed on these three patients and 75 additional HLHS patients suggest a rather complex than monogenic inheritance model since it did not reveal individual genes showing enriched mutations. Therefore, as part of an additional collaboration, parental inherited variances were further analysed. Here, an enrichment of mutations in genes crucial for cardiogenesis was found, supporting our data of defective cardiac differentiation in patient material and during cardiac differentiation of the HLHS hiPSC lines.

We were further interested if particular *de novo* mutations of our patient hiPSCs could also be involved in cardiogenesis. Therefore, we performed *in vivo* studies in zebrafish and *Xenopus*, well-established model systems for cardiac development. Several morpholino knockdown studies have been performed suggesting a role of particular genes in the onset of cardiac diseases^{363–365}. In this context, we were especially interested if *de novo* mutations of our HLHS patients could recapitulate the cardiac phenotype seen in the hiPSC system. We were able to show a significantly impaired heart development upon DENND5B morpholino knockdown in *Xenopus*, including dramatic reduction of atrial and ventricular structures along with mild truncation of the outflow tract (Fig. 34). These observations could be confirmed in zebrafish morpholino knockdown of DENND5B, which also led to cardiac structural anomalies. Additionally, published data suggest an involvement of FGFR1 and MACF1, which were targets of *de novo* mutations in the other two patient lines, in cardiogenesis, supporting the idea of an contribution of *de novo* mutations in the development of HLHS. The role of FGFR1 in cardiac development has been previously published by the group of Cresta. They could prove that FGFR1 signalling is required for mesoderm formation and subsequent cardiogenesis in mice, showing that *fgfr1*^{-/-} knockout mice die before the heart is formed and that in embryonic bodies (EBs) derived from *fgfr1*^{-/-} mouse ES cells less beating foci were found. Additionally, the expression of mesodermal, cardiovascular progenitor as well as cardiac genes was lower, while mRNA levels of markers for other germ layers were not altered. The same effect could be seen by FGFR1 inhibition in *fgfr1*^{+/-} mES cells³⁵⁷. Knockout of MACF1 prevented primitive streak, node, and mesoderm formation and mice died during gastrulation. MACF1 interacts with AXIN and other components of the WNT inhibitory complex and upon siRNA knockdown of MACF1, WNT signalling,

important for cardiogenesis among others, was reduced³⁵⁶. This work supports the theory that our *de novo* mutations might be one reason for the development of CHD.

However, the fact that genes in which *de novo* mutations are found are by far not identical and additionally do only cluster in gene ontology groups such as cardiac developmental genes, leads to the conclusion that those findings can only be seen as an indication of a novel candidate gene. It is more likely a complex disease caused by the combination of different mutations including *de novo* mutation as well as variances inherited by the parents as already describe above. Moreover, *in vivo* gene knockout studies are solely partially transferrable to the human being and can only describe the effect of single variants on the onset of the disease, but single knockouts do not recapitulate the multifaceted phenotype. Hence, understanding the onset of HLHS ideally requires *in vivo* or *in vitro* model systems in which it is possible to introduce the multigenic background, favourable in a human setting. Current techniques allowing genetic modifications in *in vitro* and *in vivo* systems are restricted. Targeted introduction of single mutations has been successfully established in the recent decades, including homologous recombination, zinc finger (ZNF), TALEN, adeno- associated viruses (AAVs) and the latest CRISPR/Cas9 technology. Nonetheless, these techniques are still not very efficient and are very time-demanding, and targeted introduction of multiple specific mutations to closer resemble the genetic background of HLHS patients *via* Multiplex gene editing is still in its early stage. *In silico*, analytical methods to evaluate combined effects of more than a single gene variant exist only in a premature form and need to be developed further.

The restriction in genetic manipulation in *in vivo* or *in vitro* systems to model HLHS highlights the advantage of patient-specific hiPSCs in disease modelling. These cells harbour the whole set of genetic variances of the individual patient. Thus, for the discovery of mechanisms altered in HLHS, these cells represent the most promising tool. Additionally, by targeted correction of predicted disease-causing mutations using the CRISPR/Cas technology, the role of particular genes in the origin of the disease can be assessed. But here, the same restrictions described for disease modelling by introduction of disease causing mutations account, since it would also require multiple rounds of correction. Another important question in the understanding of HLHS is “what are the mechanistic consequences behind the detected gene variants and differential expression profiles?”

In general, all these *de novo* mutations can be assigned to cytoskeleton dynamics, closely linked to ciliogenesis. The abovementioned analysis of transcriptional differences in HLHS hearts by Gambetta *et al.* reveals, besides the differential expression of cell cycle genes and chromatin modifiers, abnormal transcription of microtubule polymerization genes including dyneins and microtubule associated proteins, directing towards a vesicular transport and ciliogenesis defect in HLHS hearts³⁵⁸.

4.2. Perturbations in cilia and autophagy as basis for defective cardiogenesis and CHD

Further analysis of the exome sequencing of 78 trios unravelled a significantly enriched number of *de novo* and inherited mutations in the GO category “cilia” (Fig. 25) thereby, along with the *de novo* mutations involvement in ciliogenesis, directing the focus on the role of cilia and associated mechanisms in the onset of this cardiac disorder. To investigate whether cilia structure and function are abnormal during cardiogenesis in HLHS patients compared to healthy controls, we assessed this organelle on cardiac progenitor cells and found a significantly altered number of ciliated cells and differences in cilia length in hiPSC-derived progenitors of the HLHS patients (Fig. 27). In addition, altered GLI1 expression, a major component of the ciliary SHH signalling, could be detected on mRNA and protein level (Fig. 26).

Current knowledge suggests a strong connection of cilia dysfunction with CHDs, indicating a crucial role of cilia during cardiogenesis^{176,189}. Recently, Li *et al.* published a mutagenesis study unravelling several mutations in cilia-related genes leading to congenital cardiac malformations¹⁹¹. Interestingly, a study published in 2016 revealed a significantly enriched occurrence of cilia-mutations in children with HLHS that show an additional neurodevelopmental retardation supporting our hypothesis of an involvement of ciliary malfunction in the onset of HLHS³⁶⁶.

The cilia defect seen in HLHS hiPSC could be recapitulated by targeted knockdown of DENND5B in zebrafish, a well-established model system for ciliogenesis, analysing several cilia-related phenotypes (Fig. 35). Hence, by using this *in vivo* system we could strengthen the hypothesis of an involvement of cilia in the development of the cardiac phenotype discovered in the hiPSC system. Interestingly, ciliogenesis defects in zebrafish and *Xenopus* have been discovered also after FGFR1 morpholino. Neugebauer

et al. could prove that cilia length is reduced in FGFR1 morphants as well as after treatment with FGFR1 inhibitors. Moreover, mRNA levels of cilia genes were down-regulated upon FGFR1 signalling inhibition³⁶⁷. Additionally, May-Simera *et al.* could show that ciliogenesis is interrupted through MACF1 ablation, linking also the third *de novo* mutations to ciliogenesis^{356,368}.

Connection of ciliary defect within a cell cycle-autophagy axis

The link between cilia defects and the differentiation capacity of cardiac progenitors in HLHS is still elusive. Recently, it was shown that a connection of ciliogenesis with autophagy and cell cycle progression is crucial for specific early cell fate decisions by the discovery of the so called “Primary Cilium-Autophagy-Nrf2 (PAN) axis”. This axis connects changes in the length of G₁ phase to progress in neuroectoderm and mesoderm lineage specification, the earliest decision following hESC differentiation induction. This, in turn, changes the ciliation patterning on the cells resulting in autophagy induction. Lineage specific markers are thereby turned on, while pluripotency gene expression is downregulated¹⁹². Congenital defects caused by anomalies in one of these interconnected axis components might range from a dramatic malformation to non-existence of specific tissues rising from these lineages. Hereby, the defective component influences all the other components resulting in misexpression of important markers that define and initiate tissue patterning. Thus, the discovered ciliation defect in cardiac progenitors derived from HLHS hiPSCs might be connected with cell cycle and autophagy defects resulting in the observed dysregulation of specific cardiac progenitor markers, making it worthwhile to investigate these processes in our hiPSC system as well.

As mentioned above, the second factor of the described axis is the cell cycle, another key regulator of differentiation progression, closely connected to the proliferation speed. We saw that proliferation and cell cycle changes occurring during specification progression towards a cardiac progenitor state are delayed in HLHS hiPSCs (Fig. 23 and 24), suggesting that patient cells stay longer in a less differentiated state, showing a higher proliferation rate and shorter G₁ phase, indicated by a decreased number of cells in the G₁ phase. It is well known that pluripotent stem cells have a high proliferation rate due to a short cell cycle length (16-18h), mainly defined by an abbreviated G₁ phase (2.5h); upon differentiation induction, proliferation speed is reduced by prolongation of the G₁ phase³⁶⁹. As described in the introduction, strict temporally and spatially defined prolifer-

eration is crucial for sufficient development of the heart field populations. Gambetta *et al.* showed a dysregulation of cell cycle gene expression directing towards a block of cell cycle progression HLHS hearts³⁵⁸. This study supports our hypothesis, even though the results were obtained in a static context of human differentiated tissue, while we were able to bring these findings in the dynamic context of the cardiac development process, thus helping to better understand the direct effect of those anomalies. At day 3 of cardiac progenitor differentiation the number of patient cells caught up with the control cell levels, this suggests that HLHS iPSCs are able to differentiate towards cardiac progenitors but it requires more time. One reason for this delay could be reduced autophagy activity that might lead to delayed protein clearance.

The third component of the PAN axis is the process of autophagy. Hence, we tried to induce autophagy in our patient hiPSC lines to examine if this process is defective as well. Upon autophagy stimulation by Brefeldin A during hiPSC differentiation towards cardiac progenitors, we observed a non-response of patient cells to this induction compared to control lines, indicating a defect in the autophagic process (Fig. 28). Autophagy is required for the rapid removal of proteins during cell fate determination acting through different developmental pathways. Therefore, autophagy plays a major role in differentiation progression as well as pluripotency maintenance³⁷⁰. Increasing autophagy by mTOR inhibition or autophagy stimulation leads to an accelerated and more efficient reprogramming for instance, relieving the somatic cells from a senescence state after reprogramming induction and supporting cell cycle progression. Autophagy induction is even described to support pluripotency by expression of pluripotent marker genes^{371,372}. In recently published papers it has been claimed that autophagy is directly connected to different phases of the cell cycle, thereby eventually regulating the switch between proliferation and differentiation through midbody accumulation and induction of cell cycle arrest, among others. In pancreatic cancer cells, autophagy induction led to a G₂/M phase arrest along with a downregulation of proteins that control cell cycle progression thereby inhibiting proliferation^{224,230,231,373}. However, the direct translation of autophagy activity to differentiation processes during embryogenesis remains subject of future studies.

Interestingly, not only cilia but also autophagy is closely connected to all three *de novo* mutations found in our patient lines. The predicted disease-causing mutation in the gene DENND5B interrupts its RAB39 binding (Fig. 33) and in literature, RAB39 has been

described as a protein involved in the fusion step of the autophagosome with the lysosome^{374–376}. Moreover, the autophagy activator Brefeldin A, used in the experiments, interacts with RAB proteins to induce autophagy^{377–379}, which might explain why autophagy induction was reduced in the HLHS patient line carrying the DENND5B mutation. Additionally, mediated by its RAB interaction, DENND5B is involved in vesicular trafficking, an important component in ciliogenesis as mentioned before^{380–383}. So far, RAB39 has not been directly connected to ciliogenesis. However, many other RAB family members, such as RAB12 that directly activates DENND3, are known to induce autophagy³⁸⁴. Overall, very little is known about the role of RAB39; thus, it will be of interest to further investigate its involvement in ciliogenesis. The predicted disease-causing mutation in the FGFR1 gene, carried by the second patient line, is well known to play a crucial role in cardiogenesis along with its function in the ciliary signalling centre as mentioned above^{357,367}. Interestingly, recent publications could show a role in autophagy as well. Lin *et al.* discovered an inhibitory effect on autophagy by FGFR1 signalling via mTOR activation, confirmed by the finding that FGFR inhibition in breast cancer cells leads to activation of autophagy mediating a protective effect^{385,386}. Finally, FGFR1 is involved in cell cycle regulation in cardiac progenitors³⁸⁷, which might explain the very specific heart phenotype in this patient, most likely resulting from a combination with additional inherited mutations. Finally, the microtubule-associating factor MACF1 is not only known for its function in mesoderm formation and ciliogenesis, it can also be linked to the autophagy defect seen in the correspondent HLHS hiPSC line through its interaction with p230, a *Trans*-Golgi protein that mediates the transport of the autophagic protein ATG9 from the Golgi to the phagophores³⁸⁸.

We obtained an intriguing result that brought us a step closer in the understanding of this presumed axis in the context of HLHS by inhibiting autophagy in control lines. The administration of the autophagy inhibitor CQ to control hiPSC lines induced a similar phenotype seen in the patient lines, with a lower number of progenitor cells in G₁ phase at day 2 of differentiation as well as a decreased expression of specific cardiac progenitor genes such as TBX5 while other markers such as ISL1 remained unaltered (Fig. 29). Taken together, these findings show for the first time that manipulation of defined processes such as autophagy and cell cycle changes can influence the differentiation ability of early cardiac progenitor cells and could be assigned to a congenital malformation. Moreover, they suggest common regulatory mechanisms to be responsible for the onset

of HLHS rather than single gene variants. Another logical inference regarding these findings raise the idea of investigating autophagy inducers as a therapeutic option in HLHS, though this approach is very hypothetical since very early stages of embryogenesis are very difficult to target and prenatal screening for HLHS is not yet established due to the lack of markers and defined causative genes.

Autophagy manipulation as a therapeutic intervention

The role of autophagy with its diverse functions in keeping a healthy condition has been investigated in several disorders, leading to first trials that test autophagy inducers or inhibitors for therapeutic interventions. For instance, in cancer, autophagic genes encoding proteins such as G₁/S-specific cyclin-D1 also known as B-cell CLL/lymphoma 1 (BCL1), and many ATGs could be assigned to an anti-oncogenic function. By monoallelic knockdown of these tumour suppressor genes, spontaneous tumorigenesis occurred suggesting that anti-oncogenic pathways may stimulate autophagy. Controversially, in established tumours, autophagy might be advantageous for the survival of cancerogenic cells, thereby inhibition of autophagy was tested as a therapeutic option in combatting tumour progression and has been also shown to increase cell killing during chemotherapy³⁸⁹. Another potential treatment using autophagy manipulation can be found in the field of neurodegenerative diseases that are manifested by an accumulation of protein aggregates. It could be shown that defect autophagic pathway function is associated with the onset of Huntington disease for instance. Mice showing an autophagy deficiency develop neurodegeneration and applying autophagy inducers in those mice could alleviate the symptoms^{390,391}. The same autophagic function of protein clearance is discussed to be beneficial in pulmonary diseases such as cystic fibrosis or cigarette smoke-induced chronic obstructive pulmonary disease (COPD), where impaired autophagy leads to protein accumulation as well^{392,393}.

With its role in the regulation of the innate and adaptive immune response by degradation of invasive pathogens, autophagy has been discussed in the treatment of infectious diseases as well. In this context, several mutations in autophagy-related genes could be associated with a higher susceptibility to specific inflammatory and infectious diseases. Since pathogens developed strategies to evade the autophagy clearance and, upon negative manipulation of autophagy, increased susceptibility to specific pathogens could be observed, counteracting this condition by opposite autophagy manipulation could repre-

sent a novel therapeutic option^{394,395}. Notably, the replication Human immunodeficiency virus (HIV) could be abolished by the application of vitamin D and Rapamycin, two pro-autophagic substances^{396,397}. The involvement of autophagy proteins in the process of adaptive immune response might furthermore open possibilities in the development of vaccines. Moreover, metabolic diseases such as diabetes and Glycogen storage disease have also been connected to impaired autophagic function due to its role in the homeostasis of metabolic precursors. Thus, influencing the availability of specific metabolites through autophagic degradation might be beneficial in particular metabolic conditions such as diabetes or storage diseases³⁹⁸.

Also in the field of adult cardiac diseases, genetic variations in autophagy genes such as Lysosome-associated membrane protein 2 (LAMP2) could be linked to these pathogenic conditions. An increased number of autophagosomes in cardiomyocytes of patients affected by cardiomyopathy as well as in cardiac tissues of patients suffering heart failure could be detected^{399,400}. Interestingly, higher autophagy activity could be proven to be cardioprotective in a mouse model for cardiomyopathy⁴⁰¹. Additionally, macrophages isolated from atherosclerotic plaques presented an enrichment of autophagosomes. Hereby, autophagy eventually inhibits apoptosis and plaque necrosis due to its role in the stabilization of atherosclerotic plaques^{402,403}. Moreover, in experimental ischemia–reperfusion injury autophagic activity could be detected, most likely due to stress-response including hypoxia, Ca²⁺ level alterations and ATP depletion⁴⁰⁴. However, a role of deficient autophagy processes in the onset of congenital cardiac disorders has not been examined yet and was the last main focus of this thesis, hopefully unravelling potential treatment options for congenital disorders by autophagy inhibition or activation.

Primary cilium-autophagy axis order in HLHS

In our system we hypothesize cilia defects, caused by mutations, as main regulator of the axis, negatively influencing autophagy induction. The defective autophagy pathway then leads to the differentiation defect of cardiac progenitors due to delayed cell cycle and proliferation changes. This axis order varies from the “PAN axis”, suggested by Jang *et al.*¹⁹². However, several recent publications raised the question which of these processes stands first influencing the other. Current findings suggest a rather tissue- and time-dependent individual axis order, with a reciprocal cilia and autophagy interaction in which the front standing partner varies dependent on specific conditions. For instance

Tang *et al.* showed that autophagy induces ciliogenesis through the degradation of the ciliary protein OFD1. Supportive findings have been reported by Lam *et al.*, who could prove that cigarette smoke-induced autophagy in tracheal epithelial cells results in cilia shortening. Moreover, Lee *et al.* discovered that inhibition of autophagy restored abnormal ciliogenesis in thyroid cancer cells^{219,220,405}. In contrast, other research groups could show that ciliary signalling influences autophagy. It could be shown on the one hand, that the ciliary SHH signalling cascade stimulates autophagy in vascular smooth muscle cells and neural cells by upregulating autophagy-related gene expression, while it on the other hand inhibits autophagosome formation in HeLa cells and MEFs. Moreover, in the neurodegenerative Huntington disease, impaired ciliary interaction with the defective HTT protein results in an incomplete autophagy induction and consequently an accumulation of the diseased protein^{217,406,407}. Pampliega *et al.* detected a reciprocal cilium-autophagy regulation: they could show that SHH is directly linked to autophagic proteins in the ciliary pocket and that autophagy is reduced upon impaired ciliogenesis, whereas autophagy negatively regulates cilia formation by degradation of IFT proteins. This bidirectional interplay was also seen in a study conducted by Wang *et al.* where cells with repressed ciliogenesis exhibited lower autophagy levels due to enhanced mTOR activity, while cells with inhibited autophagy displayed cilia shortening, confirmed in mouse knockout models for autophagic ATG proteins^{408,409}.

The same bi-directional interplay was observed for cell cycle and cilia. While the cell cycle is defining the phases in which ciliogenesis occurs due to centrosome availability and regulation by cell cycle-associated proteins, ciliary signalling pathways such as SHH signalling can induce expression of cell cycle genes along with changes in cell cycle phase transitions and thereby directly or indirectly influence this process^{159,163,410}. Besides cilia, also autophagy can be linked to the cell cycle. For instance, stress-induced signals translated to autophagy initiation lead to cell cycles changes. Additionally, the expression of cell cycle genes such as cyclin dependent kinases is negatively correlated with the expression of autophagy-related genes in cancer cells, where the cell cycle control is defective^{411,412}. Whether autophagy can be reciprocally induced by cell cycle-related genes needs to be examined in future studies. With our autophagy manipulation experiments we showed a strong indication of autophagy as the regulator of cell cycle length and cardiac marker gene expression. Nevertheless, rescue experiments in the patient lines would be necessary to fully understand this interplay, though this remains

challenging since the cells do not respond to autophagy activators. Genetic manipulation or overexpression vectors are required to answer this question. Moreover, it would be exciting to manipulate cell cycle or cilia in the control lines or rescue those phenotypes in the patient lines to further analyse which defect stands at the first position of the axis affecting the following processes. Cilia represent a highly complex signalling centre including several pathways. Also the cell cycle with its many checkpoints and steps is very difficult to manipulate without interrupting too many crucial cellular functions.

4.3. Limitations of the study

3D in vitro models of cardiogenesis

Since CHDs display cardiac structural abnormalities, one of the main challenges is to model this complex cardiac remodelling phenotype *in vitro*. To investigate patterning processes and steps such as cardiac looping and the influence of cilia and autophagy defects among others on these processes in the onset of HLHS cannot be investigated in 2D monolayers. The lack of appropriate 3D *in vitro* models in the cardiac field made the usage of 2D monolayer assays currently indispensable. However, 3D models such as heart-on-a-chip approaches or human cardiac organoids (hCOs) that have recently been started to be used in several disease modelling approaches⁴¹³ might help to examine the process of cardiac development in the future. An advantage of these models could be the application of different flow dynamics to the cells to observe structural changes during development or the seeding of these devices with diseased cardiomyocytes or precursor cells to investigate the influence of particular mutations or genetic backgrounds on heart chamber formation among others. First trials exerted some promising efforts in myocyte alignment and microvascularization of the native cardiac structure using bioprinting strategies. Moreover, wall structure-like formation could be induced by the cellularization of flexible substrates. One major restriction at present seems to be the measurement of electrophysiological and cell signalling parameters. Methods such as optical mapping or stainings have been tested but could barely provide accurate information. Recently, a heart-on-a-chip device was fabricated where sensors to measure contractility were integrated using a 3D multi-material extrusion printer that resulted in more reliable measurements⁴¹⁴. However, seeding of 3D models with different cardiac

cell types, even in a progenitor state, thereby inducing the development of cardiac structures, remains a major challenge in the field of *in vitro* human cardiac remodelling.

Distinction of FHF vs. SHF cardiac populations

Our results of a dysregulation of TBX5 and NKX2.5 hint to a possible defect in FHF progenitor cells in HLHS. Expression of markers known for SHF progenitors is unaltered, supporting the hypothesis of a subtype specific defect. However, we cannot distinguish whether a FHF population is formed in HLHS patients and in case it is formed, whether the substantial defects seen in cell cycle, autophagy and cilia formation can be assigned to this specific population. The group of Harvey reported that upon knockout of Nkx2.5 in mice, cardiac precursors are over-specialized followed by impaired SHF proliferation and shortening of the OFT due to an upregulation of genes that define and maintain cardiac progenitor. Moreover, FHF population seems to form *in vivo* also without Nkx2.5, though with altered expression profile population¹⁰³. Thus, one could speculate that if the aberrant NKX2.5 expression seen in our HLHS hiPSC lines was the cause of the onset of the disease, a FHF population would arise but is defective. However, the NKX2.5 downregulation could also be a secondary consequence of the described altered ciliogenesis or autophagy. Which role FHF cells plays in the human system and whether NKX2.5 downregulation is a cause or consequence of dysregulated FHF population formation needs to be further investigated.

Another interesting observation in terms of hypothetical FHF-related defects in HLHS is that we find a higher expression of *Dennd5b* in mESC-derived FHF cardiac progenitors forming the left ventricle of mice, marked by Nkx2.5 enhancer activation (Fig. 31). However, the phenotype induced by *Dennd5b* knockdown in *Xenopus* showed an additional mild effect in structures derived from SHF cells (e.g. OFT). This could result from dosage and temporal differences in the induced morpholino knockdown compared to the physiological situation in HLHS patients or be a consequence of abnormal FHF development.

Building on these results, a well-established way for the identification and subsequent separation of these two hypothetical progenitor populations is necessary to further analyse if the observed defects are specific for a FHF-like population. For mice, a Nkx.5 enhancer marking system has successfully been developed, that, if cloned into a reporter vector and transfected into mESCs, was able to mark a distinct population characterized

by the expression of typical FHF markers⁴¹⁵. Now it needs to be tested whether this cardiac specific murine enhancer can be transferred into the human system. We were able to clone the enhancer sequence linked to a GFP marker gene into a PiggyBac™ system allowing us to bring high copy numbers of the sequence into the human genome. First results after transfection of the NKX2.5-enhancer construct into hiPSCs showed a promising specific marker expression during cardiac differentiation. However, further evaluation and characterization is required as well as a way to isolate the two distinct populations for a possible assignment of the described HLHS phenotype to one of the progenitor populations.

5. References

1. Bruneau, B. G. The developmental genetics of congenital heart disease. *Nature* **451**, 943–948 (2008).
2. Hoffman, J. I. E. & Kaplan, S. The incidence of congenital heart disease. *J. Am. Coll. Cardiol.* **39**, 1890–900 (2002).
3. Zaidi, S. & Brueckner, M. Genetics and genomics of congenital heart disease. *Circ. Res.* **120**, 923–940 (2017).
4. Canfield, M. A. *et al.* National estimates and race/ethnic-specific variation of selected birth defects in the United States, 1999–2001. *Birth Defects Res. Part A Clin. Mol. Teratol.* **76**, 747–756 (2006).
5. Fixler, D. E., Pastor, P., Chamberlin, M., Sigman, E. & Eifler, C. W. Trends in congenital heart disease in Dallas County births. 1971-1984. *Circulation* **81**, 137–142 (1990).
6. Grech, V. Spectrum of congenital heart disease in Malta. An excess of lesions causing right ventricular outflow tract obstruction in a population-base study. *Eur. Heart J.* **19**, 521–525 (1998).
7. Grech, V. Trends in presentation of congenital heart disease in a population-based study in Malta. *Eur. J. Epidemiol.* **15**, 881–887 (1999).
8. McBride, K. L. *et al.* Inheritance analysis of congenital left ventricular outflow tract obstruction malformations: Segregation, multiplex relative risk, and heritability. *Am. J. Med. Genet. Part A* **134A**, 180–186 (2005).
9. McBride, K. L. *et al.* Epidemiology of noncomplex left ventricular outflow tract obstruction malformations (aortic valve stenosis, coarctation of the aorta, hypoplastic left heart syndrome) in Texas, 1999-2001. *Birth Defects Res. Part A Clin. Mol. Teratol.* **73**, 555–561 (2005).
10. Muir, C. S. Incidence of congenital heart disease in Singapore. *Br. Heart J.* **22**, 243–254 (1960).
11. Pradat, P., Francannet, C., Harris, J. A. & Robert, E. The epidemiology of cardiovascular defects, part I and II: A study based on data from three large registries of congenital malformations. *Pediatr. Cardiol.* **24**, 195–235 (2003).
12. Schrire, V. Experience with congenital heart disease at Groote Schuur hospital, Cape Town. An analysis of 1,439 patients over an eleven-year period. *South African Med. J.* **37**, 1175–1180 (1963).
13. Shann, M. K. Congenital heart disease in Taiwan, Republic of China. *Circulation* **39**, 251–258 (1969).
14. Burn, J. *et al.* Recurrence risks in offspring of adults with major heart defects: results from first cohort of British collaborative study. *Lancet* **351**, 311–316 (1998).
15. Digilio, M. C. *et al.* Complete transposition of the great arteries: patterns of congenital heart disease in familial precurrence. *Circulation* **104**, 2809–2814 (2001).
16. Gill, H. K., Splitt, M., Sharland, G. K. & Simpson, J. M. Patterns of recurrence of congenital heart disease: an analysis of 6,640 consecutive pregnancies evaluated by detailed fetal echocardiography. *J. Am. Coll. Cardiol.* **42**, 923–929 (2003).

17. Hoess, K., Goldmuntz, E. & Pyeritz, R. E. Genetic counseling for congenital heart disease: new approaches for a new decade. *Curr. Cardiol. Rep.* **4**, 68–75 (2002).
18. Hoffman, J. I. Congenital heart disease: incidence and inheritance. *Pediatr. Clin. North Am.* **37**, 25–43 (1990).
19. Lewin, M. B. *et al.* Echocardiographic evaluation of asymptomatic parental and sibling cardiovascular anomalies associated with congenital left ventricular outflow tract lesions. *Pediatrics* **114**, 691–696 (2004).
20. Meijer, J. M. *et al.* Pregnancy, fertility, and recurrence risk in corrected tetralogy of Fallot. *Heart* **91**, 801–805 (2005).
21. Oyen, N. *et al.* Recurrence of congenital heart defects in families. *Circulation* **120**, 295–301 (2009).
22. Leirgul, E. *et al.* Birth prevalence of congenital heart defects in Norway 1994–2009. A nationwide study. *Am. Heart J.* **168**, 956–964 (2014).
23. Piacentini, G. *et al.* Familial recurrence of heart defects in subjects with congenitally corrected transposition of the great arteries. *Am. J. Med. Genet. Part A* **137A**, 176–180 (2005).
24. Siu, S. The risk of congenital heart disease recurrence in the offspring of adults with major heart defects. *Evid. Based. Cardiovasc. Med.* **2**, 70 (1998).
25. Whittemore, R., Wells, J. A. & Castellsague, X. A second-generation study of 427 probands with congenital heart defects and their 837 children. *J. Am. Coll. Cardiol.* **23**, 1459–1467 (1994).
26. Badaruddoza, Afzal, M. & Akhtaruzzaman. Inbreeding and congenital heart diseases in a north Indian population. *Clin. Genet.* **45**, 288–291 (1994).
27. Becker, S. & Al Halees, Z. First-cousin matings and congenital heart disease in Saudi Arabia. *Community Genet.* **2**, 69–73 (1999).
28. Becker, S. M., Al Halees, Z., Molina, C. & Paterson, R. M. Consanguinity and congenital heart disease in Saudi Arabia. *Am. J. Med. Genet.* **99**, 8–13 (2001).
29. Chehab, G., Chedid, P., Saliba, Z. & Bouvagnet, P. Congenital cardiac disease and inbreeding: specific defects escape higher risk due to parental consanguinity. *Cardiol. Young* **17**, 414–422 (2007).
30. Nabulsi, M. M. *et al.* Parental consanguinity and congenital heart malformations in a developing country. *Am. J. Med. Genet. A* **116A**, 342–347 (2003).
31. Ramegowda, S. & Ramachandra, N. B. Parental consanguinity increases congenital heart diseases in South India. *Ann. Hum. Biol.* **33**, 519–528 (2006).
32. Cripe, L., Andelfinger, G., Martin, L. J., Shooner, K. & Benson, D. W. Bicuspid aortic valve is heritable. *J. Am. Coll. Cardiol.* **44**, 138–143 (2004).
33. Hinton, R. B. *et al.* Hypoplastic left heart syndrome is heritable. *J. Am. Coll. Cardiol.* **50**, 1590–1595 (2007).
34. Insley, J. The heritability of congenital heart disease. *Br. Med. J.* **294**, 662–663 (1987).
35. Bentham, J. & Bhattacharya, S. Genetic mechanisms controlling cardiovascular development. *Ann. N. Y. Acad. Sci.* **1123**, 10–19 (2008).
36. Lalani, S. R. & Belmont, J. W. Genetic basis of congenital cardiovascular malformations. *Eur. J. Med. Genet.* **57**, 402–413 (2014).

37. Hartman, R. J. *et al.* The contribution of chromosomal abnormalities to congenital heart defects: a population-based study. *Pediatr. Cardiol.* **32**, 1147–1157 (2011).
38. Breckpot, J. *et al.* Array comparative genomic hybridization as a diagnostic tool for syndromic heart defects. *J. Pediatr.* **156**, 810–817 (2010).
39. Greenway, S. C. *et al.* De novo copy number variants identify new genes and loci in isolated sporadic tetralogy of Fallot. *Nat. Genet.* **41**, 931–935 (2009).
40. Syrmou, A. *et al.* Array comparative genomic hybridization as a clinical diagnostic tool in syndromic and nonsyndromic congenital heart disease. *Pediatr. Res.* **73**, 772–776 (2013).
41. Warburton, D. *et al.* The contribution of de novo and rare inherited copy number changes to congenital heart disease in an unselected sample of children with conotruncal defects or hypoplastic left heart disease. *Hum. Genet.* **133**, 11–27 (2014).
42. Zaidi, S. *et al.* De novo mutations in histone-modifying genes in congenital heart disease. *Nature* **498**, 220–223 (2013).
43. Nielsen, G. L. *et al.* Risk of specific congenital abnormalities in offspring of women with diabetes. *Diabet. Med.* **22**, 693–696 (2005).
44. Gillian M Blue, Edwin P Kirk, Gary F Sholler, Richard P Harvey & David S Winlaw. Congenital heart disease: current knowledge about causes and inheritance. *Med. J. Aust.* **197**, 155–159 (2012).
45. Sinning, A. R. Role of vitamin A in the formation of congenital heart defects. *Anat. Rec.* **253**, 147–153 (1998).
46. Hall, J. & Solehdin, F. Folic acid for the prevention of congenital anomalies. *Eur. J. Pediatr.* **157**, 445–450 (1998).
47. Liu, S. *et al.* Environmental risk factors for congenital heart disease in the Shandong Peninsula, China: a hospital-based case-control study. *J. Epidemiol.* **19**, 122–130 (2009).
48. Jenkins, K. J. *et al.* Noninherited risk factors and congenital cardiovascular defects: current knowledge. *Circulation* **115**, 2995–3014 (2007).
49. Lage, K. *et al.* Dissecting spatio-temporal protein networks driving human heart development and related disorders. *Mol. Syst. Biol.* **6**, 30–35 (2010).
50. Hornberger, L. K., Need, L. & Benacerraf, B. R. Development of significant left and right ventricular hypoplasia in the second and third trimester fetus. *J. Ultrasound Med.* **15**, 655–659 (1996).
51. Ferencz, C. *et al.* Congenital heart disease: prevalence at livebirth. The Baltimore-Washington Infant Study. *Am. J. Epidemiol.* **121**, 31–36 (1985).
52. Tweddell, J. S. *et al.* Intermediate-term mortality and cardiac transplantation in infants with single-ventricle lesions: Risk factors and their interaction with shunt type. *J. Thorac. Cardiovasc. Surg.* **144**, 152–159 (2012).
53. Ghanayem, N. S. *et al.* Interstage mortality after the Norwood procedure: results of the multicenter single ventricle reconstruction trial. *J. Thorac. Cardiovasc. Surg.* **144**, 896–906 (2012).
54. Norwood, W. I., Kirklin, J. K. & Sanders, S. P. Hypoplastic left heart syndrome: experience with palliative surgery. *Am. J. Cardiol.* **45**, 87–91 (1980).
55. Puga, F. J. Modified Fontan procedure for hypoplastic left heart syndrome after palliation with the Norwood operation. *J. Am. Coll. Cardiol.* **17**, 1150–1151 (1991).

56. Feinstein, J. A. *et al.* Hypoplastic left heart syndrome: current considerations and expectations. *J. Am. Coll. Cardiol.* **59**, S1–S42 (2012).
57. Chintala, K., Tian, Z., Du, W., Donaghue, D. & Rychik, J. Fetal pulmonary venous Doppler patterns in hypoplastic left heart syndrome: relationship to atrial septal restriction. *Heart* **94**, 1446–1449 (2008).
58. Harh, J. Y., Paul, M. H., Gallen, W. J., Friedberg, D. Z. & Kaplan, S. Experimental production of hypoplastic left heart syndrome in the chick embryo. *Am. J. Cardiol.* **31**, 51–56 (1973).
59. Groenendijk, B. C. W., Van der Heiden, K., Hierck, B. P. & Poelmann, R. E. The role of shear stress on ET-1, KLF2, and NOS-3 expression in the developing cardiovascular system of chicken embryos in a venous ligation model. *Physiology* **22**, 380–389 (2007).
60. Midgett, M. & Rugonyi, S. Congenital heart malformations induced by hemodynamic altering surgical interventions. *Front. Physiol.* **5**, 1–8 (2014).
61. Hickey, E. J., Caldarone, C. A. & McCrindle, B. W. Left ventricular hypoplasia: a spectrum of disease involving the left ventricular outflow tract, aortic valve and aorta. *J. Am. Coll. Cardiol.* **59**, S43–S54 (2012).
62. Hinton, R. B. *et al.* Hypoplastic left heart syndrome is heritable. *J. Am. Coll. Cardiol.* **50**, 1590–1595 (2007).
63. Hinton, R. B. *et al.* Hypoplastic left heart syndrome links to chromosomes 10q and 6q and is genetically related to bicuspid aortic valve. *J. Am. Coll. Cardiol.* **53**, 1065–1071 (2009).
64. Guenthard, J., Buehler, E., Jaeggi, E. & Wyler, F. Possible genes for left heart formation on 11q23.3. *Ann. Genet.* **37**, 143–146 (1994).
65. Shokeir, M. H. Hypoplastic left heart. Evidence for possible autosomal recessive inheritance. *Birth Defects Orig. Artic. Ser.* **10**, 223–227 (1974).
66. Allen, R. H., Benson, C. B. & Haug, L. W. Pregnancy outcome of fetuses with a diagnosis of hypoplastic left ventricle on prenatal sonography. *J. Ultrasound Med.* **24**, 1199–1203 (2005).
67. Fruitman, D. S. Hypoplastic left heart syndrome: prognosis and management options. *Paediatr. Child Health* **5**, 219–225 (2000).
68. Payne, A. R., Chang, S.-W., Koenig, S. N., Zinn, A. R. & Garg, V. Submicroscopic chromosomal copy number variations identified in children with hypoplastic left heart syndrome. *Pediatr. Cardiol.* **33**, 757–763 (2012).
69. Hitz, M.-P. *et al.* Rare copy number variants contribute to congenital left-sided heart disease. *PLoS Genet.* **8**, e1002903 (2012).
70. Dasgupta, C. *et al.* Identification of connexin43 (alpha1) gap junction gene mutations in patients with hypoplastic left heart syndrome by denaturing gradient gel electrophoresis (DGGE). *Mutat. Res.* **479**, 173–186 (2001).
71. Elliott, D. A. *et al.* Cardiac homeobox gene NKX2-5 mutations and congenital heart disease: associations with atrial septal defect and hypoplastic left heart syndrome. *J. Am. Coll. Cardiol.* **41**, 2072–2076 (2003).
72. McBride, K. L. *et al.* NOTCH1 mutations in individuals with left ventricular outflow tract malformations reduce ligand-induced signaling. *Hum. Mol. Genet.* **17**, 2886–2893 (2008).
73. Iacone, M. *et al.* Identification of de novo mutations and rare variants in hypoplastic left heart syndrome. *Clin. Genet.* **81**, 542–554 (2012).

74. Theis, J. L. *et al.* Recessive MYH6 mutations in hypoplastic left heart with reduced ejection fraction. *Circ. Cardiovasc. Genet.* **8**, 564–571 (2015).
75. Reamon-Buettner, S. M., Ciribilli, Y., Inga, A. & Borlak, J. A loss-of-function mutation in the binding domain of HAND1 predicts hypoplasia of the human hearts. *Hum. Mol. Genet.* **17**, 1397–1405 (2008).
76. Bruneau, B. G. The developing heart and congenital heart defects: a make or break situation. *Clin. Genet.* **63**, 252–261 (2003).
77. Benson, D. W., Martin, L. J. & Lo, C. W. Genetics of hypoplastic left heart syndrome. *J. Pediatr.* **173**, 25–31 (2016).
78. Fitzgerald, K. K., Bhat, A. M., Conard, K., Hyland, J. & Pizarro, C. Novel SMAD3 mutation in a patient with hypoplastic left heart syndrome with significant aortic aneurysm. *Case Rep. Genet.* **2014**, 1–4 (2014).
79. McBride, K. L. *et al.* Association of common variants in ERBB4 with congenital left ventricular outflow tract obstruction defects. *Birth Defects Res.* **91**, 162–168 (2011).
80. Ware, S. M. *et al.* Identification and functional analysis of ZIC3 mutations in heterotaxy and related congenital heart defects. *Am. J. Hum. Genet.* **74**, 93–105 (2004).
81. Iacone, M. *et al.* Identification of de novo mutations and rare variants in hypoplastic left heart syndrome. *Clin. Genet.* **81**, 542–554 (2012).
82. Zaidi, S. *et al.* De novo mutations in histone-modifying genes in congenital heart disease - Supplementary information. *Nature* **498**, (2013).
83. Moorman, A., Webb, S., Brown, N. A., Lamers, W. & Anderson, R. H. Development of the heart: formation of the cardiac chambers and arterial trunks. *Hear.* **89**, 806–814 (2003).
84. Rawles, M. E. The heart-forming areas of the early chick blastoderm. *Physiol. Zool.* **16**, 22–42 (1943).
85. Beddington, R. S., Rashbass, P. & Wilson, V. Brachyury- a gene affecting mouse gastrulation and early organogenesis. *Development* 157–165 (1992).
86. Furtado, M. B. *et al.* BMP/SMAD1 signaling sets a threshold for the left/right pathway in lateral plate mesoderm and limits availability of SMAD4. *Genes Dev.* **22**, 3037–3049 (2008).
87. Lu, C. C. & Robertson, E. J. Multiple roles for Nodal in the epiblast of the mouse embryo in the establishment of anterior-posterior patterning. *Dev. Biol.* **273**, 149–159 (2004).
88. Schlange, T., André, B., Arnold, H. H. & Brand, T. BMP2 is required for early heart development during a distinct time period. *Mech. Dev.* **91**, 259–70 (2000).
89. Madabhushi, M. & Lacy, E. Anterior visceral endoderm directs ventral morphogenesis and placement of head and heart via BMP2 expression. *Dev. Cell* **21**, 907–919 (2011).
90. Zhang, H. & Bradley, A. Mice deficient for BMP2 are nonviable and have defects in amnion/chorion and cardiac development. *Development* **122**, 2977–2986 (1996).
91. Kitajima, S., Takagi, A., Inoue, T. & Saga, Y. MesP1 and MesP2 are essential for the development of cardiac mesoderm. *Dev.* **127**, 3215–3226 (2000).
92. Arai, A., Yamamoto, K. & Toyama, J. Murine cardiac progenitor cells require visceral embryonic endoderm and primitive streak for terminal differentiation. *Dev. Dyn.* **210**, 344–353 (1997).
93. Tam, P. P., Parameswaran, M., Kinder, S. J. & Weinberger, R. P. The allocation of epiblast cells to

- the embryonic heart and other mesodermal lineages: the role of ingression and tissue movement during gastrulation. *Development* **124**, 1631–1642 (1997).
94. von Gise, A. & Pu, W. T. Endocardial and epicardial epithelial to mesenchymal transitions in heart development and disease. *Circ. Res.* **110**, 1628–1645 (2012).
 95. Bondue, A. *et al.* Mesp1 acts as a master regulator of multipotent cardiovascular progenitor specification. *Cell Stem Cell* **3**, 69–84 (2008).
 96. Rosenquist, G. C. & DeHaan, R. L. Migration of precardiac cells in the chick embryo : a radioautographic study. *Carnegie Inst. Wash. Publ. 625. Contrib. to Embryol.* **38**, 111–121 (1966).
 97. de la Cruz, M. V, Sánchez Gómez, C., Arteaga, M. M. & Argüello, C. Experimental study of the development of the truncus and the conus in the chick embryo. *J. Anat.* **123**, 661–686 (1977).
 98. Cai, C.-L. *et al.* Isl1 identifies a cardiac progenitor population that proliferates prior to differentiation and contributes a majority of cells to the heart. *Dev. Cell* **5**, 877–889 (2003).
 99. Kelly, R. G., Brown, N. A. & Buckingham, M. E. The arterial pole of the mouse heart forms from Fgf10-expressing cells in pharyngeal mesoderm. *Dev. Cell* **1**, 435–440 (2001).
 100. Waldo, K. L. *et al.* Conotruncal myocardium arises from a secondary heart field. *Dev.* **128**, 3179–3188 (2001).
 101. Sun, Y. *et al.* Islet 1 is expressed in distinct cardiovascular lineages, including pacemaker and coronary vascular cells. *Dev. Biol.* **304**, 286–296 (2007).
 102. Ma, Q., Zhou, B. & Pu, W. T. Reassessment of Isl1 and Nkx2-5 cardiac fate maps using a Gata4-based reporter of Cre activity. *Dev. Biol.* **323**, 98–104 (2008).
 103. Prall, O. W. J. *et al.* An Nkx2-5/Bmp2/Smad1 negative feedback loop controls heart progenitor specification and proliferation. *Cell* **128**, 947–959 (2007).
 104. Vliet, P. Van, Wu, S. M., Phane Zaffran, S. & Pucé At, M. Early cardiac development: a view from stem cells to embryos. *Cardiovasc. Res.* **96**, 352–362 (2012).
 105. Mosimann, C. *et al.* Chamber identity programs drive early functional partitioning of the heart. *Nat. Commun.* **6**, (2015).
 106. Brade, T., Pane, L. S., Moretti, A., Chien, K. R. & Laugwitz, K.-L. Embryonic heart progenitors and cardiogenesis. *Cold Spring Harb. Perspect. Med.* **3**, a013847 (2013).
 107. Schneider, V. A. & Mercola, M. Wnt antagonism initiates cardiogenesis in *Xenopus laevis*. *Genes Dev.* **15**, 304–315 (2001).
 108. Marvin, M. J., Di Rocco, G., Gardiner, A., Bush, S. M. & Lassar, A. B. Inhibition of Wnt activity induces heart formation from posterior mesoderm. *Genes Dev.* **15**, 316–327 (2001).
 109. Cohen, E. D. *et al.* Wnt/ β -catenin signaling promotes expansion of Isl-1–positive cardiac progenitor cells through regulation of FGF signaling. *J. Clin. Invest.* **117**, 1794–1804 (2007).
 110. Pandur, P., Läsche, M., Eisenberg, L. M. & Kühl, M. Wnt-11 activation of a non-canonical Wnt signalling pathway is required for cardiogenesis. *Nature* **418**, 636–641 (2002).
 111. Palpant, N. J., Yasuda, S., MacDougald, O. & Metzger, J. M. Non-canonical Wnt signaling enhances differentiation of Sca1+/c-kit+ adipose-derived murine stromal vascular cells into spontaneously beating cardiac myocytes. *J. Mol. Cell. Cardiol.* **43**, 362–370 (2007).
 112. Garriock, R. J., D’Agostino, S. L., Pilcher, K. C. & Krieg, P. A. Wnt11-R, a protein closely related to

- mammalian Wnt11, is required for heart morphogenesis in *Xenopus*. *Dev. Biol.* **279**, 179–192 (2005).
113. Schleiffarth, J. R. *et al.* Wnt5a is required for cardiac outflow tract septation in mice. *Pediatr. Res.* **61**, 386–391 (2007).
114. Zhou, W. *et al.* Modulation of morphogenesis by noncanonical Wnt signaling requires ATF/CREB family-mediated transcriptional activation of TGF β 2. *Nat. Genet.* **39**, 1225–1234 (2007).
115. Chu, G. C., Dunn, N. R., Anderson, D. C., Oxburgh, L. & Robertson, E. J. Differential requirements for Smad4 in TGF β -dependent patterning of the early mouse embryo. *Development* **131**, 3501–3512 (2004).
116. Schultheiss, T. M., Burch, J. B. & Lassar, A. B. A role for bone morphogenetic proteins in the induction of cardiac myogenesis. *Genes Dev.* **11**, 451–462 (1997).
117. Monzen, K. *et al.* Bone morphogenetic proteins induce cardiomyocyte differentiation through the mitogen-activated protein kinase kinase kinase TAK1 and cardiac transcription factors Csx/Nkx-2.5 and GATA-4. *Mol. Cell. Biol.* **19**, 7096–7105 (1999).
118. Shi, Y., Katsev, S., Cai, C. & Evans, S. BMP signaling is required for heart formation in vertebrates. *Dev. Biol.* **224**, 226–237 (2000).
119. Somi, S., Buffing, A. A. M., Moorman, A. F. M. & Van Den Hoff, M. J. B. Dynamic patterns of expression of BMP isoforms 2, 4, 5, 6, and 7 during chicken heart development. *Anat. Rec.* **279**, 636–651 (2004).
120. Dyer, L. A. & Kirby, M. L. The role of secondary heart field in cardiac development. *Dev. Biol.* **336**, 137–144 (2009).
121. Dyer, L. A. & Kirby, M. L. Sonic hedgehog maintains proliferation in secondary heart field progenitors and is required for normal arterial pole formation. *Dev. Biol.* **330**, 305–317 (2009).
122. Zhang, X. M., Ramalho-Santos, M. & McMahon, A. P. Smoothed mutants reveal redundant roles for Shh and Ihh signaling including regulation of L/R asymmetry by the mouse node. *Cell* **105**, 781–792 (2001).
123. Schilling, T. F., Concordet, J.-P. & Ingham, P. W. Regulation of left–right asymmetries in the zebrafish by Shh and BMP4. *Dev. Biol.* **210**, 277–287 (1999).
124. Briscoe, J. & Théron, P. P. The mechanisms of Hedgehog signalling and its roles in development and disease. *Nat. Rev. Mol. Cell Biol.* **14**, 418–431 (2013).
125. Levin, M., Johnson, R. L., Stern, C. D., Kuehn, M. & Tabin, C. A molecular pathway determining left-right asymmetry in chick embryogenesis. *Cell* **82**, 803–814 (1995).
126. Belmonte, J. C. I. *et al.* The novel Cer-like protein Caronte mediates the establishment of embryonic left-right asymmetry. *Nature* **401**, 243–251 (1999).
127. Isaac, A., Sargent, M. G. & Cooke, J. Control of vertebrate left-right asymmetry by a snail-related zinc finger gene. *Sci.* **275**, 1301–1304 (1997).
128. Piedra, M. E., Icardo, J. M., Albajar, M., Rodriguez-Rey, J. C. & Ros, M. A. Pitx2 participates in the late phase of the pathway controlling left-right asymmetry. *Cell* **94**, 319–324 (1998).
129. Itoh, N., Ohta, H., Nakayama, Y. & Konishi, M. Roles of FGF signals in heart development, health, and disease. *Front. Cell Dev. Biol.* **4**, (2016).
130. Alsan, B. H. & Schultheiss, T. M. Regulation of avian cardiogenesis by Fgf8 signaling. *Development* **129**, 1935–1943 (2002).

131. Gannon, M. & Bader, D. Initiation of cardiac differentiation occurs in the absence of anterior endoderm. *Development* **121**, 2439–2450 (1995).
132. Sun, X., Meyers, E. N., Lewandoski, M. & Martin, G. R. Targeted disruption of *Fgf8* causes failure of cell migration in the gastrulating mouse embryo. *Genes Dev.* **13**, 1834–1846 (1999).
133. Abu-Issa, R., Smyth, G., Smoak, I., Yamamura, K. & Meyers, E. N. *Fgf8* is required for pharyngeal arch and cardiovascular development in the mouse. *Development* **129**, 4613–4625 (2002).
134. Park, I.-H. *et al.* Disease-specific induced pluripotent stem cells. *Cell* **134**, 877–886 (2008).
135. Kwon, C. *et al.* A regulatory pathway involving Notch1/ β -catenin/*Isl1* determines cardiac progenitor cell fate. *Nat. Cell Biol.* **11**, 951–957 (2009).
136. McCright, B. *et al.* Defects in development of the kidney, heart and eye vasculature in mice homozygous for a hypomorphic Notch2 mutation. *Dev.* **128**, 491–502 (2001).
137. Ronces, M. S., McLaughlin, K. A., Raffin, M. & Mercola, M. Serrate and Notch specify cell fates in the heart field by suppressing cardiomyogenesis. *Development* **127**, 3865–3876 (2000).
138. Niessen, K. & Karsan, A. Notch signaling in cardiac development. *Circ. Res.* **102**, 1169–1181 (2008).
139. Nosedá, M. *et al.* Notch activation results in phenotypic and functional changes consistent with Endothelial-to-Mesenchymal Transformation. *Circ. Res.* **94**, 910–917 (2004).
140. Fischer, A. *et al.* Combined loss of *Hey1* and *HeyL* causes congenital heart defects because of impaired Epithelial to Mesenchymal Transition. *Circ. Res.* **100**, 856–863 (2007).
141. Satir, P. & Christensen, S. T. Structure and function of mammalian cilia. *Histochem. Cell Biol.* **129**, 687–693 (2008).
142. Scholey, J. M. Intraflagellar transport motors in cilia: moving along the cell’s antenna. *J. Cell Biol.* **180**, 23–29 (2008).
143. Takao, D. & Verhey, K. J. Gated entry into the ciliary compartment. *Cell. Mol. Life Sci.* **73**, 119–127 (2016).
144. Goetz, S. C. & Anderson, K. V. The primary cilium: a signalling centre during vertebrate development. *Nat. Rev. Genet.* **11**, 331–344 (2010).
145. Oro, A. E. The primary cilia, a ‘Rab-id’ transit system for hedgehog signaling. *Curr. Opin. Cell Biol.* **19**, 691–696 (2007).
146. Grosshans, B. L., Ortiz, D. & Novick, P. Rabs and their effectors: achieving specificity in membrane traffic. *Proc. Natl. Acad. Sci. U. S. A.* **103**, 11821–11827 (2006).
147. Pennekamp, P. *et al.* The ion channel polycystin-2 is required for left-right axis determination in mice. *Curr. Biol.* **12**, 938–943 (2002).
148. Brown, N. A. & Wolpert, L. The development of handedness in left/right asymmetry. *Dev.* **109**, 1–9 (1990).
149. Enuka, Y., Hanukoglu, I., Edelheit, O., Vaknine, H. & Hanukoglu, A. Epithelial sodium channels (ENaC) are uniformly distributed on motile cilia in the oviduct and the respiratory airways. *Histochem. Cell Biol.* **137**, 339–353 (2012).
150. Sawamoto, K. *et al.* New neurons follow the flow of cerebrospinal fluid in the adult brain. *Science (80-)*. **311**, 629–632 (2006).

151. Luo, W. *et al.* Cilia distribution and polarity in the epithelial lining of the mouse middle ear cavity. *Sci. Rep.* **7**, 45870 (2017).
152. Shah, A. S., Ben-Shahar, Y., Moninger, T. O., Kline, J. N. & Welsh, M. J. Motile cilia of human airway epithelia are chemosensory. *Sci.* **325**, 1131–1134 (2009).
153. Davenport, J. R. *et al.* Disruption of intraflagellar transport in adult mice leads to obesity and slow-onset cystic kidney disease. *Curr. Biol.* **17**, 1586–1594 (2007).
154. Christensen, S. T., Pedersen, S. F., Satir, P., Veland, I. R. & Schneider, L. The Primary Cilium Coordinates Signaling Pathways in Cell Cycle Control and Migration During Development and Tissue Repair. *Curr. Top. Dev. Biol.* **85**, 261–301 (2008).
155. Kuehn, E. W., Walz, G. & Benzing, T. Von hippel-lindau: a tumor suppressor links microtubules to ciliogenesis and cancer development. *Cancer Res.* **67**, 4537–4540 (2007).
156. Mans, D. A. *et al.* Mobility of the von Hippel–Lindau tumour suppressor protein is regulated by kinesin-2. *Exp. Cell Res.* **314**, 1229–1236 (2008).
157. Michaud, E. J. & Yoder, B. K. The primary cilium in cell signaling and cancer. *Cancer Res.* **66**, 6463–6467 (2006).
158. Nielsen, S. K. *et al.* Characterization of primary cilia and Hedgehog signaling during development of the human pancreas and in human pancreatic duct cancer cell lines. *Dev. Dyn.* **237**, 2039–2052 (2008).
159. Plotnikova, O. V, Golemis, E. A. & Pugacheva, E. N. Cell cycle-dependent ciliogenesis and cancer. *Cancer Res.* **68**, 2058–2061 (2008).
160. Wong, S. Y. *et al.* Primary cilia can both mediate and suppress Hedgehog pathway–dependent tumorigenesis. *Nat. Med.* **15**, 1055–1061 (2009).
161. Han, Y.-G. *et al.* Dual and opposing roles of primary cilia in medulloblastoma development. *Nat. Med.* **15**, 1062–1065 (2009).
162. Izawa, I., Goto, H., Kasahara, K. & Inagaki, M. Current topics of functional links between primary cilia and cell cycle. *Cilia* **4**, (2015).
163. Plotnikova, O. V, Pugacheva, E. N. & Golemis, E. A. Primary cilia and the cell cycle. *Methods Cell Biol.* **94**, 137–160 (2009).
164. Inoko, A. *et al.* Trichoplein and Aurora A block aberrant primary cilia assembly in proliferating cells. *J. Cell Biol.* **197**, 391–405 (2012).
165. Kim, S. *et al.* Nde1-mediated inhibition of ciliogenesis affects cell cycle re-entry. *Nat. Cell Biol.* **13**, 351–360 (2011).
166. Li, A. *et al.* Ciliary transition zone activation of phosphorylated Tctex-1 controls ciliary resorption, S-phase entry and fate of neural progenitors. *Nat. Cell Biol.* **13**, 402–411 (2011).
167. Kenney, A. M. & Rowitch, D. H. Sonic hedgehog promotes G(1) cyclin expression and sustained cell cycle progression in mammalian neuronal precursors. *Mol. Cell. Biol.* **20**, 9055–9067 (2000).
168. Phua, S. C. *et al.* Dynamic remodeling of membrane composition drives cell cycle through primary cilia excision. *Cell* **168**, 264–279 (2017).
169. Irigoín, F. & Badano, J. L. Keeping the balance between proliferation and differentiation: the primary cilium. *Curr. Genomics* **12**, 285–297 (2011).
170. Nonaka, S. *et al.* Randomization of left-right asymmetry due to loss of nodal cilia generating

- leftward flow of extraembryonic fluid in mice lacking KIF3B motor protein. *Cell* **95**, 829–837 (1998).
171. McGrath, J., Somlo, S., Makova, S., Tian, X. & Brueckner, M. Two populations of node monocilia initiate left-right asymmetry in the mouse. *Cell* **114**, 61–73 (2003).
172. Komatsu, Y. & Mishina, Y. Establishment of left-right asymmetry in vertebrate development: the node in mouse embryos. *Cell. Mol. Life Sci.* **70**, 4659–4666 (2013).
173. Ramsdell, A. F. Left-right asymmetry and congenital cardiac defects: getting to the heart of the matter in vertebrate left-right axis determination. *Dev. Biol.* **288**, 1–20 (2005).
174. Samsa, L. A., Yang, B. & Liu, J. Embryonic cardiac chamber maturation: Trabeculation, conduction, and cardiomyocyte proliferation. *Am. J. Med. Genet.* **163**, 157–168 (2013).
175. Myklebust, R., Engedal, H., Saetersdal, T. S. & Ulstein, M. Primary 9 + 0 cilia in the embryonic and the adult human heart. *Anat. Embryol. (Berl.)* **151**, 127–139 (1977).
176. Clement, C. a *et al.* The primary cilium coordinates early cardiogenesis and hedgehog signaling in cardiomyocyte differentiation. *J. Cell Sci.* **122**, 3070–3082 (2009).
177. Willaredt, M. A., Gorgas, K., Gardner, H. a R. & Tucker, K. L. Multiple essential roles for primary cilia in heart development. *Cilia* **1**, 23 (2012).
178. Gerhardt, C., Lier, J. M., Kuschel, S. & R  ther, U. The ciliary protein Ftm is required for ventricular wall and septal development. *PLoS One* **8**, e57545 (2013).
179. Ngan, E. S.-W., Kim, K.-H. & Hui, C.-C. Sonic hedgehog signaling and VACTERL association. *Mol. Syndromol.* **4**, 32–45 (2013).
180. Lim, J.-Y., Kim, W. H., Kim, J. & Park, S. I. Involvement of TGF-beta1 signaling in cardiomyocyte differentiation from P19CL6 cells. *Mol. Cells* **24**, 431–436 (2007).
181. Clement, C. A. *et al.* TGF- β signaling is associated with endocytosis at the pocket region of the primary cilium. *Cell Rep.* **3**, 1806–1814 (2013).
182. Fakhro, K. A. *et al.* Rare copy number variations in congenital heart disease patients identify unique genes in left-right patterning. *Proc. Natl. Acad. Sci.* **108**, 2915–2920 (2011).
183. Schneider, L. *et al.* PDGFR α signaling is regulated through the primary cilium in fibroblasts. *Curr. Biol.* **15**, 1861–1866 (2005).
184. Price, R. L. *et al.* Effects of platelet-derived growth factor-AA and -BB on embryonic cardiac development. *Anat. Rec.* **272A**, 424–433 (2003).
185. Schatteman, G. C., Motley, S. T., Effmann, E. L. & Bowen-Pope, D. F. Platelet-derived growth factor receptor alpha subunit deleted Patch mouse exhibits severe cardiovascular dysmorphogenesis. *Teratology* **51**, 351–366 (1995).
186. Zilber, Y. *et al.* The PCP effector Fuzzy controls ciliary assembly and signaling by recruiting Rab8 and Dishevelled to the primary cilium. *Mol. Biol. Cell* **24**, 555–565 (2013).
187. Ocbina, P. J. R., Tuson, M. & Anderson, K. V. Primary cilia are not required for normal canonical Wnt signaling in the mouse embryo. *PLoS One* **4**, e6839 (2009).
188. Ezratty, E. J. *et al.* A role for the primary cilium in Notch signaling and epidermal differentiation during skin development. *Cell* **145**, 1129–1141 (2011).
189. Slough, J., Cooney, L. & Brueckner, M. Monocilia in the embryonic mouse heart imply a direct role for cilia in cardiac morphogenesis. *Dev. Dyn.* **237**, 2304–2314 (2008).

190. Follit, J. A. *et al.* The golgin GMAP210/TRIP11 anchors IFT20 to the golgi complex. *PLoS Genet.* **4**, e1000315 (2008).
191. Li, Y. *et al.* Global genetic analysis in mice unveils central role for cilia in congenital heart disease. *Nature* **521**, 520–524 (2015).
192. Jang, J. *et al.* Primary Cilium-Autophagy-Nrf2 (PAN) axis activation commits human embryonic stem cells to a neuroectoderm fate. *Cell* **165**, 410–420 (2016).
193. Ryter, S. W., Cloonan, S. M. & Choi, A. M. K. Autophagy: A critical regulator of cellular metabolism and homeostasis. *Mol. Cells* **36**, 7–16 (2013).
194. Glick, D., Barth, S. & Macleod, K. F. Autophagy: cellular and molecular mechanisms. *J. Pathol.* **221**, 3–12 (2010).
195. Ogata, M. *et al.* Autophagy is activated for cell survival after endoplasmic reticulum stress. *Mol. Cell. Biol.* **26**, 9220–9231 (2006).
196. Ding, W.-X. *et al.* Linking of autophagy to ubiquitin-proteasome system is important for the regulation of Endoplasmic Reticulum stress and cell viability. *Am. J. Pathol.* **171**, 513–524 (2007).
197. Kondratyev, M., Avezov, E., Shenkman, M., Groisman, B. & Lederkremer, G. Z. PERK-dependent compartmentalization of ERAD and unfolded protein response machineries during ER stress. *Exp. Cell Res.* **313**, 3395–3407 (2007).
198. Høyer-Hansen, M. *et al.* Control of macroautophagy by calcium, calmodulin-dependent kinase kinase- β , and Bcl-2. *Mol. Cell* **25**, 193–205 (2007).
199. Papandreou, I., Lim, A. L., Laderoute, K. & Denko, N. C. Hypoxia signals autophagy in tumor cells via AMPK activity, independent of HIF-1, BNIP3, and BNIP3L. *Cell Death Differ.* **15**, 1572–1581 (2008).
200. Huang, Q., Wu, Y.-T., Tan, H.-L., Ong, C.-N. & Shen, H.-M. A novel function of poly(ADP-ribose) polymerase-1 in modulation of autophagy and necrosis under oxidative stress. *Cell Death Differ.* **16**, 264–277 (2009).
201. Nobukuni, T. *et al.* Amino acids mediate mTOR/raptor signaling through activation of class 3 phosphatidylinositol 3OH-kinase. *Proc. Natl. Acad. Sci.* **102**, 14238–14243 (2005).
202. Budovskaya, Y. V., Stephan, J. S., Reggiori, F., Klionsky, D. J. & Herman, P. K. The Ras/cAMP-dependent protein kinase signaling pathway regulates an early step of the autophagy process in *Saccharomyces cerevisiae*. *J. Biol. Chem.* **279**, 20663–20671 (2004).
203. Delgado, M. A., Elmaoued, R. A., Davis, A. S., Kyei, G. & Deretic, V. Toll-like receptors control autophagy. *EMBO J.* **27**, 1110–1121 (2008).
204. Axe, E. L. *et al.* Autophagosome formation from membrane compartments enriched in phosphatidylinositol 3-phosphate and dynamically connected to the endoplasmic reticulum. *J. Cell Biol.* **182**, 685–701 (2008).
205. Simonsen, A. & Tooze, S. A. Coordination of membrane events during autophagy by multiple class III PI3-kinase complexes. *J. Cell Biol.* **186**, 773–782 (2009).
206. Pankiv, S. *et al.* p62/SQSTM1 binds directly to Atg8/LC3 to facilitate degradation of ubiquitinated protein aggregates by autophagy. *J. Biol. Chem.* **282**, 24131–24145 (2007).
207. Kim, P. K., Hailey, D. W., Mullen, R. T. & Lippincott-Schwartz, J. Ubiquitin signals autophagic degradation of cytosolic proteins and peroxisomes. *Proc. Natl. Acad. Sci.* **105**, 20567–20574 (2008).

208. Scott, S. V, Guan, J., Hutchins, M. U., Kim, J. & Klionsky, D. J. Cvt19 is a receptor for the cytoplasm-to-vacuole targeting pathway. *Mol. Cell* **7**, 1131–1141 (2001).
209. Shintani, T., Huang, W.-P., Stromhaug, P. E. & Klionsky, D. J. Mechanism of cargo selection in the cytoplasm to vacuole targeting pathway. *Dev. Cell* **3**, 825–837 (2002).
210. He, C. & Klionsky, D. J. Regulation mechanisms and signaling pathways of autophagy. *Annu. Rev. Genet.* 67–93 (2009). doi:10.1146/annurev-genet-102808-114910.Regulation
211. Köchl, R., Hu, X. W., Chan, E. Y. W. & Tooze, S. A. Microtubules facilitate autophagosome formation and fusion of autophagosomes with endosomes. *Traffic* **7**, 129–145 (2006).
212. Iwata, A., Riley, B. E., Johnston, J. A. & Kopito, R. R. HDAC6 and microtubules are required for autophagic degradation of aggregated huntingtin. *J. Biol. Chem.* **280**, 40282–40292 (2005).
213. Ravikumar, B. *et al.* Dynein mutations impair autophagic clearance of aggregate-prone proteins. *Nat. Genet.* **37**, 771–776 (2005).
214. Ao, X., Zou, L. & Wu, Y. Regulation of autophagy by the Rab GTPase network. *Cell Death Differ.* **21**, 348–358 (2014).
215. Boehlke, C. *et al.* Primary cilia regulate mTORC1 activity and cell size through Lkb1. *Nat. Cell Biol.* **12**, 1115–1122 (2010).
216. Li, H. *et al.* Sonic hedgehog promotes autophagy of vascular smooth muscle cells. *Am. J. Physiol. Heart Circ. Physiol.* **303**, H1319–H1331 (2012).
217. Petralia, R. S. *et al.* Sonic hedgehog promotes autophagy in hippocampal neurons. *Biol. Open* **2**, 499–504 (2013).
218. Pampliega, O. *et al.* Functional interaction between autophagy and ciliogenesis. *Nature* **502**, 194–200 (2013).
219. Lam, H. C. *et al.* Histone deacetylase 6-mediated selective autophagy regulates COPD-associated cilia dysfunction. *J. Clin. Invest.* **123**, 5212–5230 (2013).
220. Tang, Z. *et al.* Autophagy promotes primary ciliogenesis by removing OFD1 from centriolar satellites. *Nature* **502**, 254–257 (2013).
221. Orhon, I., Dupont, N., Pampliega, O., Cuervo, A. M. & Codogno, P. Autophagy and regulation of cilia function and assembly. *Cell Death Differ.* **22**, 389–397 (2015).
222. Tasdemir, E. *et al.* Cell cycle-dependent induction of autophagy, mitophagy and reticulophagy. *Cell Cycle* **6**, 2263–2267 (2007).
223. Kaminsky, V., Abdi, A. & Zhivotovsky, B. A quantitative assay for the monitoring of autophagosome accumulation in different phases of the cell cycle. *Autophagy* **7**, 83–90 (2011).
224. Kuo, T.-C. *et al.* Midbody accumulation through evasion of autophagy contributes to cellular reprogramming and tumorigenicity. *Nat. Cell Biol.* **13**, 1214–1223 (2011).
225. Eskelinen, E.-L. *et al.* Inhibition of autophagy in mitotic animal cells. *Traffic* **3**, 878–893 (2002).
226. Furuya, T. *et al.* Negative regulation of Vps34 by Cdk mediated phosphorylation. *Mol. Cell* **38**, 500–511 (2010).
227. Tasdemir, E. *et al.* Regulation of autophagy by cytoplasmic p53. *Nat. Cell Biol.* **10**, 676–687 (2008).
228. Kenzelmann Broz, D. *et al.* Global genomic profiling reveals an extensive p53-regulated

- autophagy program contributing to key p53 responses. *Genes Dev.* **27**, 1016–1031 (2013).
229. Gewirtz, D. A. Autophagy and senescence. a partnership in search of definition. *Autophagy* **9**, 808–812 (2013).
230. García-Prat, L. *et al.* Autophagy maintains stemness by preventing senescence. *Nature* **529**, 37–42 (2016).
231. Kang, C. *et al.* The DNA damage response induces inflammation and senescence by inhibiting autophagy of GATA4. *Sci.* **349**, aaa5612 (2015).
232. Cecconi, F. & Levine, B. The role of autophagy in mammalian development: cell makeover rather than cell death. *Dev. Cell* **15**, 344–357 (2008).
233. Tsukamoto, S. *et al.* Autophagy is essential for preimplantation development of mouse embryos. *Science (80-.)*. **321**, 117–120 (2008).
234. Kuma, A. *et al.* The role of autophagy during the early neonatal starvation period. *Nature* **432**, 1032–1036 (2004).
235. Yue, Z., Jin, S., Yang, C., Levine, A. J. & Heintz, N. Beclin 1, an autophagy gene essential for early embryonic development, is a haploinsufficient tumor suppressor. *Proc. Natl. Acad. Sci.* **100**, 15077–15082 (2003).
236. Maria Fimia, G. *et al.* Ambra1 regulates autophagy and development of the nervous system. *Nature* **447**, 1121–1125 (2007).
237. Zhang, Y. *et al.* Adipose-specific deletion of autophagy-related gene 7 (atg7) in mice reveals a role in adipogenesis. *Proc. Natl. Acad. Sci.* **106**, 19860–19865 (2009).
238. Mizushima, N. & Levine, B. Autophagy in mammalian development and differentiation. *Nat. Cell Biol.* **12**, 823–830 (2010).
239. Gan, B. *et al.* Role of FIP200 in cardiac and liver development and its regulation of TNF α and TSC–mTOR signaling pathways. *J. Cell Biol.* **175**, 121–133 (2006).
240. Lee, E. *et al.* Autophagy is essential for cardiac morphogenesis during vertebrate development. *Autophagy* **10**, 572–587 (2014).
241. Zhang, J., Liu, J., Liu, L., McKeenan, W. L. & Wang, F. The fibroblast growth factor signaling axis controls cardiac stem cell differentiation through regulating autophagy. *Autophagy* **8**, 690–691 (2012).
242. Jia, Z. *et al.* Autophagy eliminates cytoplasmic β -catenin and NICD to promote the cardiac differentiation of P19CL6 cells. *Cell. Signal.* **26**, 2299–2305 (2014).
243. Gao, C. *et al.* Autophagy negatively regulates Wnt signalling by promoting Dishevelled degradation. *Nat. Cell Biol.* **12**, 781–790 (2010).
244. Jimenez-Sanchez, M. *et al.* The Hedgehog signalling pathway regulates autophagy. *Nat. Commun.* **3**, 1200 (2012).
245. Suzuki, H. I., Kiyono, K. & Miyazono, K. Regulation of autophagy by transforming growth factor- β (TGF- β) signaling. *Autophagy* **6**, 645–647 (2010).
246. Kiyono, K. *et al.* Autophagy is activated by TGF-beta and potentiates TGF-beta-mediated growth inhibition in human hepatocellular carcinoma cells. *Cancer Res.* **69**, 8844–8852 (2009).
247. Settembre, C. *et al.* Proteoglycan desulfation determines the efficiency of chondrocyte autophagy and the extent of FGF signaling during endochondral ossification. *Genes Dev.* **22**,

- 2645–2650 (2008).
248. Jerome, L. A. & Papaioannou, V. E. DiGeorge syndrome phenotype in mice mutant for the T-box gene, *Tbx1*. *Nat. Genet.* **27**, 286–291 (2001).
249. Lindsay, E. A. *et al.* *Tbx1* haploinsufficiency in the DiGeorge syndrome region causes aortic arch defects in mice. *Nature* **410**, 97–101 (2001).
250. Merscher, S. *et al.* *TBX1* is responsible for cardiovascular defects in velo-cardio-facial/DiGeorge syndrome. *Cell* **104**, 619–629 (2001).
251. Zhang, Z., Huynh, T. & Baldini, A. Mesodermal expression of *Tbx1* is necessary and sufficient for pharyngeal arch and cardiac outflow tract development. *Development* **133**, 3587–3595 (2006).
252. Araki, T. *et al.* Mouse model of Noonan syndrome reveals cell type- and gene dosage-dependent effects of *Ptpn11* mutation. *Nat. Med.* **10**, 849–857 (2004).
253. Dietz, H. C. *et al.* Marfan syndrome caused by a recurrent de novo missense mutation in the fibrillin gene. *Nature* **352**, 337–339 (1991).
254. Isogai, Z. *et al.* Latent transforming growth factor beta -binding protein 1 interacts with fibrillin and is a microfibril-associated protein. *J. Biol. Chem.* **278**, 2750–2757 (2003).
255. Neptune, E. R. *et al.* Dysregulation of TGF-beta activation contributes to pathogenesis in Marfan syndrome. *Nat. Genet.* **33**, 407–411 (2003).
256. Pereira, L. *et al.* Targetting of the gene encoding fibrillin-1 recapitulates the vascular aspect of Marfan syndrome. *Nat. Genet.* **17**, 218–222 (1997).
257. Naito, T. *et al.* Angiotensin II induces thrombospondin-1 production in human mesangial cells via p38 MAPK and JNK: a mechanism for activation of latent TGF- 1. *Am. J. Physiol. Ren. Physiol.* **286**, 278–287 (2004).
258. Habashi, J. P. *et al.* Losartan, an AT1 antagonist, prevents aortic aneurysm in a mouse model of Marfan syndrome. *Science (80-)*. **312**, 117–121 (2006).
259. Yashiro, K., Shiratori, H. & Hamada, H. Haemodynamics determined by a genetic programme govern asymmetric development of the aortic arch. *Nature* **450**, 285–288 (2007).
260. High, F. A. *et al.* An essential role for Notch in neural crest during cardiovascular development and smooth muscle differentiation. *J. Clin. Invest.* **117**, 353–363 (2007).
261. Grossfeld, P. D. The genetics of hypoplastic left heart syndrome. *Cardiol. Young* **9**, 627–632 (1999).
262. Grossfeld, P., Ye, M. & Harvey, R. Hypoplastic left heart syndrome: new genetic insights. *J. Am. Coll. Cardiol.* **53**, 1072–1074 (2009).
263. Krishnan, A. *et al.* A detailed comparison of mouse and human cardiac development. *Pediatr. Res.* **76**, 500–507 (2014).
264. Takahashi, K. *et al.* Induction of pluripotent stem cells from adult human fibroblasts by defined factors. *Cell* **131**, 861–872 (2007).
265. Yu, J. *et al.* Induced pluripotent stem cell lines derived from human somatic cells. *Science (80-)*. **318**, 1917–1920 (2007).
266. Takahashi, K. & Yamanaka, S. Induction of pluripotent stem cells from mouse embryonic and adult fibroblast cultures by defined factors. *Cell* **126**, 663–676 (2006).

267. Aasen, T. *et al.* Efficient and rapid generation of induced pluripotent stem cells from human keratinocytes. *Nat. Biotechnol.* **26**, 1276–1284 (2008).
268. Ruiz, S. *et al.* High-efficient generation of induced pluripotent stem cells from human astrocytes. *PLoS One* **5**, e15526 (2010).
269. Loh, Y.-H. *et al.* Reprogramming of T cells from human peripheral blood. *Cell Stem Cell* **7**, 15–19 (2010).
270. Staerk, J. *et al.* Reprogramming of human peripheral blood cells to induced pluripotent stem cells. *Cell Stem Cell* **7**, 20–24 (2010).
271. Seki, T. *et al.* Generation of induced pluripotent stem cells from human terminally differentiated circulating T cells. *Cell Stem Cell* **7**, 11–14 (2010).
272. Stadtfeld, M., Nagaya, M., Utikal, J., Weir, G. & Hochedlinger, K. Induced pluripotent stem cells generated without viral integration. *Science (80-.)*. **322**, 945–949 (2008).
273. Fusaki, N., Ban, H., Nishiyama, A., Saeki, K. & Hasegawa, M. Efficient induction of transgene-free human pluripotent stem cells using a vector based on Sendai virus, an RNA virus that does not integrate into the host genome. *Proc. Japan Acad. Ser. B* **85**, 348–362 (2009).
274. Deng, X.-Y. *et al.* Non-viral methods for generating integration-free, induced pluripotent stem cells. *Curr. Stem Cell Res. Ther.* **10**, 153–158 (2015).
275. Kim, D. *et al.* Generation of human induced pluripotent stem cells by direct delivery of reprogramming proteins. *Cell Stem Cell* **4**, 472–476 (2009).
276. Warren, L., Ni, Y., Wang, J. & Guo, X. Feeder-free derivation of human induced pluripotent stem cells with messenger RNA. *Sci. Rep.* **2**, (2012).
277. Mandal, P. K. & Rossi, D. J. Reprogramming human fibroblasts to pluripotency using modified mRNA. *Nat. Protoc.* **8**, 568–582 (2013).
278. Anokye-Danso, F. *et al.* Highly efficient miRNA-mediated reprogramming of mouse and human somatic cells to pluripotency. *Cell Stem Cell* **8**, 376–388 (2011).
279. Miyoshi, N. *et al.* Reprogramming of mouse and human cells to pluripotency using mature microRNAs. *Cell Stem Cell* **8**, 633–638 (2011).
280. Bayart, E. & Cohen-Haguenaer, O. Technological overview of iPSC induction from human adult somatic cells. *Curr. Gene Ther.* **13**, 73–92 (2013).
281. Hu, K. All roads lead to induced pluripotent stem cells: the technologies of iPSC generation. *Stem Cells Dev.* **23**, 1285–1300 (2014).
282. Chun, Y. S., Chaudhari, P. & Jang, Y.-Y. Applications of patient-specific induced pluripotent stem cells; focused on disease modeling, drug screening and therapeutic potentials for liver disease. *Int. J. Biol. Sci.* **6**, 796–805 (2010).
283. Avior, Y., Sagi, I. & Benvenisty, N. Pluripotent stem cells in disease modelling and drug discovery. *Nat. Rev. Mol. Cell Biol.* **17**, 170–182 (2016).
284. Devalla, H. D. *et al.* Atrial-like cardiomyocytes from human pluripotent stem cells are a robust preclinical model for assessing atrial-selective pharmacology. *EMBO Mol. Med.* **7**, 394–410 (2015).
285. Barbuti, A. & Robinson, R. B. Stem cell-derived nodal-like cardiomyocytes as a novel pharmacologic tool: insights from sinoatrial node development and function. *Pharmacol. Rev.* **67**, 368–388 (2015).

286. Witty, A. D. *et al.* Generation of the epicardial lineage from human pluripotent stem cells. *Nat. Biotechnol.* **32**, 1026–1035 (2014).
287. Kehat, I. *et al.* Human embryonic stem cells can differentiate into myocytes with structural and functional properties of cardiomyocytes. *J. Clin. Invest.* **108**, 407–414 (2001).
288. Takei, S. *et al.* Bone morphogenetic protein-4 promotes induction of cardiomyocytes from human embryonic stem cells in serum-based embryoid body development. *Am. J. Physiol. Heart Circ. Physiol.* **296**, H1793–H1803 (2009).
289. Bu, L. *et al.* Human ISL1 heart progenitors generate diverse multipotent cardiovascular cell lineages. *Nature* **460**, 113–117 (2009).
290. Shimoji, K. *et al.* G-CSF promotes the proliferation of developing cardiomyocytes in vivo and in derivation from ESCs and iPSCs. *Cell Stem Cell* **6**, 227–237 (2010).
291. Yang, L. *et al.* Human cardiovascular progenitor cells develop from a KDR+ embryonic-stem-cell-derived population. *Nature* **453**, 524–528 (2008).
292. Elliott, D. A. *et al.* NKX2-5eGFP/w hESCs for isolation of human cardiac progenitors and cardiomyocytes. *Nat. Methods* **8**, 1037–1040 (2011).
293. Kattman, S. J. *et al.* Stage-specific optimization of activin/nodal and BMP signaling promotes cardiac differentiation of mouse and human pluripotent stem cell lines. *Cell Stem Cell* **8**, 228–240 (2011).
294. Burridge, P. W., Keller, G., Gold, J. D. & Wu, J. C. Production of de novo cardiomyocytes: human pluripotent stem cell differentiation and direct reprogramming. *Cell Stem Cell* **10**, 16–28 (2012).
295. McDevitt, T. C., Laflamme, M. A. & Murry, C. E. Proliferation of cardiomyocytes derived from human embryonic stem cells is mediated via the IGF/PI 3-kinase/Akt signaling pathway. *J. Mol. Cell. Cardiol.* **39**, 865–873 (2005).
296. Ng, E. S., Davis, R. P., Azzola, L., Stanley, E. G. & Elefanty, A. G. Forced aggregation of defined numbers of human embryonic stem cells into embryoid bodies fosters robust, reproducible hematopoietic differentiation. *Blood* **106**, 1601–1603 (2005).
297. Khademhosseini, A. *et al.* Co-culture of human embryonic stem cells with murine embryonic fibroblasts on microwell-patterned substrates. *Biomaterials* **27**, 5968–5977 (2006).
298. Bauwens, C. L. *et al.* Control of human embryonic stem cell colony and aggregate size heterogeneity influences differentiation trajectories. *Stem Cells* **26**, 2300–2310 (2008).
299. Mummery, C. *et al.* Differentiation of human embryonic stem cells to cardiomyocytes: role of coculture with visceral endoderm-like cells. *Circulation* **107**, 2733–2740 (2003).
300. Passier, R. *et al.* Increased cardiomyocyte differentiation from human embryonic stem cells in serum-free cultures. *Stem Cells* **23**, 772–780 (2005).
301. Graichen, R. *et al.* Enhanced cardiomyogenesis of human embryonic stem cells by a small molecular inhibitor of p38 MAPK. *Differentiation* **76**, 357–370 (2008).
302. Laflamme, M. A. *et al.* Cardiomyocytes derived from human embryonic stem cells in pro-survival factors enhance function of infarcted rat hearts. *Nat. Biotechnol.* **25**, 1015–1024 (2007).
303. Ng, E. S., Davis, R., Stanley, E. G. & Elefanty, A. G. A protocol describing the use of a recombinant protein-based, animal product-free medium (APEL) for human embryonic stem cell differentiation as spin embryoid bodies. *Nat. Protoc.* **3**, 768–776 (2008).
304. Zhang, J. *et al.* Extracellular matrix promotes highly efficient cardiac differentiation of human

- pluripotent stem cells: the matrix sandwich method. *Circ. Res.* **111**, 1125–1136 (2012).
305. Lian, X. *et al.* Robust cardiomyocyte differentiation from human pluripotent stem cells via temporal modulation of canonical Wnt signaling. *Proc. Natl. Acad. Sci. U. S. A.* **109**, 1848–1857 (2012).
306. Burridge, P. W. *et al.* Chemically defined generation of human cardiomyocytes. *Nat. Methods* **11**, 855–860 (2014).
307. Minami, I. *et al.* A small molecule that promotes cardiac differentiation of human pluripotent stem cells under defined, cytokine- and xeno-free conditions. *Cell Rep.* **2**, 1448–1460 (2012).
308. Cao, N. *et al.* Highly efficient induction and long-term maintenance of multipotent cardiovascular progenitors from human pluripotent stem cells under defined conditions. *Cell Res.* **23**, 1119–1132 (2013).
309. Birket, M. J. *et al.* Expansion and patterning of cardiovascular progenitors derived from human pluripotent stem cells. *Nat. Biotechnol.* **33**, 970–979 (2015).
310. Moretti, A. *et al.* Patient-specific induced pluripotent stem-cell models for long-QT syndrome. *N. Engl. J. Med.* **363**, 1397–1409 (2010).
311. Wang, Q. *et al.* SCN5A mutations associated with an inherited cardiac arrhythmia, long QT syndrome. *Cell* **80**, 805–811 (1995).
312. Splawski, I. *et al.* Spectrum of mutations in long-QT syndrome genes. KVLQT1, HERG, SCN5A, KCNE1, and KCNE2. *Circulation* **102**, 1178–1185 (2000).
313. Crotti, L., Celano, G., Dagradi, F. & Schwartz, P. J. Congenital long QT syndrome. *Orphanet J. Rare Dis.* **3**, (2008).
314. Moretti, A. *et al.* SUPPLEMENT - Mouse and human induced pluripotent stem cells as a source for multipotent Isl1+ cardiovascular progenitors. *FASEB J.* **24**, 700–711 (2010).
315. Itzhaki, I. *et al.* Calcium handling in human induced pluripotent stem cell derived cardiomyocytes. *PLoS One* **6**, e18037 (2011).
316. Matsa, E. *et al.* Drug evaluation in cardiomyocytes derived from human induced pluripotent stem cells carrying a long QT syndrome type 2 mutation. *Eur. Heart J.* **32**, 952–962 (2011).
317. Lahti, A. L. *et al.* Model for long QT syndrome type 2 using human iPS cells demonstrates arrhythmogenic characteristics in cell culture. *Dis. Model. Mech.* **5**, 220–230 (2012).
318. Egashira, T. *et al.* Disease characterization using LQTS-specific induced pluripotent stem cells. *Cardiovasc. Res.* **95**, 419–429 (2012).
319. Bellin, M. *et al.* Isogenic human pluripotent stem cell pairs reveal the role of a KCNH2 mutation in long-QT syndrome. *EMBO J.* **32**, 3161–3175 (2013).
320. Mehta, A. *et al.* Re-trafficking of hERG reverses long QT syndrome 2 phenotype in human iPS-derived cardiomyocytes. *Cardiovasc. Res.* **102**, 497–506 (2014).
321. Ma, D. *et al.* Modeling type 3 long QT syndrome with cardiomyocytes derived from patient-specific induced pluripotent stem cells. *Int. J. Cardiol.* **168**, 5277–5286 (2013).
322. Malan, D. *et al.* Human iPS cell model of type 3 long QT syndrome recapitulates drug-based phenotype correction. *Basic Res. Cardiol.* **111**, (2016).
323. Terrenoire, C. *et al.* Induced pluripotent stem cells used to reveal drug actions in a long QT syndrome family with complex genetics. *J. Gen. Physiol.* **141**, 61–72 (2013).

324. Priori, S. G. *et al.* Mutations in the cardiac ryanodine receptor gene (hRyR2) underlie catecholaminergic polymorphic ventricular tachycardia. *Circulation* **103**, 196–200 (2001).
325. Beard, N. A., Laver, D. R. & Dulhunty, A. F. Calsequestrin and the calcium release channel of skeletal and cardiac muscle. *Prog. Biophys. Mol. Biol.* **85**, 33–69 (2004).
326. Song, L. *et al.* Calsequestrin 2 (CASQ2) mutations increase expression of calreticulin and ryanodine receptors, causing catecholaminergic polymorphic ventricular tachycardia. *J. Clin. Invest.* **117**, 1814–1823 (2007).
327. Novak, A. *et al.* Cardiomyocytes generated from CPVTD307H patients are arrhythmogenic in response to β -adrenergic stimulation. *J. Cell. Mol. Med.* **16**, 468–482 (2012).
328. Jung, C. B. *et al.* Dantrolene rescues arrhythmogenic RYR2 defect in a patient-specific stem cell model of catecholaminergic polymorphic ventricular tachycardia. *EMBO Mol. Med.* **4**, 180–191 (2012).
329. Itzhaki, I. *et al.* Modeling of catecholaminergic polymorphic ventricular tachycardia with patient-specific human-induced pluripotent stem cells. *J. Am. Coll. Cardiol.* **60**, 990–1000 (2012).
330. Di Pasquale, E. *et al.* CaMKII inhibition rectifies arrhythmic phenotype in a patient-specific model of catecholaminergic polymorphic ventricular tachycardia. *Cell Death Dis.* **4**, e843 (2013).
331. Maron, B. J. & Maron, M. S. Hypertrophic cardiomyopathy. *Lancet* **381**, 242–255 (2013).
332. Lan, F. *et al.* Abnormal calcium handling properties underlie familial hypertrophic cardiomyopathy pathology in patient-specific induced pluripotent stem cells. *Cell Stem Cell* **12**, 101–113 (2013).
333. Siu, C.-W. *et al.* Modeling of lamin A/C mutation premature cardiac aging using patient-specific induced pluripotent stem cells. *Aging (Albany, NY)*. **4**, 803–822 (2012).
334. Tse, H.-F. *et al.* Patient-specific induced-pluripotent stem cells-derived cardiomyocytes recapitulate the pathogenic phenotypes of dilated cardiomyopathy due to a novel DES mutation identified by whole exome sequencing. *Hum. Mol. Genet.* **22**, 1395–403 (2013).
335. Sun, N. *et al.* Patient-specific induced pluripotent stem cells as a model for familial dilated cardiomyopathy. *Sci. Transl. Med.* **4**, 130ra47 (2012).
336. Gramlich, M. *et al.* Antisense-mediated exon skipping: a therapeutic strategy for titin-based dilated cardiomyopathy. *EMBO Mol. Med.* **7**, 562–576 (2015).
337. Hershberger, R. E. & Siegfried, J. D. Update 2011: Clinical and genetic issues in familial dilated cardiomyopathy. *J. Am. Coll. Cardiol.* **57**, 1641–1649 (2011).
338. Ma, D. *et al.* Generation of patient-specific induced pluripotent stem cell-derived cardiomyocytes as a cellular model of arrhythmogenic right ventricular cardiomyopathy. *Eur. Heart J.* **34**, 1122–1133 (2013).
339. Caspi, O. *et al.* Modeling of arrhythmogenic right ventricular cardiomyopathy with human induced pluripotent stem cells. *Circ. Cardiovasc. Genet.* **6**, 557–568 (2013).
340. Kim, C. *et al.* Studying arrhythmogenic right ventricular dysplasia with patient-specific iPSCs. *Nature* **494**, 105–110 (2013).
341. Kobayashi, J. *et al.* Directed differentiation of patient-specific induced pluripotent stem cells identifies the transcriptional repression and epigenetic modification of NKX2-5, HAND1, and NOTCH1 in hypoplastic left heart syndrome. *PLoS One* **9**, e102796 (2014).
342. Jiang, Y. *et al.* An induced pluripotent stem cell model of hypoplastic left heart syndrome (HLHS)

- reveals multiple expression and functional differences in HLHS-derived cardiac myocytes. *Stem Cells Transl. Med.* **3**, 416–423 (2014).
343. Theis, J. L. *et al.* Compound heterozygous NOTCH1 mutations underlie impaired cardiogenesis in a patient with hypoplastic left heart syndrome. *Hum. Genet.* **134**, 1003–1011 (2015).
344. Hrstka, S. C. L., Li, X., Nelson, T. J. & Wanek Program Genetics Pipeline Group. NOTCH1-dependent Nitric Oxide signaling deficiency in Hypoplastic Left Heart Syndrome revealed through patient-specific phenotypes detected in bioengineered cardiogenesis. *Stem Cells* **35**, 1106–1119 (2017).
345. Bohlmeier, T. J. *et al.* Hypoplastic left heart syndrome myocytes are differentiated but possess a unique phenotype. *Cardiovasc. Pathol.* **12**, 23–31 (2003).
346. Tomita-Mitchell, A. *et al.* Impact of MYH6 variants in hypoplastic left heart syndrome. *Physiol. Genomics* **48**, 912–921 (2016).
347. Lyons, G. E., Schiaffino, S., Sassoon, D., Barton, P. & Buckingham, M. Developmental regulation of myosin gene expression in mouse cardiac muscle. *J. Cell Biol.* **111**, 2427–2436 (1990).
348. Zhao, S. *et al.* PiggyBac transposon vectors: the tools of the human gene encoding. *Transl. Lung Cancer Res.* **5**, 120–125 (2016).
349. Burridge, P. W. *et al.* Chemically defined generation of human cardiomyocytes. *Nat. Methods* **11**, 855–860 (2014).
350. Cooper, G. in *The Cell: A Molecular Approach. 2nd edition.* (2000).
351. Salic, A. & Mitchison, T. J. A chemical method for fast and sensitive detection of DNA synthesis in vivo. *Proc. Natl. Acad. Sci. U. S. A.* **105**, 2415–2420 (2008).
352. Calder, A. *et al.* Lengthened G1 phase indicates differentiation status in human embryonic stem cells. *Stem Cells Dev.* **22**, 279–295 (2013).
353. Krishan, A. Rapid flow cytofluorometric analysis of mammalian cell cycle by propidium iodide staining. *J. Cell Biol.* **66**, 188–193 (1975).
354. Colanzi, A. *et al.* Molecular mechanism and functional role of brefeldin A-mediated ADP-ribosylation of CtBP1/BARS. *Proc. Natl. Acad. Sci. U. S. A.* **110**, 9794–9799 (2013).
355. Yang, Y. *et al.* Application and interpretation of current autophagy inhibitors and activators. *Acta Pharmacol. Sin.* **34**, 625–635 (2013).
356. Chen, H.-J. *et al.* The role of microtubule actin cross-linking factor 1 (MACF1) in the Wnt signaling pathway. *Genes Dev.* **20**, 1933–1945 (2006).
357. Dell’Era, P. *et al.* Fibroblast growth factor receptor-1 is essential for in vitro cardiomyocyte development. *Circ. Res.* **93**, 414–420 (2003).
358. Gambetta, K., Al-Ahdab, M. K., Ilbawi, M. N., Hassaniya, N. & Gupta, M. Transcription repression and blocks in cell cycle progression in hypoplastic left heart syndrome. *Am. J. Physiol. Heart Circ. Physiol.* **294**, 2268–2275 (2008).
359. Davies, B. *et al.* Differences in extra-cellular matrix and myocyte homeostasis between the neonatal right ventricle in hypoplastic left heart syndrome and truncus arteriosus. *Eur. J. Cardio-thoracic Surg.* **34**, 738–744 (2008).
360. Bedada, F. B., Wheelwright, M. & Metzger, J. M. Maturation status of sarcomere structure and function in human iPSC-derived cardiac myocytes. *Biochim. Biophys. Acta. Mol. Cell Res.* **1863**, 1829–1838 (2016).

361. Li, Q. Y. *et al.* Holt-Oram syndrome is caused by mutations in TBX5, a member of the Brachyury (T) gene family. *Nat. Genet.* **15**, 21–29 (1997).
362. Bruneau, B. G. *et al.* A murine model of Holt-Oram syndrome defines roles of the T-box transcription factor Tbx5 in cardiogenesis and disease. *Cell* **106**, 709–721 (2001).
363. Warkman, A. S. & Krieg, P. A. *Xenopus* as a model system for vertebrate heart development. *Semin. Cell Dev. Biol.* **18**, 46–53 (2007).
364. Nguyen, C. T., Lu, Q., Wang, Y. & Chen, J.-N. Zebrafish as a model for cardiovascular development and disease. *Drug Discov. Today. Dis. Models* **5**, 135–140 (2008).
365. Kaltenbrun, E. *et al.* *Xenopus*: an emerging model for studying congenital heart disease. *Birth Defects Res. A. Clin. Mol. Teratol.* **91**, 495–510 (2011).
366. Geddes, G. C., Stamm, K., Mitchell, M., Mussatto, K. A. & Tomita-Mitchell, A. Ciliopathy variant burden and developmental delay in children with hypoplastic left heart syndrome. *Genet. Med.* (2016). doi:10.1038/gim.2016.167
367. Neugebauer, J. M., Amack, J. D., Peterson, A. G., Bisgrove, B. W. & Yost, H. J. FGF signalling during embryo development regulates cilia length in diverse epithelia. *Nature* **458**, 651–654 (2009).
368. May-Simera, H. L. *et al.* Loss of MACF1 abolishes ciliogenesis and disrupts apicobasal polarity establishment in the retina. *Cell Rep.* **17**, 1399–1413 (2016).
369. Ghule, P. N. *et al.* Reprogramming the pluripotent cell cycle: restoration of an abbreviated G1 phase in human induced pluripotent stem (iPS) cells. *J. Cell Physiol.* **226**, 1149–1156 (2011).
370. Wu, X., Won, H. & Rubinsztein, D. C. Autophagy and mammalian development. *Biochem. Soc. Trans.* **41**, 1489–1494 (2013).
371. Menendez, J. A., Vellon, L., Oliveras-Ferraros, C., Cufí, S. & Vazquez-Martin, A. mTOR-regulated senescence and autophagy during reprogramming of somatic cells to pluripotency: A roadmap from energy metabolism to stem cell renewal and aging. *Cell Cycle* **10**, 3658–3677 (2011).
372. Pospelova, T. V. *et al.* Rapamycin induces pluripotent genes associated with avoidance of replicative senescence. *Cell Cycle* **12**, 3841–3851 (2013).
373. Pathania, A. S. *et al.* Interplay between cell cycle and autophagy induced by boswellic acid analog. *Sci. Rep.* **6**, (2016).
374. Seto, S., Tsujimura, K. & Koide, Y. Rab GTPases regulating phagosome maturation are differentially recruited to mycobacterial phagosomes. *Traffic* **12**, 407–420 (2011).
375. Seto, S. *et al.* Rab39a interacts with phosphatidylinositol 3-kinase and negatively regulates autophagy induced by lipopolysaccharide stimulation in macrophages. *PLoS One* **8**, e83324 (2013).
376. Sellier, C. *et al.* Loss of C9ORF72 impairs autophagy and synergizes with polyQ Ataxin-2 to induce motor neuron dysfunction and cell death. *EMBO J.* **35**, 1276–1297 (2016).
377. Alvarez, C. & Sztul, E. S. Brefeldin A (BFA) disrupts the organization of the microtubule and the actin cytoskeletons. *Eur. J. Cell Biol.* **78**, 1–14 (1999).
378. Ivessa, N. E., Gravotta, D., De Lemos-Chiarandini, C. & Kreibich, G. Functional protein prenylation is required for the brefeldin A-dependent retrograde transport from the Golgi apparatus to the endoplasmic reticulum. *J. Biol. Chem.* **272**, 20828–20834 (1997).
379. Dong, C. *et al.* ADP-ribosylation factors modulate the cell surface transport of G protein-coupled

- receptors. *J. Pharmacol. Exp. Ther.* **333**, 174–183 (2010).
380. Fernandes, H., Franklin, E. & Khan, A. R. Crystallization of an engineered RUN domain of Rab6-interacting protein 1/DENND5. *Acta Crystallogr. Sect. F. Struct. Biol. Cryst. Commun.* **67**, 556–560 (2011).
381. Fernandes, H., Franklin, E., Jollivet, F., Bliedtner, K. & Khan, A. R. Mapping the interactions between a RUN domain from DENND5/Rab6IP1 and sorting nexin 1. *PLoS One* **7**, e35637 (2012).
382. Marat, A. L., Dokainish, H. & McPherson, P. S. DENN domain proteins: regulators of Rab GTPases. *J. Biol. Chem.* **286**, 13791–800 (2011).
383. Yoshimura, S., Gerondopoulos, A., Linford, A., Rigden, D. J. & Barr, F. a. Family-wide characterization of the DENN domain Rab GDP-GTP exchange factors. *J. Cell Biol.* **191**, 367–381 (2010).
384. Xu, J. & McPherson, P. S. Regulation of DENND3, the exchange factor for the small GTPase Rab12 through an intramolecular interaction. *J. Biol. Chem.* **292**, 7274–7282 (2017).
385. Lin, X. *et al.* FRS2 α is essential for the fibroblast growth factor to regulate the mTOR pathway and autophagy in mouse embryonic fibroblasts. *Int. J. Biol. Sci.* **7**, 1114–1121 (2011).
386. Chen, Y. *et al.* FGFR antagonist induces protective autophagy in FGFR1-amplified breast cancer cell. *Biochem. Biophys. Res. Commun.* **474**, 1–7 (2016).
387. Goetz, S. C. & Conlon, F. L. Cardiac progenitors and the embryonic cell cycle. *Cell cycle* **6**, 1974–1981 (2007).
388. Sohda, M. *et al.* Trans-Golgi protein p230/golgin-245 is involved in phagophore formation. *Biochem. Biophys. Res. Commun.* **456**, 275–281 (2015).
389. Ávalos, Y. *et al.* Tumor suppression and promotion by autophagy. *Biomed Res. Int.* **2014**, 603980 (2014).
390. Williams, A. *et al.* Novel targets for Huntington’s disease in an mTOR-independent autophagy pathway. *Nat. Chem. Biol.* **4**, 295–305 (2008).
391. Ravikumar, B. *et al.* Inhibition of mTOR induces autophagy and reduces toxicity of polyglutamine expansions in fly and mouse models of Huntington disease. *Nat. Genet.* **36**, 585–595 (2004).
392. Luciani, A. *et al.* Cystic fibrosis: a disorder with defective autophagy. *Autophagy* **7**, 104–106 (2011).
393. Mizumura, K., Cloonan, S. M., Haspel, J. A. & Choi, A. M. K. The emerging importance of autophagy in pulmonary diseases. *Chest* **142**, 1289–1299 (2012).
394. Deretic, V., Saitoh, T. & Akira, S. Autophagy in infection, inflammation and immunity. *Nat. Rev. Immunol.* **13**, 722–737 (2013).
395. Ganesan, R. *et al.* Salmonella Typhimurium disrupts Sirt1/AMPK checkpoint control of mTOR to impair autophagy. *PLoS Pathog.* **13**, e1006227 (2017).
396. Campbell, G. R. & Spector, S. A. Autophagy induction by vitamin D inhibits both Mycobacterium tuberculosis and human immunodeficiency virus type 1. *Autophagy* **8**, 1523–1525 (2012).
397. Donia, M., McCubrey, J. A., Bendtzen, K. & Nicoletti, F. Potential use of rapamycin in HIV infection. *Br. J. Clin. Pharmacol.* **70**, 784–793 (2010).
398. Ryter, S. W., Koo, J. K. & Choi, A. M. K. Molecular regulation of autophagy and its implications for metabolic diseases. *Curr. Opin. Clin. Nutr. Metab. Care* **17**, 329–337 (2014).

399. Saftig, P. *et al.* Accumulation of autophagic vacuoles and cardiomyopathy in LAMP-2-deficient mice. *Nature* **406**, 902–906 (2000).
400. Shimomura, H. *et al.* Autophagic degeneration as a possible mechanism of myocardial cell death in dilated cardiomyopathy. *Jpn. Circ. J.* **65**, 965–968 (2001).
401. Eisenberg, T. *et al.* Cardioprotection and lifespan extension by the natural polyamine spermidine. *Nat. Med.* **22**, 1428–1438 (2016).
402. Liao, X. *et al.* Macrophage autophagy plays a protective role in advanced atherosclerosis. *Cell Metab.* **15**, 545–553 (2012).
403. Razani, B. *et al.* Autophagy links inflammasomes to atherosclerotic progression. *Cell Metab.* **15**, 534–544 (2012).
404. Chen-Scarabelli, C. *et al.* The role and modulation of autophagy in experimental models of myocardial ischemia-reperfusion injury. *J. Geriatr. Cardiol.* **11**, 338–348 (2014).
405. Lee, J. *et al.* Defective ciliogenesis in thyroid hürthle cell tumors is associated with increased autophagy. *Oncotarget* **7**, 79117–79130 (2016).
406. Jimenez-Sanchez, M., Thomson, F., Zavodszky, E. & Rubinsztein, D. C. Autophagy and polyglutamine diseases. *Prog. Neurobiol.* **97**, 67–82 (2012).
407. Kaliszewski, M., Knott, A. B. & Bossy-Wetzel, E. Primary cilia and autophagic dysfunction in Huntington’s disease. *Cell Death Differ.* **22**, 1413–1424 (2015).
408. Wang, S., Livingston, M. J., Su, Y. & Dong, Z. Reciprocal regulation of cilia and autophagy via the MTOR and proteasome pathways. *Autophagy* **11**, 607–616 (2015).
409. Pampliega, O. *et al.* Functional interaction between autophagy and ciliogenesis. *Nature* **502**, 194–200 (2013).
410. Avidor-Reiss, T. & Gopalakrishnan, J. Cell cycle regulation of the centrosome and cilium. *Drug Discov. Today. Dis. Mech.* **10**, e119–e124 (2013).
411. Kroemer, G., Mariño, G. & Levine, B. Autophagy and the integrated stress response. *Mol. Cell* **40**, 280–293 (2010).
412. Polager, S., Ofir, M. & Ginsberg, D. E2F1 regulates autophagy and the transcription of autophagy genes. *Oncogene* **27**, 4860–4864 (2008).
413. Clevers, H. Modeling development and disease with organoids. *Cell* **165**, 1586–1597 (2016).
414. Zhang, Y. S. & Yu, C. Towards engineering integrated cardiac organoids: beating recorded. *J. Thorac. Dis.* **8**, 1683–1687 (2016).
415. Wu, S. M. *et al.* Developmental origin of a bipotential myocardial and smooth muscle cell precursor in the mammalian heart. *Cell* **127**, 1137–1150 (2006).

Acknowledgements

First of all I would like to thank Prof. Karl-Ludwig Laugwitz and Prof. Alessandra Moretti for giving me the opportunity to work in their group and for supervising my thesis. I am very thankful for your support and guidance.

A big thank you goes to Ilaria, who was the greatest support within my project, always motivating me, contributing with many ideas to the outcome of my thesis and finally always having an open ear also outside work, thereby becoming a very good friend. Moreover, I want to thank Zhifi who was a very helpful colleague and good friend throughout my PhD thesis. And of course I have to thank Tatu, who was such a great support at work, answering all my questions and discussing with me so patiently, who taught me a lot and also became more than a colleague for me within the last years. You guys let me enjoy my work life so much more! Finally, I would like to thank Birgit for so many nice talks at work, not only concerning our projects, Alex for carefully reading my thesis, Tine, Dorota, Kathi, Farah, Luna, Elvira, Jessy, Lisa, Tom, Christina and Diana for your support at work and some fun outside work as well.

I also would like to thank all my friends from home, abroad and in Munich for filling the often stressful time of my thesis with so many wonderful moments.

But the biggest thank you goes to my family: to my parents, who supported me so much not only during this thesis, and to my sister Janina, for always encouraging me, for visiting me so often in Munich and for planning the greatest trips.